RESEARCH IN SEISMOLOGY

by

Carl Kisslinger

Department of Earth and Atmospheric Sciences
Saint Louis University
St. Louis, Missouri 63103

Contract No F19628-70-C-0036
Project No. 8652

ANNUAL TECHNICAL REPORT No. 1

1 September 1969 — 31 August 1970
1 September 1970

Contract Monitor: Henry A. Ossing
Terrestrial Sciences Laboratory

Sponsored by
Advanced Research Projects Agency
ARPA Order No. 0292

Monitored by
Air Force Cambridge Research Laboratories
Air Force Systems Command
United States Air Force
Bedford, Massachusetts 01730

DISCLAIMER NOTICE

THIS DOCUMENT IS THE BEST QUALITY AVAILABLE.

COPY FURNISHED CONTAINED A SIGNIFICANT NUMBER OF PAGES WHICH DO NOT REPRODUCE LEGIBLY.

AFCRL-70-0582

RESEARCH IN SEISMOLOGY

by

Carl Kisslinger

Department of Earth and Atmospheric Sciences
Saint Louis University
St. Louis, Missouri 63103

Contract No. F19628-70-C-0036
Project No. 8652

ANNUAL TECHNICAL REPORT No. 1

1 September 1969 — 31 August 1970
1 September 1970

Contract Monitor: Henry A. Ossing
Terrestrial Sciences Laboratory

Sponsored by
Advanced Research Projects Agency
ARPA Order No. 0292

Monitored by
Air Force Cambridge Research Laboratories
Air Force Systems Command
United States Air Force
Bedford, Massachusetts 01730

ABSTRACT

Research related to the detection, location, and identification of underground nuclear explosion devoted to several major problem areas has been completed. Effects of earth structure and focal mechanism on body-wave magnitude determinations have been investigated, and empirical relations between nuclear yield and Rayleigh wave magnitudes established for selected seismograph stations. Calculations of crustal transmission coefficients for P-waves have been extended to take into account dip and the results applied to observations of laboratory explosion and deep earthquakes. A model for the triggering of earthquakes by explosions based on finite-strain theory has been suggested, the superposition of the explosion-generated and triggered-earthquake-generated P-wave computed for single models, and aftershocks of the Benham event analyzed. Methods of using P-wave and Rayleigh wave spectra for determining earthquake mechanisms have been developed and applied. A small local network for detecting and locating low magnitude earthquakes in southeast Missouri has yielded good data on current local seismicity.

Table of Contents

Magnitude, Yield, and Energy Determination.

1. On the Problems of Determining Body-Wave Magnitude

Otto W. Nuttli

One of the most successful means of discriminating between earthquakes and underground explosions compares the body and surface wave magnitudes of the event. This discrimination method was developed for larger magnitude events (m_b between about 5 and 6.5) and is gradually being extended to smaller ones.

At least two classes of problems arise when smaller magnitude events are considered. The first concerns the physics of the source mechanism. For earthquakes of small magnitude the volume of the source region and the time duration of the source become small, so that the earthquake source will more closely approximate an impulse in time applied at a point. For this reason the differences in seismic signals from earthquakes and underground explosions are expected to become less pronounced as their magnitudes become smaller. The second class of problems peculiar to small magnitude events results from the fact that the amplitudes of the seismic signals are smaller, so that they are recorded by perhaps only a few seismograph stations or arrays. As a consequence certain factors which affect the amplitude of the <u>recorded</u> signal take on a new significance. For the larger magnitude events these factors can to a large extent be ignored, by assuming that they randomly affect the ground motion at a

large number of seismograph stations. Although the scatter in magnitude values from individual stations will be large, the statistical average of all such magnitudes appears to give a reasonable approximation to the actual magnitude. However, when data from only a few stations are available, the effects of crustal structure, azimuthal-dependent radiation pattern of the source and the attenuation of wave motion with distance take on much more importance.

In another paper in this report (Effect of Regional Correction on the Value of m_b), Syed offers a methodology for correcting for the azimuthal-dependent radiation pattern of the source. His procedure, which can be applied in a routine manner, does not require that a focal mechanism solution be determined for each event. Furthermore, his study enables him to determine which seismograph stations will receive anomalously small amplitude P waves from earthquakes in a particular geographic region because of the focal mechanism pattern of the region. For example, LASA will have smaller than average amplitude P waves from earthquakes beneath the Aleutian Islands, but normal or larger than average amplitude P waves for earthquakes beneath the Aleutian Trench.

The effects of the crust and upper mantle structure on the ground motion can, in theory, be compensated by using the crustal transfer function. These effects include the frequency-dependent constructive and destructive interference of waves reflected at the crustal boundaries and/or converted from P to SV motion. However, in practice, the inverse

problem of determining crustal structure from observations of the crustal transfer function only has been successful for long-period P waves. Attempts at using the short-period P spectral ratios for crustal structure determinations have proved inconclusive or unsatisfactory (Utsu, 1966, and Hasegawa, 1970). This can be attributed in great part to the fact that the maxima and minima of the crustal transfer function, when considered as a function of earth period, are much more closely spaced together at periods of about 0.5 to 2.0 seconds than at periods of about 5 to 10 seconds.

The extent to which crustal structure can influence the short-period P wave ground motion may be seen in the plot of the maximum A/T for the vertical component of the P motion produced by LONGSHOT (Lambert et al, 1970, fig. 4). At distances of 20° to 100° the spread in A/T values at any given distance is at least one and as much as two orders of magnitude (differences of 10 to 100 times). As a second example, the data in Table 1, which contains m_b values from short-period PZ for two Soviet underground explosions at Kazakh, indicate a spread of one magnitude unit between m_b values at the various WWSSN stations. However, at no station does the difference in m_b for the two events exceed 0.27 magnitude units, the average value of the absolute difference being only 0.12. This indicates that the variation in magnitude values between stations for a single event is not caused principally by noise or errors in reading, but rather is reproducible. Such reproducibility is to be expected if the observed amplitudes depend strongly upon the crustal structure.

crust and upper mantle structure has a lesser modifying effect upon the amplitude of the incident P wave for the long-period waves, as compared to the short-period ones. Figure 1.1 gives the A/T values of P for the underground explosion at Novaya Zemlaya on Oct. 27, 1966. The circles correspond to the maximum value of A/T in the first three cycles of the P motion, as obtained from the short-period WWSSN seismograms. The crosses correspond to the A/T value of the first half-cycle of the P motion as recorded by the long-period WWSSN seismographs. The solid line is the expected value of A/T, based on Gutenberg and Richter's (1956) magnitude chart, for $m_b = 6.4$. Note that in general there is more scatter among the short-period values than the long-period ones. There are three anomalously large values of the long-period data between 65° and 70°. These anomalous amplitudes, which are from stations on islands in the western Pacific, will be discussed later.

Similar examples can be given for LASA, with large variations in short-period P wave amplitude across the array (Broome et al, 1967, fig. A-1) but practically no variations in long-period P wave amplitudes across the array (Syed, 1969).

Ben-Menahem, et al (1965, fig. 9) gave the impulse response of a long-period, vertical component seismograph system ($T_s = 30$ sec., $T_g = 100$ sec.) to an incident P wave for a half-space model and five models including a layered crust over a half-space. The crustal models include extreme types, such as thin oceanic and thick mountainous ones. For these two

extreme models the P wave first half amplitude was 1.5 to 2 times larger than that of the half-space (0.2 to 0.3 of an order of magnitude) whereas for the other three models the amplitudes were almost the same as for the half-space. This figure not only helps to explain the three anomalously large amplitudes of P for the Novaya Zemlya event as recorded at the island stations at distances of 65° to 70°, but also serves to explain why the scatter of A/T values of long-period P waves is relatively small.

Evne, et al (1970) note that m_b values of earthquakes as determined by the U.S.C.G.S. are consistently smaller than those determined by the seismological stations of the U.S.S.R. The differences are sometimes as large as 0.7 magnitude unit. They believe the discrepancies are caused by differences in the frequency response of the seismograph systems, the U.S.C.G.S. values being based upon data from peaked short-period systems.

All the reasons mentioned above argue for m_b determinations based upon A/T values of the first half-cycle of the long-period P wave motion. At present this is only practical for earthquakes or explosions with $m_b \geq 6.0$, because the P waves of smaller magnitude events as recorded by WWSSN seismographs (most with a peak magnification of 1500 or 3000) are too small to be seen on the seismograms. However, the new high-gain, long-period seismographs (Pomeroy et al, 1969) which can be operated at peak magnifications of several hundred thousand should allow P waves to be detected at teleseismic distances for $m_b \geq 4.0$.

It is recommended that, whenever possible, body wave magnitude values be determined from long-period as well as short-period P wave data. The long-period magnitude might be called m_B, to distinguish it from the short-period magnitude. A set of statistics should be accumulated, relating m_B to M_S and also comparing the standard deviation of m_B to that of m_b. It is expected that the m_B-M_S relation will not show such a strong regional dependence as has been found for the m_b-M_S relation. Furthermore, it is expected that the standard deviation of m_B will be less than that of m_b.

In magnitude determinations the effect of attenuation on the P wave amplitude appears in the Q term, where

$$m_b = Q(\Delta, h) + \log A/T$$

and Δ is epicentral distance, h focal depth, A the amplitude of the ground motion and T its period. All seismologists, except those in eastern Europe and the Soviet Union, presently use the Q values given by Gutenberg and Richter (1956) for teleseismic distances. For smaller distances Evernden (1967) has shown that lateral variations in crust and upper mantle structure are large enough so that different Q functions are required for different geographic regions at distances less than about 2500 km. Soviet seismologists use the Q function of Vanek et al (1962) for their m_b determinations. Recently Duda (1970) has presented a new set of $Q(\Delta, h)$ values for P waves, based on the assumption that the P wave attenuation is caused only by geometrical spreading (effects of anelasticity are negligible) and utilizing the 1968 P Travel-Time Tables of Herrin et al (1968).

Fig. 1.7 compares A/T values of the vertical component of P for an event with m_b = 6.4, using the Gutenberg-Richter, Vanek et al and Duda Q functions, as well as a fourth derived from the Jeffreys-Bullen travel-time tables. All the curves were made to coincide at 60°. The greatest differences between the curves occur from about 25° to 45°, where they can be as large as the equivalent of 0.5 magnitude unit. Between 45° and 95° the differences are smaller, never exceeding 0.3 magnitude unit and more commonly about 0.1 unit.

If sufficient data are available over a large range of epicentral distances, all four calibration functions will give approximately the same magnitude for a given event. However, if only a few amplitude data are available and particularly if they are at distances less than 45°, then the choice of the calibration function will have a greater effect on the computed body-wave magnitude. The question thus arises: Which of the various magnitude calibration functions is closest to the one that applies to the real Earth?

Gutenberg and Richter's Q function is based on theoretical calculations using their travel-time tables, the calculated values then being modified to conform better to actual amplitude data. There is a very large amount of scatter present in the amplitude data they used (see, for example, Gutenberg, 1958, fig. 1), so much so that the existence of the majority of maxima and minima in the curve seems questionable. The amplitude data also scatter widely about the Q curve of Vanek et al (Bune et al, 1970, fig. 7). These

authors, however, elected to construct a more smooth, monotonically decreasing amplitude-distance curve; an exception to this statement is a shallow minimum in the curve between 63° and 70°. The amplitude-distance curves calculated from the smoothed Jeffreys-Bullen and the Herrin et al tables (Duda, 1970) also are generally monotonically decreasing functions of distance; exceptions occur where there is a greater than average curvature of the travel-time curve (large amplitude) or a lesser than average curvature (small amplitude).

Nuclear explosions, with their almost symmetrical P wave radiation pattern, have been recognized to be a valuable source of data for improving the Q function or the amplitude-distance curve. Carpenter et al (1967) and Kaila (1970) constructed such curves using A/T values of short-period PZ waves from large underground explosions. In general the scatter in their data is large, which can best be seen by comparing the two radically different amplitude-distance curves which they derived as best fitting the data.

To avoid the problem of scatter which appears to be inherent when using short-period amplitude data, we have measured A/T values of PZ recorded by long-period WWSSN seismographs for underground explosions at Novaya Zemlya (Oct. 27, 1966), Nevada (GREELEY, Dec. 20, 1966 and BOXCAR, Apr. 26, 1968) and Amchitka (MILROW, Oct 2, 1969). Fig. 1.3 presents the data. In it the MILROW values have been scaled down by 0.5 magnitude unit to make them comparable to the

values for the other three explosions, all of which are taken to have a body-wave magnitude of 6.4. The bigger A/T values of MILROW are caused not only by larger amplitudes, but also by shorter periods. Crosses, circles and triangles serve to distinguish data from Novaya Zemlya, Nevada and Amchitka, respectively. Small symbols indicate less reliable values, resulting either from the presence of microseismic noise or the fact that the trace amplitude of PZ was less than 0.8 mm. Five data points with anomalously large A/T values have been omitted from the figure. Two curves are included, the one the Gutenberg-Richter for $m_b = 6.4$, the other a curve drawn more or less intuitively as a "by eye" fit to the data. Differences between the two curves are greatest from 40° to 70°, where they are as large as 0.4 magnitude unit.

Both amplitude curves of Fig. 1.3 are empirical ones which have been constructed in a rather arbitrary manner. To this point in the discussion they have not yet been subjected to the constraints imposed upon them by the travel-time curve.

For an event with zero focal depth, the amplitude A beneath the station is

$$A = C \sqrt{\left|di/d\Delta\right| \tan i / \sin \Delta}$$

where C is a constant, i is the angle of incidence at the focus and Δ the epicentral distance. The earth model is assumed to be spherically symmetric and the effects, if any,

of anelasticity are ignored. The amplitude $\bar{A}_Z$ of the vertical component of the surface P motion is related to A by

$$\bar{A}_Z = A \cos \bar{i}$$

where $\bar{i}$ is the apparent angle of incidence at the station. Nuttli (1964) experimentally determined the relation of $\bar{i}$ to Δ for P waves of various periods.

The slope of the travel-time curve, $dT/d\Delta$, for a surface focus is

$$dT/d\Delta = r \sin i/v$$

where r is the radius of the earth model, v the velocity and i the angle of incidence at the surface.

The three equations above provide implicit relations between the dependent variables $\bar{A}_Z$, i, $dT/d\Delta$ and the independent variable Δ . Because the $dT/d\Delta$ vs Δ relation for P waves is known with a high degree of accuracy, the i vs Δ and $\bar{A}_Z$ vs Δ relations are severely constrained. For example, it was found by calculations based on the above equations that the amplitudes of both empirical curves of Fig. 1.3 are too large between about 35° and 45°. As drawn they would imply errors of up to five or more seconds in the travel-time curve at those distances, which is obviously not acceptable.

Detailed calculations show that much of the "topography," that is, the existence of pronounced maxima and minima in the amplitude-distance curves of Fig. 1,3, is not compatible with the Jeffreys-Bullen or the Herrin et al P tables. From this it follows that the Gutenberg-Richter magnitude calibration

function for zero focal depth is inconsistent with observed travel times.

A trial and error method was used to calculate an amplitude-distance curve which satisfied the travel-time tables (maximum permissible difference of one second) and, as well as possible, the amplitude data of Fig. 1.3. From this curve a Q magnitude calibration function was calculated and tabulated. Its values are given in Table 2.

Fig. 1.4 compares the new Q function with those of Gutenberg and Richter and of Duda. In general it agrees well with Duda's, their separation being everywhere less than or equal to 0.1 magnitude unit except from 27° to 28°, where it is about 0.2 unit. Differences between the new Q function and that of Gutenberg and Richter are larger, being as big as 0.2 magnitude unit from 37° to 44°, 47° to 48° and 62° to 69°. The general shape of the new Q curve, or the related A/T curve, conforms with Duda's assumption that the effects of anelasticity are small compared to those of geometrical spreading.

Table 3 gives magnitudes of four underground explosions, using the amplitudes of PZ recorded by long-period WWSSN seismographs. Magnitudes were calculated using the new Q function and that of Gutenberg and Richter. For three of the four events the body-wave magnitude calculated using the new Q function has a slightly smaller standard deviation. For the fourth event, BOXCAR, the standard deviations are the same.

Table 4 compares magnitudes of two Aleutian earthquakes, using amplitude data of Syed (personal communication) which have been corrected for focal mechanism. Average magnitudes and their standard deviations are given, for magnitudes calculated using the new Q function as well as those of Duda and of Gutenberg and Richter. From the table it can be seen that the average magnitudes and standard deviations obtained using the Duda and new Q functions are the same, and they differ only slightly from those based on the Gutenberg-Richter Q function.

Summary

The purposes of this paper are to examine the factors which cause problems in body-wave magnitude determination, to assess their relative importance and, if possible, to suggest means of reducing the errors in such evaluations.

Three principal factors which can cause such problems are the azimuth-dependent radiation pattern of the earthquake source, the effects of crust and upper mantle structure at the station and an inexact knowledge of the magnitude calibration function.

The new magnitude calibration function which has been developed in this study differs so little from that of Duda (1970) that the two may be considered to be the same. They are believed to be an improvement over the Gutenberg-Richter (1956) function because they are more consistent with observed travel times. The latter function will underestimate m_b by about 0.2 magnitude unit between 37° and 44° and overestimate it by about the same amount between 62° and 69°. Otherwise

the three calibration functions will give almost the same value of m_b.

Ignoring the effects of the focal mechanism of earthquakes can lead to discrepancies as much as 0.5 magnitude unit at particular stations, depending upon the radiation pattern. However, Syed has developed a straightforward method for taking account of this phenomenon which is readily adaptable to routine calculations, so that this problem can be said to be nearly solved.

The biggest source of error in m_b determination is the effect of the crust and upper mantle structure at the station. For short-period P waves it can cause errors of as large as one magnitude unit at particular stations. Unfortunately the station correction is a complicated function of epicentral distance, the frequency content of the incident wave, the geological structure at the station and the azimuth of wave approach if there is lateral heterogeneity in geological structure near the station. Probably the only way of arriving at station corrections for short-period data is on a statistical basis, which is a formidable task. However, the use of long-period P data would avoid many of these difficulties. For such data the largest error to be expected at a particular station because of crustal structure is only about 0.3 magnitude unit. Furthermore, because the effect of the crust and upper mantle structure on the amplitude of long-period P waves requires but a coarse knowledge of the structure, simple calculations can be made to estimate this effect at individual stations.

By using the first half-amplitude of long-period P, after correcting it for crustal structure and focal mechanism, better estimates of body-wave magnitude can be expected. It seems likely that the standard deviation of m_B can be made as small as 0.2 and possibly 0.1 magnitude unit.

References

Ben-Menahem, A., S. W. Smith and T. L. Teng (1965). "A procedure for source studies from spectrums of long-period seismic body waves," Bull. Seism. Soc. Am.,vol. 55, 203-235.

Broome, P. W., F. A. Klappenberger and D. E. Frankowski (1967). Amplitude anomalies at LASA, Report no. LL-7, Lincoln Laboratories.

Bune, V. I. et al (1970). "Correlation of M_{LH} and m_{pv} by data of the network of seismic stations of the U.S.S.R.," Geophys. Journ., Roy. Astro. Soc., vol. 19, 533-542.

Carpenter, E. W., P. D. Marshall and A. Douglas (1967). "The amplitude-distance curve for short period teleseismic P-waves," Geophys. Journ., Roy. Astro. Soc., vol. 13, 61-70.

Duda, S. J. (1970). Travel times and body wave magnitude, Scientific Report no. 8, Saint Louis University, AFCRL-70-011.

Evernden, J. F. (1967). "Magnitude determination at regional and near-regional distances in the United States," Bull. Seism. Soc. Am., vol. 57, 591-639.

Gutenberg, B. (1958). "Velocity of seismic waves in the Earth's mantle," Trans. Am. Gph. Union, vol. 39, 486-489.

Gutenberg, B. and C. F. Richter (1956). "Magnitude and energy of earthquakes," Ann. Geofisica, vol. 9, 1-15.

Hasegawa, H. S. (1970). "Short-period P-coda characteristics in the eastern Canadian shield," Bull. Seism. Soc. Am., vol. 60, 839-858.

Herrin, E. et al (1968). "1968 seismological tables for P phases," Bull. Seism. Soc. Am., vol. 58, 1196-1219.

Kaila, K. L. (1970). "Decay rate of P-wave amplitudes from nuclear explosions and the magnitude relations in the epicentral distance range 1^{o} to 98^{o}," Bull. Seism. Soc. Am., vol. 60, 447-460.

Lambert, D. G., D. H. Von Seggern, S. S. Alexander, G. A. Galat (1970). The LONGSHOT experiment, vol. 1: Basic Observations and Measurements, Seismic Data Laboratory, Report no. 234.

Nuttli, O. W. (1964). "Some observations relating to the effect of the crust on long-period P-wave motion," Bull. Seism. Soc. Am., vol. 54, 141-149.

Pomeroy, P. W., G. Hade, J. Savino and R. Chander (1969). "Preliminary results from high-gain wide-band long-period electromagnetic seismograph systems," Journ. Geophys. Res., vol. 74, 3295-3298.

Syed, A. A. (1969). "Station corrections for vertical component P wave amplitudes at LASA," Earthquake Notes, vol. 40, 51-53.

Utsu, T. (1966). "Variations in spectra of P waves recorded at Canadian Arctic seismograph stations," Canadian Journ. of Earth Sciences, vol. 3, 597-621.

Vanek, J. et al (1962). "Standardization of magnitude scales," Izv. Akad. Nauk SSSR, Geophys. Ser., English Translation, 108-111.

Table 1. KAZAKH EXPLOSIONS

STA.	Δ	m_b Jan.15, 1965	m_b March 20, 1966	$\lvert m_b \rvert$
	^{o}			
AAM	86.9	6.13	5.86	0.27
ALQ	95.7	5.67	5.64	0.03
ATL	95.7	5.96	5.88	0.08
BEC	92.0	-	5.77	-
BKS	90.9	5.85	6.06	0.21
BLA	91.3	5.71	5.77	0.06
BOZ	84.6	5.99	6.17	0.18
CMC	62.3	6.04	6.19	0.15
COL	60.1	6.52	6.38	0.14
COR	84.3	6.51	-	-
DAL	97.6	6.33	-	-
DUG	90.3	-	5.92	-
FLO	91.5	5.72	5.57	0.15
GDH	56.0	-	5.98	-
GEO	89.0	6.02	5.76	0.26
GOL	91.0	5.87	5.89	0.02
GSC	94.7	6.02	5.88	0.14
JCT	100.1	-	5.59	-
LON	82.4	-	6.07	-
LUB	97.1	-	6.16	-
MDS	86.6	6.20	6.22	0.02
MNN	85.4	5.98	-	-
OGD	86.4	5.71	-	-
OXF	95.6	6.20	6.23	0.03
RCD	86.7	5.98	6.09	0.11
SCP	87.3	-	5.81	-
TUC	98.0	5.59	5.48	0.11
Average		6.00 ± 0.26	5.93 ± 0.24	0.12

Table 2. Q Values for PZ (Zero Focal Depth)

Δ	Q	Δ	Q	Δ	Q
20	6.21	48	6.67	76	6.86
21	6.23	49	6.69	77	6.86
22	6.26	50	6.71	78	6.86
23	6.28	51	6.75	79	6.86
24	6.32	52	6.78	80	6.87
25	6.37	53	6.80	81	6.87
26	6.44	54	6.82	82	6.88
27	6.63	55	6.79	83	6.89
28	6.76	56	6.76	84	6.90
29	6.78	57	6.74	85	6.91
30	6.77	58	6.72	86	6.92
31	6.72	59	6.73	87	6.92
32	6.71	60	6.75	88	6.93
33	6.71	61	6.76	89	6.94
34	6.71	62	6.78	90	6.97
35	6.71	63	6.79	91	7.01
36	6.71	64	6.81	92	7.06
37	6.63	65	6.83	93	7.11
38	6.65	66	6.85	94	7.15
39	6.65	67	6.85	95	7.20
40	6.65	68	6.83	96	7.24
41	6.65	69	6.81	97	7.29
42	6.65	70	6.80	98	7.34
43	6.65	71	6.81	99	7.38
44	6.65	72	6.83	100	7.43
45	6.65	73	6.85		
46	6.65	74	6.86		
47	6.65	75	6.86		

Table 3. m_B from Long-Period PZ (Explosions)

Location	Date	m_B New Q	m_B Gut-Rich.Q	No. of Sta.
Novaya Zemlya	Oct. 27,1966	6.44±0.19	6.49±0.23	46
Nevada (GREELEY)	Dec. 20,1966	6.35±0.19	6.38±0.23	29
Nevada (BOXCAR)	Apr. 28,1968	6.32±0.26	6.35±0.26	28
Amchitka(MILROW)	Oct. 2,1969	6.87±0.20	6.94±0.27	14

Table 4. m_B from Long-Period PZ (Aleutian Earthquakes)

Date	Lat.	Long.	Origin Time	m_B New Q	m_B Duda Q	m_B Gut-Rich.Q	No. of Sta.
July 29, 1965	50.9N	171.4W	08-29-21	6.23 ± 0.30	6.23 ± 0.30	6.26 ± 0.31	52
Oct. 1, 1965	50.1N	178.2E	08-52-04	6.34 ± 0.14	6.34 ± 0.14	6.39 ± 0.15	36

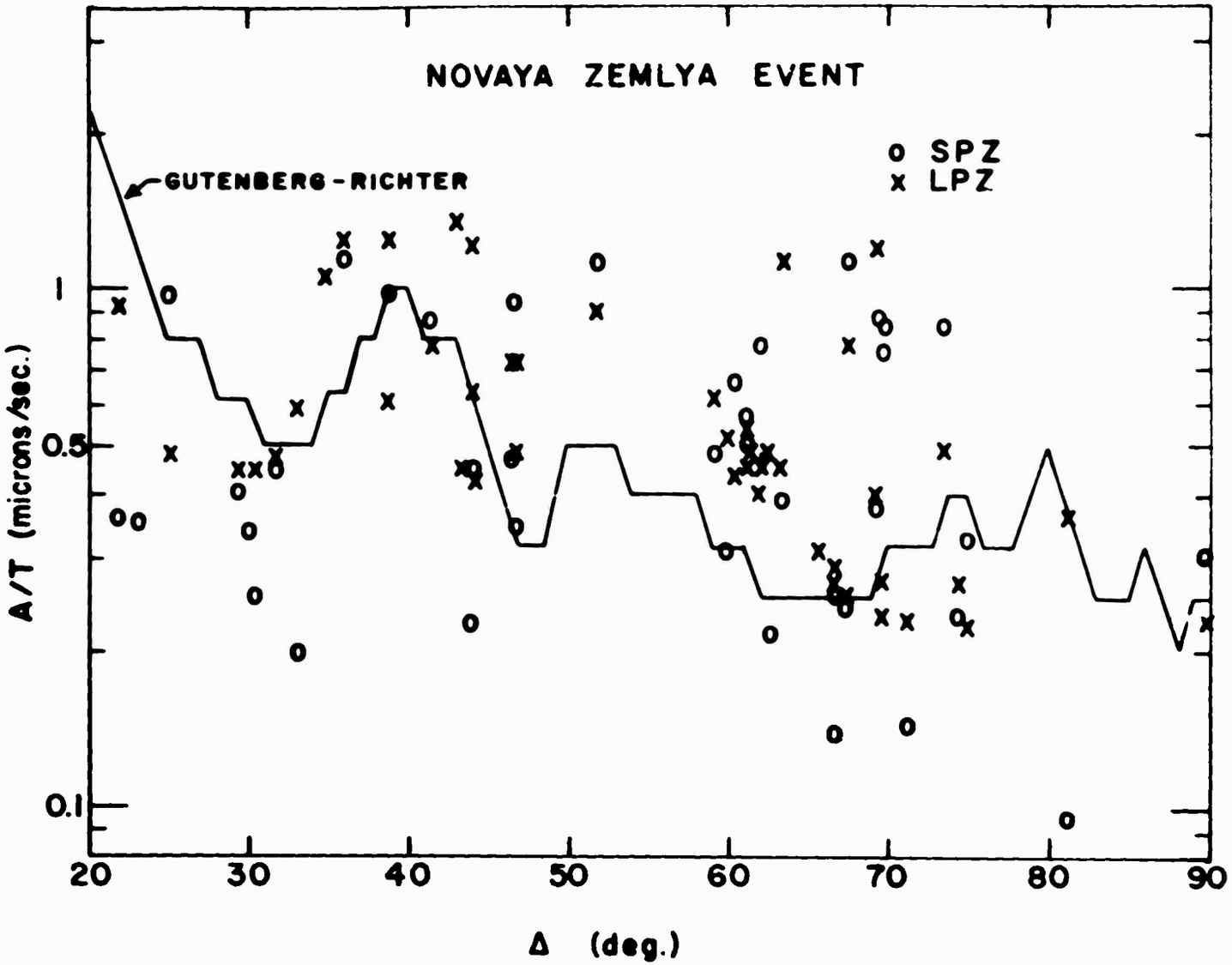
NOVAYA ZEMLYA EVENT
o SPZ
x LPZ
GUTENBERG-RICHTER
A/T (microns/sec.)
1
0.5
0.1
20
30
40
50
60
70
80
90
Δ (deg.)

Fig. 1.1

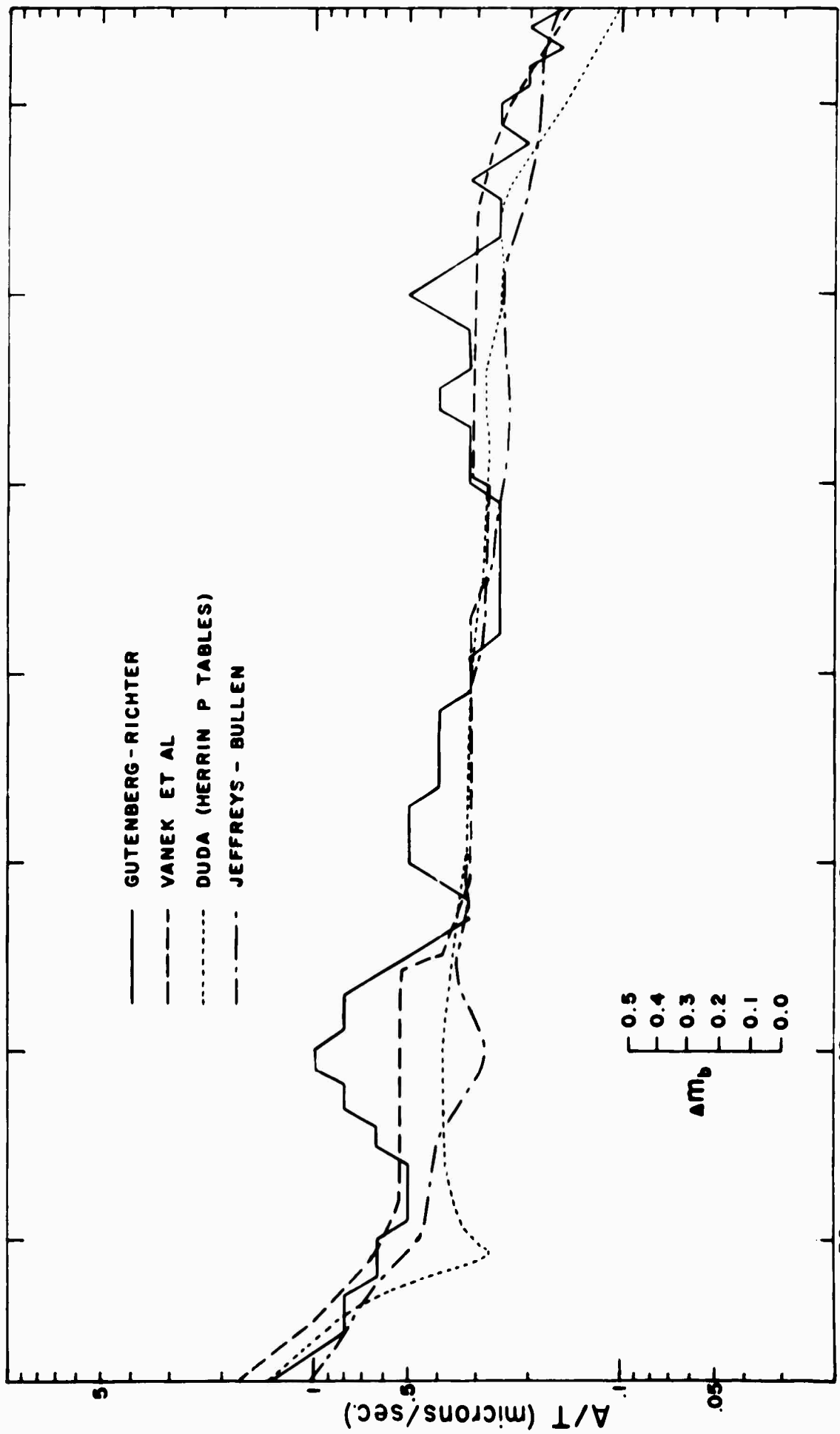
GUTENBERG-RICHTER
VANEK ET AL
DUDA (HERRIN P TABLES)
JEFFREYS - BULLEN
0.5
0.4
0.3
0.2
0.1
0.0
m_b
A/T (microns/sec.)
5
1
.5
.1
.05
30
40
50
60
70
80
90
Δ (deg.)

Fig. 1.2

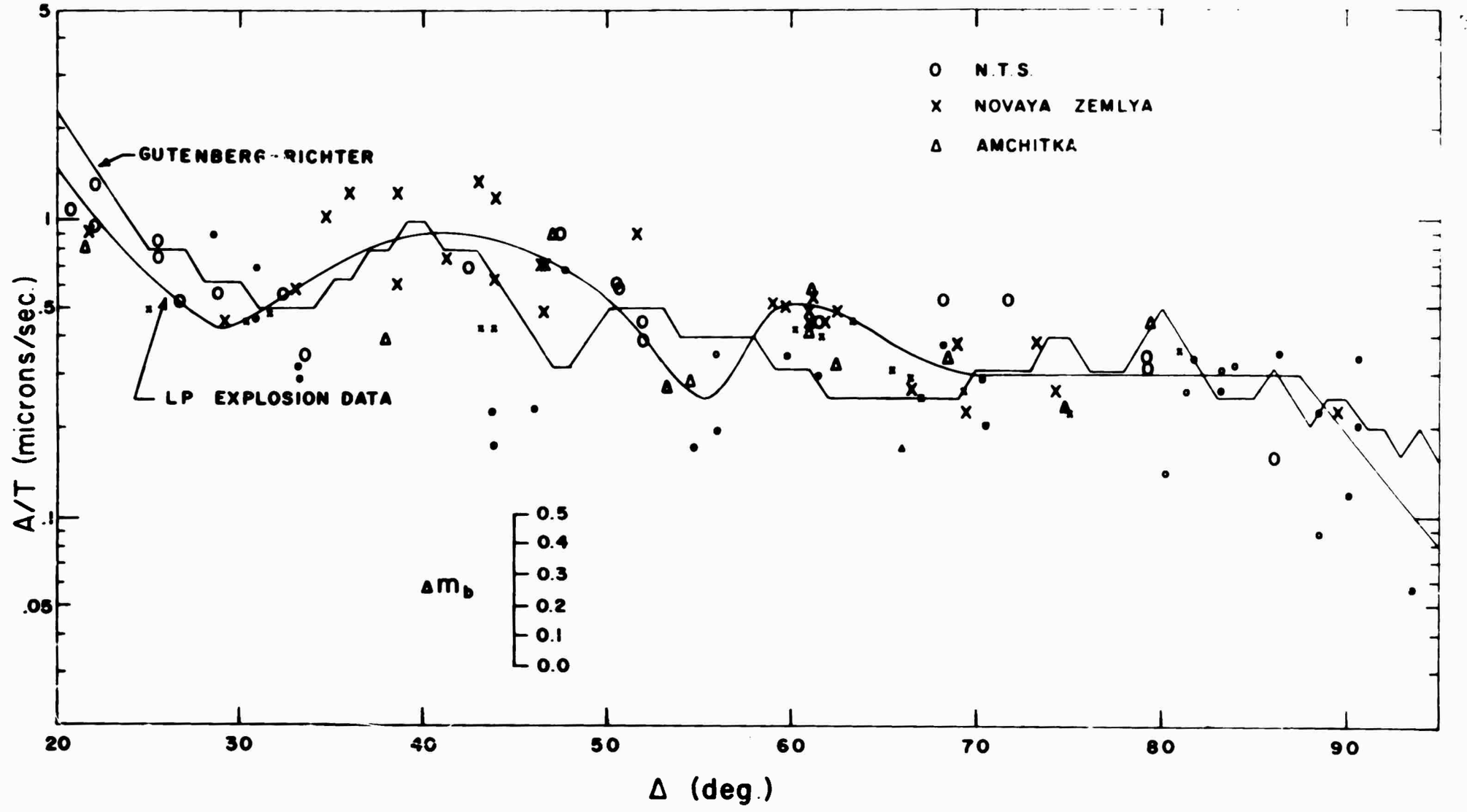
O N.T.S.
X NOVAYA ZEMLYA
Δ AMCHITKA
GUTENBERG-RICHTER
LP EXPLOSION DATA
Δm_b
0.5
0.4
0.3
0.2
0.1
0.0
A/T (microns/sec.)
5
1
.5
.1
.05
20
30
40
50
60
70
80
90
Δ (deg.)

Fig. 1.3

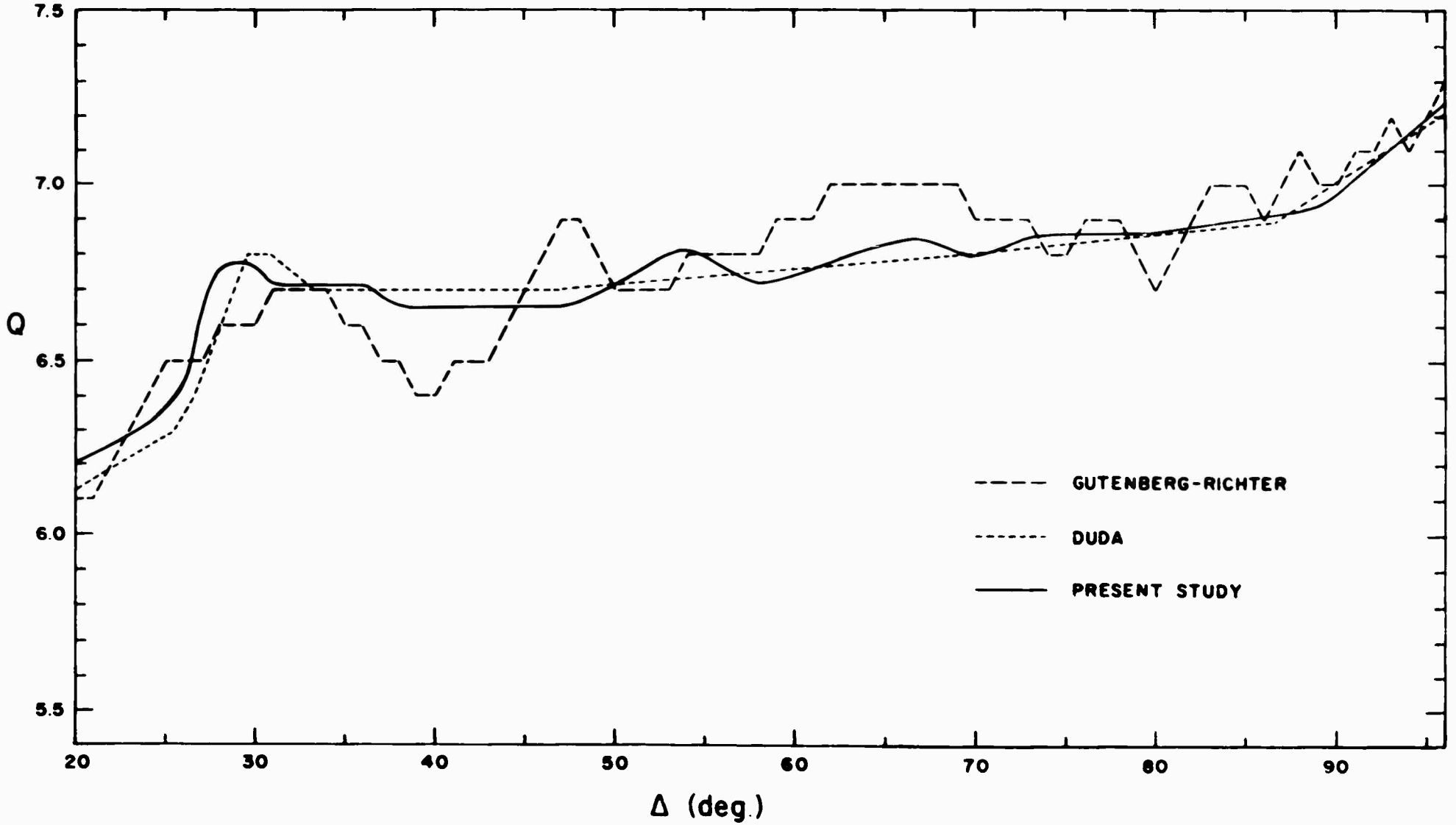
7.5
7.0
6.5
6.0
5.5
Q
20
30
40
50
60
70
80
90
Δ (deg.)
GUTENBERG-RICHTER
DUDA
PRESENT STUDY

Fig. 1.4

2. Effect of Regional Correction on the Value of m_b.

Atiq Syed

Discrepancies in magnitude determination are known to result in part from the effect of the earthquake radiation pattern on the recorded wave amplitudes. The purpose of the study reported here is to obtain a quantitative estimate of the effect of the radiation pattern on P wave amplitudes and to develop a methodology for improving body wave magnitude determinations. The results of the study may also be used as an auxiliary discriminant between earthquakes and explosions.

Correction for Mechanism

The P wave displacement at the surface of a focal sphere of radius R for a double couple point source is given by the expression

$$u_p = \frac{2xy}{4\pi\rho a^3 R^3} k'\left(t - \frac{R}{\alpha}\right) \qquad (1)$$

If for a given earthquake the observed P wave amplitudes are divided by the product 2xy the P amplitudes will be corrected relative to the maximum value of the P wave radiation. For magnitude calculations in keeping with the assumptions made in the definition of magnitude, a further normalization is required, a reduction of the P wave amplitude to the <u>average</u> value of the displacement of P over the surface

of the focal sphere. This average amplitude is obtained from the relation

$$\bar{u}_p = \frac{\int 2xy\, dS}{\int dS} = 0.424$$

or

$$\bar{u}_p = 0.424 (u_p)_{max.}$$

Thus, the total reduction of P wave amplitudes to take into account includes first the application of the 2xy factor and second multiplication by 0.424 to equate the P wave radiation from a double couple to that from a spherically symmetric source of the same strength.

It has long been observed that earthquake foci located in a given region tend to have similar orientations of the focal mechanism. This observation is in keeping with the theory of plate tectonics. Plate tectonics, in turn, provides a basis for prediction of the dominant focal mechanism. On the hypothesis that characteristic foci do exist for given hypocentral regions, P wave amplitudes can be corrected for the source mechanism and thereby magnitude estimates can be obtained which have smaller standard errors.

A procedure for applying the source mechanism correction is as follows:

1. Given the source parameters for a typical earthquake in a particular hypocentral region, compute the 2xy factor for all seismograph stations.

2. On the basis of this factor, predict which stations will record relatively large P wave amplitudes for earthquakes for the region in question, and which relatively small.

3. Select [illegible] amplitudes are best suited [illegible] earthquakes from that region. [illegible] selection of stations might be

a) Stations [illegible] the epicentral distance [illegible]

b) The [illegible] be greater than the [illegible] factor, 0.424.

The latter criterion insures that the P wave amplitude be relatively large, but also that small differences between the actual source mechanism and the average or characteristic mechanism of the region will have minimal effect on the reduced amplitudes.

4. However, if [illegible] larger than the normalizing [illegible] m_b, the magnitude determinations will be too large. It is possible to correct for the effect by subtracting from the initial m_b value the quantity $\log (2\bar{x}\bar{y}/.424)$, where $2\bar{x}\bar{y}$ is the average value of $2xy$ [illegible] all stations with $2xy$ greater than 0.424. There is a constant correction to be applied to all earthquakes in any particular geographic group. It is called the regional correction factor. In practice values of this correction in the regions studied thus far are found to vary from 0.1 to 0.25 of a magnitude unit.

5. If desirable, instead of the required correction an individual mechanism correction may be applied by subtracting the quantity $\log (2xy/.424)$ determined at each station. This

correction is applicable even to stations at which 2xy $< .424$, provided the 2xy factors be not too small. That is, stations very near nodal lines should always be excluded.

Application

In order to test this suggestion and to exemplify the order of magnitude of the corrections involved, earthquakes from two regions have been studied: earthquakes of the Aleutian Islands, and ones of the North Atlantic. Earthquakes of the Aleutian Islands (Figure 21) divide into three groups on the basis of their source mechanism as determined by Stauder (1968a,b). Similarly those of the Atlantic divide into two groups (Sykes, 1967). For each group we can calculate the average or dominant source mechanism, and then apply the various corrections indicated above.

1. Earthquake of March 30, 1965.

This earthquake belongs to group 3b of the Aleutian Island earthquakes. This group consists of earthquakes which occur along a narrow line immediately below the axis of the Aleutian trench or under the seaward slope of the trench. Foci of this group are uniformly extensional in character, with the axis of tension aligned normal to the local axis of the trench. The average focal mechanism for earthquakes in this group is characterized by two nodal planes dipping about 40°-50°.

For m_b determinations the amplitudes and periods of the first half-cycle of the vertical component long period

P waves were the basic data. The 2xy [illegible] are determined and listed in Table 1 along with the m_b [illegible] determined the ordinary way (m_b uncorrected [illegible] that for small 2xy factors the m_b values are smaller than for the larger 2xy factors. The average uncorrected magnitude using the data of all 37 stations is 7.22 ± [illegible]. The average m_b value for all stations with 2xy > [illegible] is 7.3[illegible] ± 0.15. The average value for stations with 2xy ≤ 0.424 is 7.03 ± 0.17. Applying the regional focal mechanism correction for all stations with 2xy > 0.424, m_b = 7.12 ± 0.15. Finally, correcting for individual station focal mechanism corrections we obtain for all stations m_b = 7.13 ± 0.1[illegible]. These results are summarized in Table 2.

It is noteworthy that using stations with 2xy > 0.24 and applying the constant regional correction, the m_b value is very close to that from all the stations using the individual mechanism corrections. This would seem to justify using for magnitude determinations only those stations for which 2xy is > 0.424. One may, in fact, in this way define zones on the earth's surface, identifying stations (solid circles in Figure 2.2) favorable for m_b determinations, and others (crosses in the figure) to be avoided in magnitude determinations.

2. Earthquake of November 22, 1965.

This earthquake belongs to group 1 of the Aleutian Island earthquakes. This group consists of foci on the concave side of the island arc, in the zone immediately

south of and under the island chain. Focal mechanism stations in this group have one steeply dipping nodal plane, with the other nodal plane nearly horizontal. Many stations in this case are close to the nodal plane. Consequently the number of stations suitable for P wave magnitude determination was much smaller than in group 3b. The average uncorrected magnitude using the data of all 19 stations is 6.20 ± 0.24. The average m_b for all stations with xy larger than 0.424 corrected for the regional effect is 5.99 ± 0.22. The average m_b of all stations whose amplitudes have been corrected for the source mechanism is 6.00 ± 0.26.

3. Earthquake of August 3, 1963.

This earthquake belongs to group 1 of the North Atlantic earthquakes. The events in this group are located on the equatorial fracture zone of the mid-Atlantic ridge. The mechanism of these earthquakes correspond to two near vertical nodal planes. Consequently, the 2xy factors calculated for a typical earthquake in this group at all the stations at a distance of 25-100 degrees are smaller than 0.424, which is the normalizing factor. Consequently it is not possible to satisfy the second criterion in selecting the stations suitable for P wave magnitude determination. Departing from this criterion, we have selected those stations whose 2xy factors calculated for the average focal mechanism solution are larger than 0.2 and established the appropriate regional corrections. Since the uncorrected P wave magnitudes using the data from these stations will be too low,

the regional correction has to be added to the average magnitude value. The results of the m_b calculation for this earthquake show that the average uncorrected magnitude using the data of all 31 stations is 6.51 ± 0.29. The average m_b for 15 stations whose 2xy factors are larger than 0.2 corrected for the regional effect is 6.67 ± 0.20, the average m_b for the same stations whose amplitudes have been corrected for the source mechanism is 6.73 ± 0.18.

Conclusions

From this study it can be concluded that a significant part of the scatter in the determination of earthquake magnitudes is due to the effect of the earthquake radiation pattern on the recorded P wave amplitudes. The correction for the focal mechanism becomes more important when the focal mechanism solution is one in which one or both nodal planes are steeply dipping. In these cases the average magnitude determined by using the uncorrected P wave amplitude data may be in error by as much as a quarter of a magnitude unit.

Since the observational data here examined have shown that the average m_b for stations with smaller 2xy factors is significantly smaller than the average m_b for stations with larger 2xy factors, there exists a possibility of comparing the values of uncorrected m_b from these two sets of stations in a region where the average focal mechanism solution is known to differentiate between the earthquakes

and explosions. The radiation pattern due to the explosive source being azimuthally uniform, the two sets of m_b values should be identical for explosion and different for the earthquake.

References

Stauder, W. (1968a). Mechanism of the Rat Island earthquake sequence of February 4, 1965, with relation to island arcs and sea floor spreading, JGR, 73, 3847-3858

Stauder, W. (1968b). Tensional character of earthquake foci beneath the Aleutian trench with relation to sea-floor spreading, JGR, 73, 7693-7701.

Sykes, L. R. (1967). Mechanism of earthquakes and nature of faulting on the mid-oceanic ridges, JGR, 72, 2131-2153.

Table 1. Earthquake of March 30, 1965.

Sta.	Dist.	2xy	m_b(uncorr)	m_b(corr)
LON	39.0	0.250	6.88	7.11
CMC	36.2	0.256	6.89	7.11
KIP	34.7	0.278	7.03	7.21
DUG	48.1	0.322	7.02	7.14
GUA	45.6	0.322	6.79	6.91
RCD	51.5	0.338	7.08	7.18
GSC	49.8	0.346	7.06	7.15
GOL	52.9	0.352	7.14	7.22
RAB	58.9	0.356	7.09	7.16
HNR	61.8	0.360	7.30	7.37
TUC	54.4	0.382	6.93	6.97
LUB	59.0	0.422	6.88	6.88
MDS	59.4	0.424	7.37	7.37
FLO	62.2	0.448	7.34	7.32
AAM	63.4	0.466	7.25	7.21
SHA	69.3	0.506	7.57	7.49
WES	69.5	0.532	7.05	6.95
RIV	87.3	0.594	7.50	7.35
TAU	96.9	0.624	7.23	7.06
KTG	58.4	0.636	7.57	7.39
ADE	91.9	0.638	7.42	7.25
BHP	91.0	0.642	7.35	7.17
QUI	98.8	0.646	7.17	6.99

Table 1. (cont'd)

Sta.	Dist.	2xy	m_b(uncorr)	m_b(corr)
CAR	97.3	0.664	7.20	7.00
TRN	100.3	0.672	7.13	6.93
VAL	77.6	0.674	7.33	7.07
MUN	98.6	0.714	7.40	7.18
HKC	56.5	0.744	7.25	7.01
KEV	58.1	0.780	7.43	7.16
KON	69.7	0.804	7.26	6.99
PTO	88.5	0.826	7.26	6.97
COP	73.4	0.834	7.28	6.99
TOL	89.9	0.844	7.52	7.22
MAL	93.0	0.850	7.17	6.87
STU	80.5	0.856	7.26	6.96
KOD	88.7	0.952	7.61	7.26
JER	91.6	0.966	7.51	7.15

Table 2. Average m_b values, March 30, 1965.

Uncorrected	
All stations (n = 37)	$m_b = 7.34 \pm 0.21$
For $2xy < 0.42$ (n = 13)	$m_b = 7.03 \pm 0.17$
For $2xy > 0.42$ (n = 24)	$m_b = 7.34 \pm 0.15$
Corrected	
Regional corr. (n = 24)	$m_b = 7.12 \pm 0.15$
Individual mech. corr. (n = 37)	$m_b = 7.13 \pm 0.16$

Table 3. August 3, 1963 Earthquake

Sta.	Dist.	2xy	m_b(uncorr)	m_b(corr)
NAI	36.5	0.030	6.42	7.56
BOG	38.2	0.036	5.50	6.57
KON	62.1	0.060	6.76	7.60
NUR	69.1	0.062	6.73	7.56
BUL	69.1	0.068	6.41	7.20
VAL	48.8	0.072	6.73	7.50
AAE	73.7	0.074	6.75	7.51
PRE	70.5	0.084	6.52	7.22
CAR	30.9	0.104	6.05	6.66
QUI	43.3	0.111	6.41	6.99
WIN	59.9	0.124	6.80	7.33
TRN	25.4	0.128	6.38	6.90
IST	66.0	0.154	6.75	7.19
ATU	61.4	0.180	6.93	7.30
BKS	82.5	0.194	6.17	6.51
GSC	78.4	0.198	6.32	6.66
TUC	73.3	0.212	6.33	6.63
LON	81.7	0.214	6.16	6.46
TOL	42.8	0.226	6.65	6.92
DUG	75.2	0.234	6.34	6.60
ALQ	69.8	0.242	6.53	6.77
MAL	40.6	0.252	6.70	6.92
GOL	69.4	0.260	6.45	6.66

Table 3. (Cont'd)

Sta.	Dist	2xy	m_b(uncorr)	m_b(corr)
LPA	47.3	0.266	6.97	7.17
NNA	45.3	0.268	6.61	6.81
RCD	68.5	0.276	6.39	6.58
SHA	53.9	0.312	6.70	6.83
FLO	57.9	0.322	6.45	6.55
AAM	54.4	0.366	6.61	6.57
GEO	48.4	0.398	6.67	6.69
SCP	49.8	0.398	6.69	6.72

Table 4. November 22, 1965 Earthquake

Sta.	Dist.	2xy	m_b(uncorr)	m_b(corr)
PMG	66.8	0.124	5.94	6.47
CTA	77.0	0.130	5.83	6.34
MAN	59.2	0.608	6.50	6.35
BAG	58.2	0.628	6.23	6.06
HKC	57.7	0.730	6.15	5.92
TOL	89.0	0.788	5.85	5.58
CHG	69.8	0.798	6.00	5.72
KOD	89.6	0.816	6.51	6.22
HOW	73.5	0.858	6.38	6.08
POO	85.2	0.860	6.45	6.15
KON	69.0	0.862	5.98	5.67
SHL	69.1	0.862	6.11	5.80
JER	91.5	0.886	6.14	5.82
IST	84.5	0.890	6.05	5.73
SHI	86.9	0.904	6.49	6.16
NDI	75.3	0.904	6.28	5.95
QUE	79.6	0.914	6.16	5.83
TAB	82.0	0.916	6.17	5.84
LAH	74.7	0.920	6.63	6.30

Earthquake of November 22, 1965

Av. m_b (uncorr) = 6.20 ± 0.24	n = 19
Av. m_b (uncorr) for $2xy > 0.42 = 6.24 \pm 0.22$	n = 17
Av. m_b (corr for regional effect)for $2xy > 0.42 = 5.99 \pm 0.22$	n = 17
Av. m_b (corr for focal mech) = 6.00 ± 0.26	n = 19

Earthquake of August 3, 1963

Av. m_b (uncorr) = 6.51 ± 0.29	n = 31
Av. m_b (uncorr) for $2xy > 0.20 = 6.55 \pm 0.20$	n = 15
Av. m_b (corr for regional effect) for $2xy > 0.20 = 6.67 \pm 0.20$	n = 15
Av. m_b (corr for focal mech) for $2xy > 0.20 = 6.73 \pm 0.18$	n = 15

Titles to Figures

Figure 1. Earthquakes of Aleutian Island region divided into three groups: 1) earthquakes under the islands, western portion of arc, 2) earthquakes under the islands, eastern portion of arc, 3a,b) earthquakes with foci under the trench.

Figure 2. Map indicating stations unfavorable (x) and favorable (●) for determination of m_b for Aleutian Island earthquakes of group 3a.

Figure 3. Map indicating stations unfavorable (x) and favorable (●) for determining m_b for Aleutian Island earthquakes of group 1.

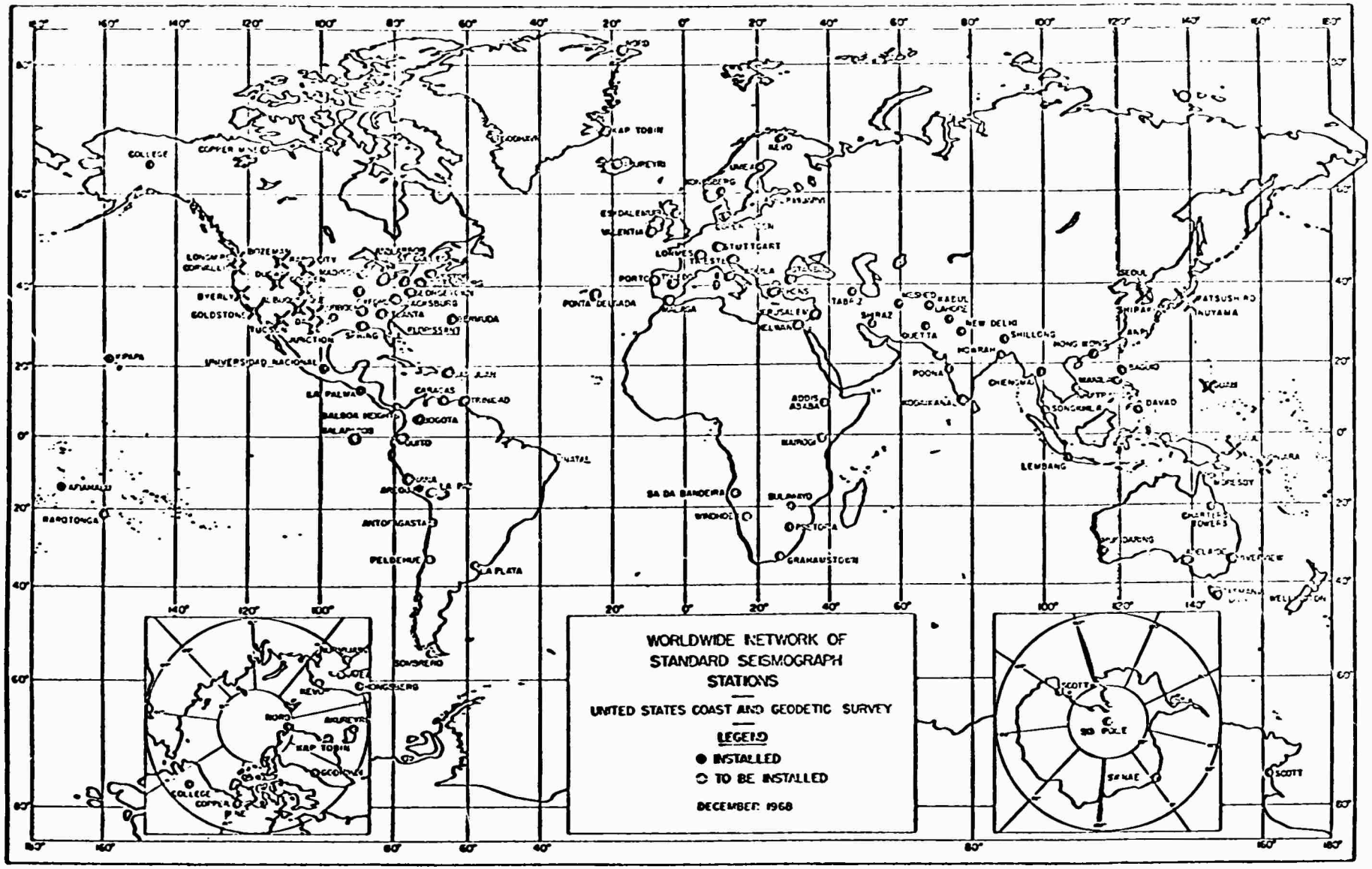
WORLDWIDE NETWORK OF
STANDARD SEISMOGRAPH
STATIONS
UNITED STATES COAST AND GEODETIC SURVEY
LEGEND
INSTALLED
TO BE INSTALLED
DECEMBER 1968
COLLEGE
KAP TOBIN
STUTTGART
NEW DELHI
SHILLONG
HONG KONG
MATSUSHIRO
INUYAMA
DAVAO
LEMBANG
ADDIS ABABA
LA PAZ
LA PLATA
SA DA BANDEIRA
PRETORIA
GRAHAMSTOWN
SCOTT
SOUTH POLE

Fig. 2.1

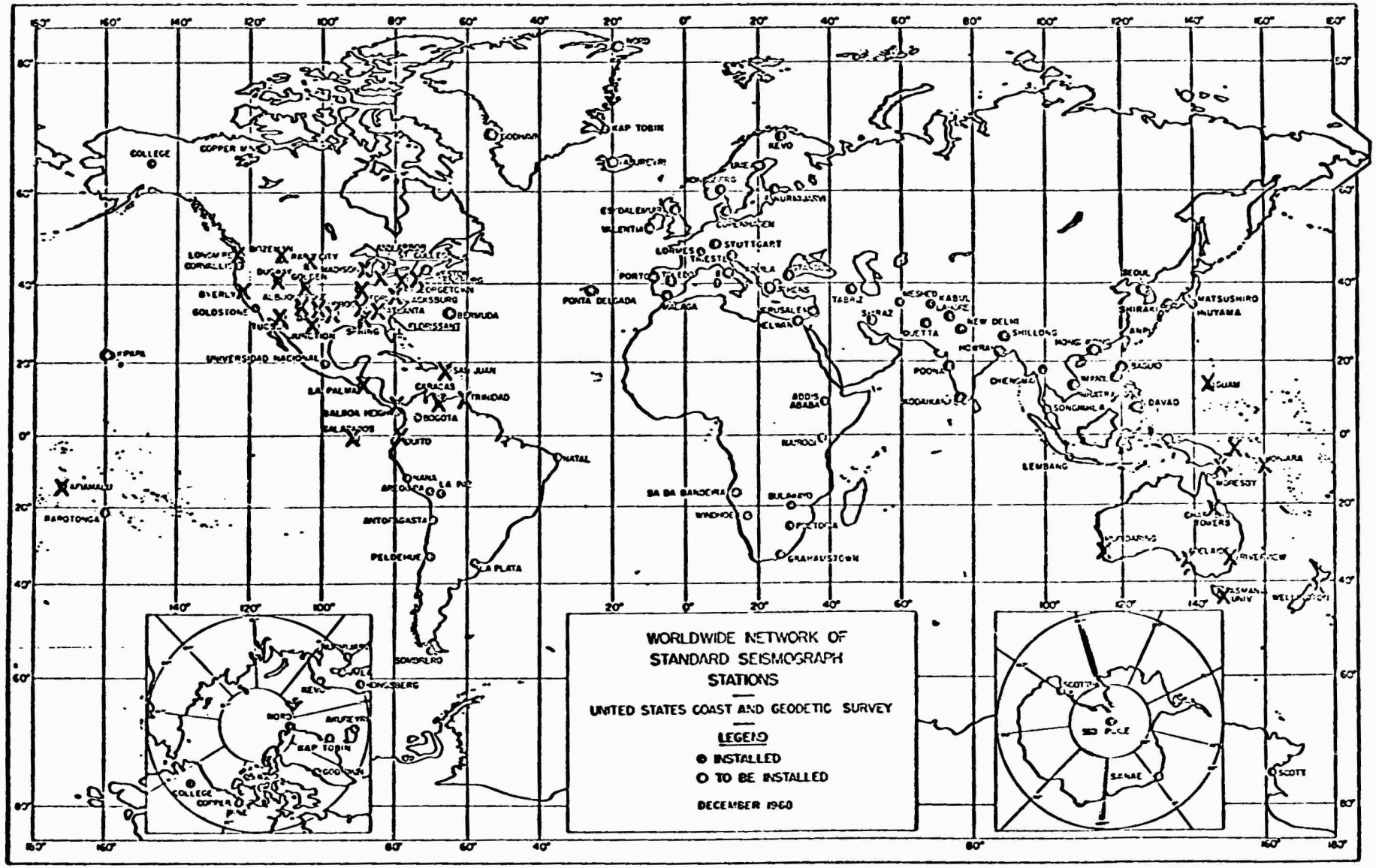

Fig 2.2

3. Nuclear Yields from Rayleigh Waves

Donald E. Wagner

Introduction

Surface waves are a function of the depth of burst, the time history of the event, and the wave guide through which they propagate. For nuclear explosions the depths vary only between 0-1 kilometer while the time history is assumed constant. Therefore, the wave guide is left as the factor controlling the observed Rayleigh wave signature at a given station. Furthermore, unlike body waves, which are affected considerably by the source medium, Rayleigh waves are a function of the average velocity and density in a layer or wave guide. Thus, they are much less susceptible to inhomogeneities or velocity contrasts both at the shot point and along the path. The distinct similarity of nuclear events at a station (see for example Fig. 2, Shurbet, 1969) encouraged the author to attempt a prediction of yield based on Rayleigh wave amplitudes.

In a recent release (Higgins, 1970), several nuclear explosions were declassified, offering a list of known-yield events observable at continental WWSSN stations. The following study applies a revised (Nuttli, 1970) surface wave magnitude formula based on maximum ratios of A/T from Rayleigh waves at all stations to develop a yield versus M_s (average) master curve for seven known energies. In a

further attempt to reduce dissimilarities owing to different wave guides, maximum A/T ratios were plotted as a function of yield at eight specific stations. All in all, nine master curves were plotted from which eleven unknown yields were predicted.

Procedure

The Richter surface wave formula $M_s = 3.1 + \log (A/T_{20}) + 1.66 \log (\Delta)$ was found to agree quite well with $M'_s = 2.4 + \log (A/T_{4-12}) + 1.66 \log (\Delta)$. Moreover, the 1.66 value was verified by measuring the slope of $(A/T)_{max}$ versus Δ (log-log) for eighteen different events. No attempt was made to measure the same period wavelet at different stations. The resulting spread in periods ranged from 5-12 seconds but remained relatively constant at a given station for all events. Next, average surface wave magnitudes were calculated using M'_s from available experimental WWSSN stations (Table 1). A master curve was drawn using known yields versus M'_s (avg) (Figure [illegible]). $(A/T)_{max}$ ratios versus known yield were plotted for eight stations (Figures 3.2 - 3.10). From the resulting nine master curves, eleven unknown yields were predicted and tabulated in Table 2.

Conclusions

A revised surface wave formula appears to be borne out by experimental data when results are based on maximum A/T ratios. Using these ratios, the yields of eleven Nevada Test Site nuclear events were predicted. The results in Table 2 indicate that the events BOXCAR, PILE DRIVER, DURYEA, CHARTREUSE, and SCOTCH are predicted within the error bounds

of one standard deviation. However, HALFBEAK is overestimated while GREELEY is underestimated. Clearly, the majority of known yield events are predictable; nothing can be inferred from the predictions of unknown yields until further declassification is forthcoming. The set of master curves (log-log) are somewhat inconclusive below 100 kiloton where the straight line appears to curve concave downward. A possible interpretation would be an increase of seismic efficiency with decreasing yield. That is, less energy would be utilized in inelastic processes such as rock vaporization, plastic flow, and crushing and cracking rock material in the near source region. The semi-log master curve tends to reinforce this hypothesis by showing increased curvature at high yields or less efficient seismic coupling.

In the future, a knowledge of more yields in the 40-1000 kiloton range would greatly enhance the resolution of the master curves especially near the change of slope which appears between 60-100 kilotons.

References

Higgins, Gary H. (1970). "Summary of nuclear explosion data for underground engineering applications," UCRL-72346, Rev. 1.

Nuttli, Otto W. (1970). Private Communication.

Shurbet, D. H. (1969). "Excitation of Rayleigh Waves," J. Geophys. Res., 74 (22), 5339-5341.

Table 1

EVENT	FAULTLESS	GREELEY	HALFBEAK	COMMODORE
Date	1-19-68	12-20-66	6-30-66	5-20-67
M_S	5.033 ± .141	4.221 ± .083	4.061 ± .130	4.562 ± .207
Number of Stations	26	18	19	15

EVENT	BOXCAR	DUMONT	PILE DRIVER	BUFF
Date	4-26-68	5-19-66	6-2-66	12-16-65
M_S	5.329 ± .167	4.219 ± .156	3.786 ± .130	3.553 ± .104
Number of Stations	16	19	15	9

EVENT	CORDUROY	BRONZE	TAN	PIRAHNA
Date	12-3-65	7-23-65	6-3-66	5-13-66
M_S	4.183 ± .148	3.864 ± .270	3.974 ± .164	3.931 ± .126
Number of Stations	16	20	17	17

EVENT	DURYEA	NOGGIN	PURSE	CHARTREUSE
Date	4-14-66	5-6-66	5-7-69	5-6-66
M_S	3.820 ± .134	4.219 ± .100	4.414 ± .207	3.908 ± .262
Number of Stations	20	14	9	16

EVENT	SCOTCH	KNICKERBOCKER
Date	5-23-67	5-26-67
M_S	4.467 ± .246	4.145 ± .239
Number of Stations	16	16

Table 2. Predicted Yields (Cont'd)

Event Criteria	M_s Yield (KT)	WES	JOR	OAF	LUB	ATL	COR	LON	SCP	AVG. YIELD
PURSE	1.6	21	19	19				19		[illegible]
CHARTREUSE (70KT)	70	[illegible]	[illegible]	61	61	61		[illegible]	[illegible]	[illegible]
SCOTCH (150 KT)	[illegible]	144	[illegible]	[illegible]	[illegible]		[illegible]		13	[illegible]
KNICKERBOCKER	96		96	[illegible]	102		[illegible]		[illegible]	[illegible]

* Denotes published value.

1 Curve was drawn through known values.

2 Based only on station criteria; not M_s.

Table 2. Predicted Yields.

Event Criteria	[1] M_s Yield (KT)	WES	COL	OXF	LUB	ATL	COR	LON	SCP	[2] AVG.YIELD
FAULTLESS	410	475	580	460		530	320	410	360	448 ± 92
HALFBEAK (300 KT)*	300	340	420	530	355			440		417 ± 76
GREELEY (825 KT)	825	805	760	760	705	800		680	790	757 ± 48
COMMODORE	170	240	155	145	180		135			171 ± 42
BOXCAR (1200 KT)	1200	1190	1120	1025		1350				1171 ± 137
DUMONT	100	100		145	91	90	95	135	126	112 ± 23
PILEDRIVER (56KT)	56	48	37	62		54	70	47		53 ± 12
BUFF	42				34				66	50 ± 23
CORDUROY	100	132		142	104	92	80	125	125	114 ± 23
BRONZE	65	32	40	62	50			53	60	50 ± 12
TAN	74	42		55	65	68	73	68	62	62 ± 10
PIRANHA	72	53	60	77	68	64	68	68	63	65 ± 7
DURYEA (65 KT)	65		60		54	61	61	63	70	62 ± 5
NOGGIN	100	102	54	170			67	90	150	106 ± 47

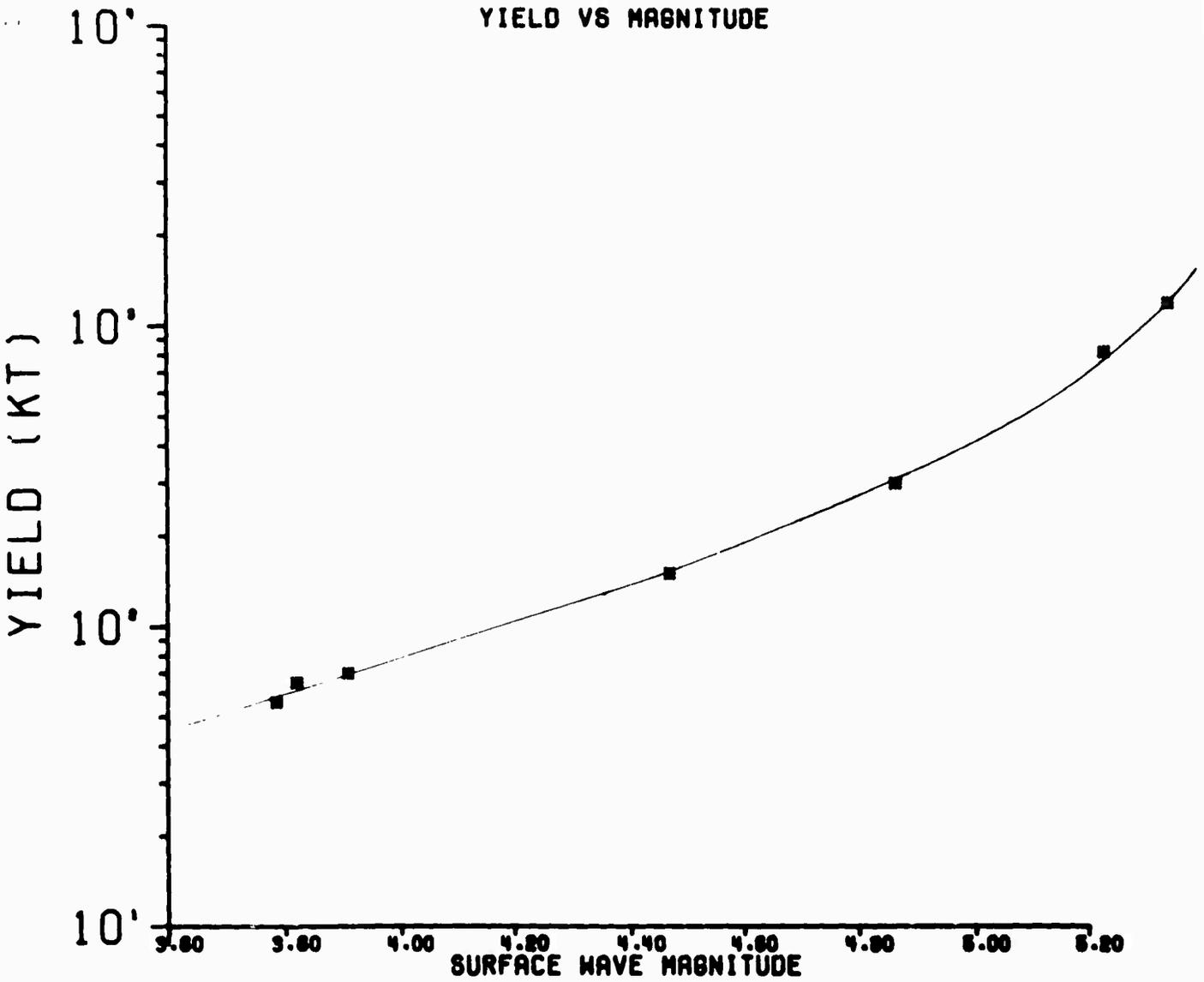
YIELD VS MAGNITUDE
YIELD (KT)
10'
10'
10'
10'
3.60
3.80
4.00
4.20
4.40
4.60
4.80
5.00
5.20
SURFACE WAVE MAGNITUDE

FIG 3.1

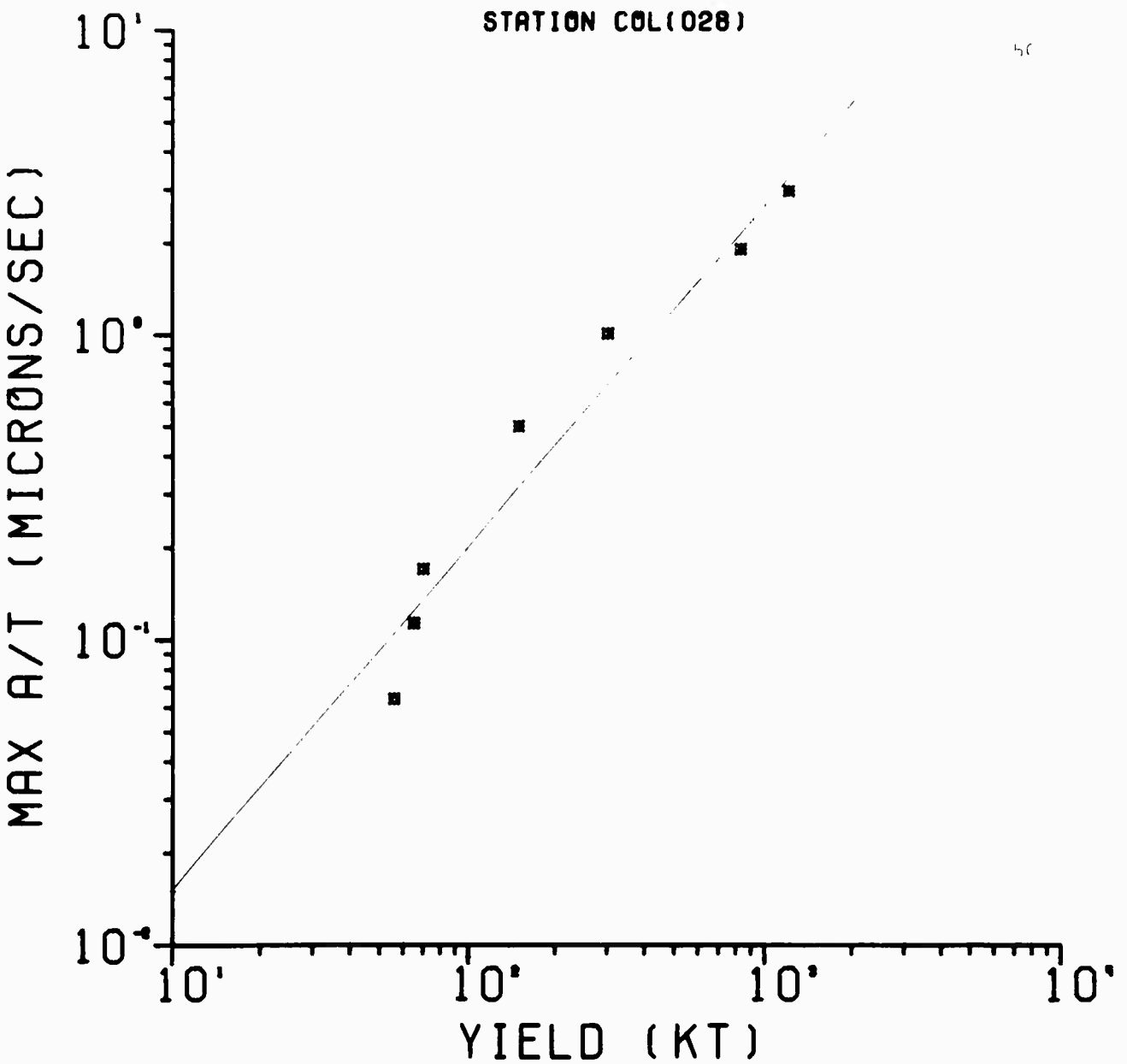
STATION COL(028)
MAX A/T (MICRONS/SEC)
10'
10°
10⁻¹
10⁻²
10'
10²
10³
10⁴
YIELD (KT)

FIG 3.2

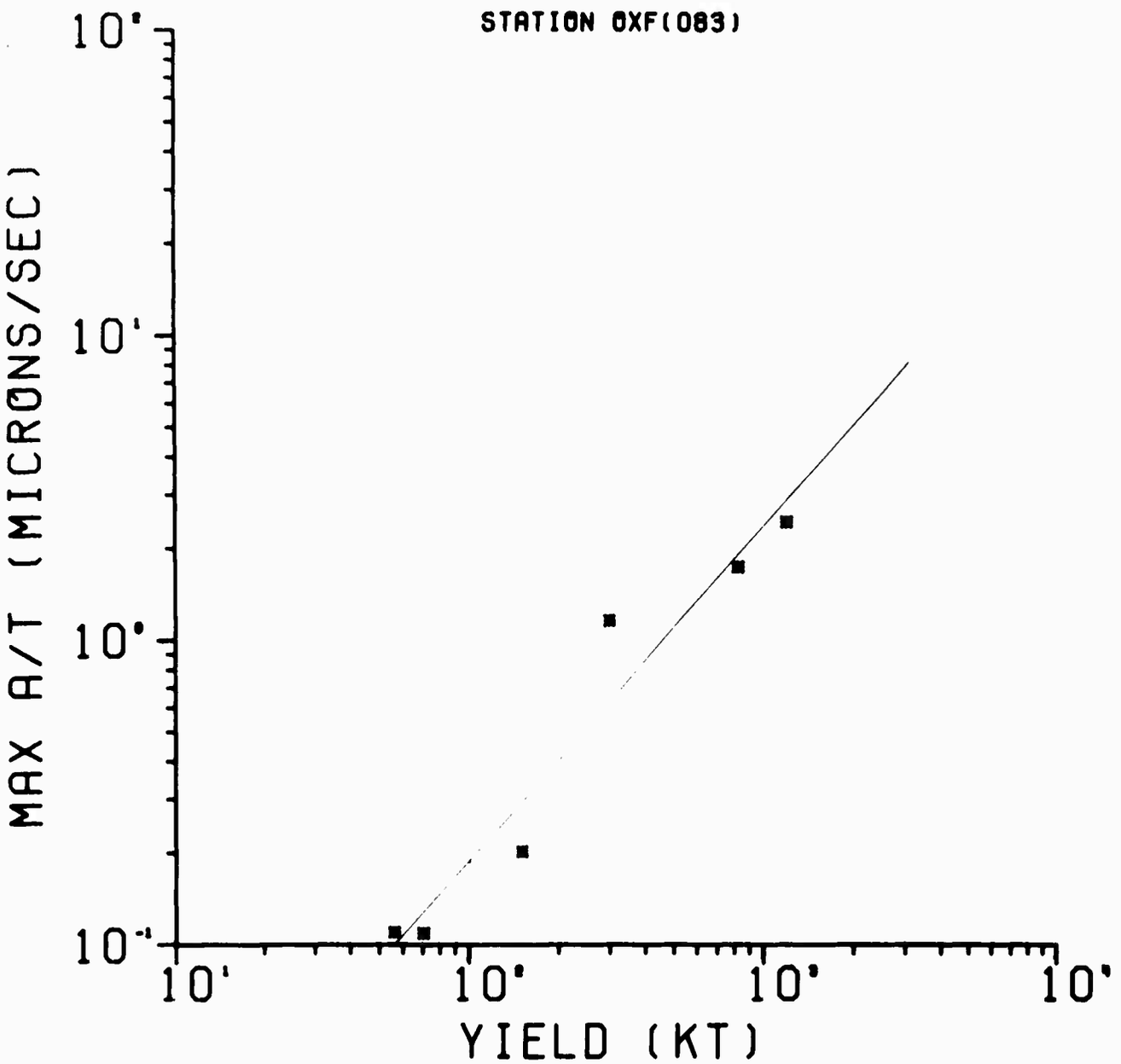
STATION 0XF(083)
MAX A/T (MICRONS/SEC)
10³
10²
10¹
10⁰
10⁻¹
10⁰
10¹
10²
10³
YIELD (KT)

FIG 33

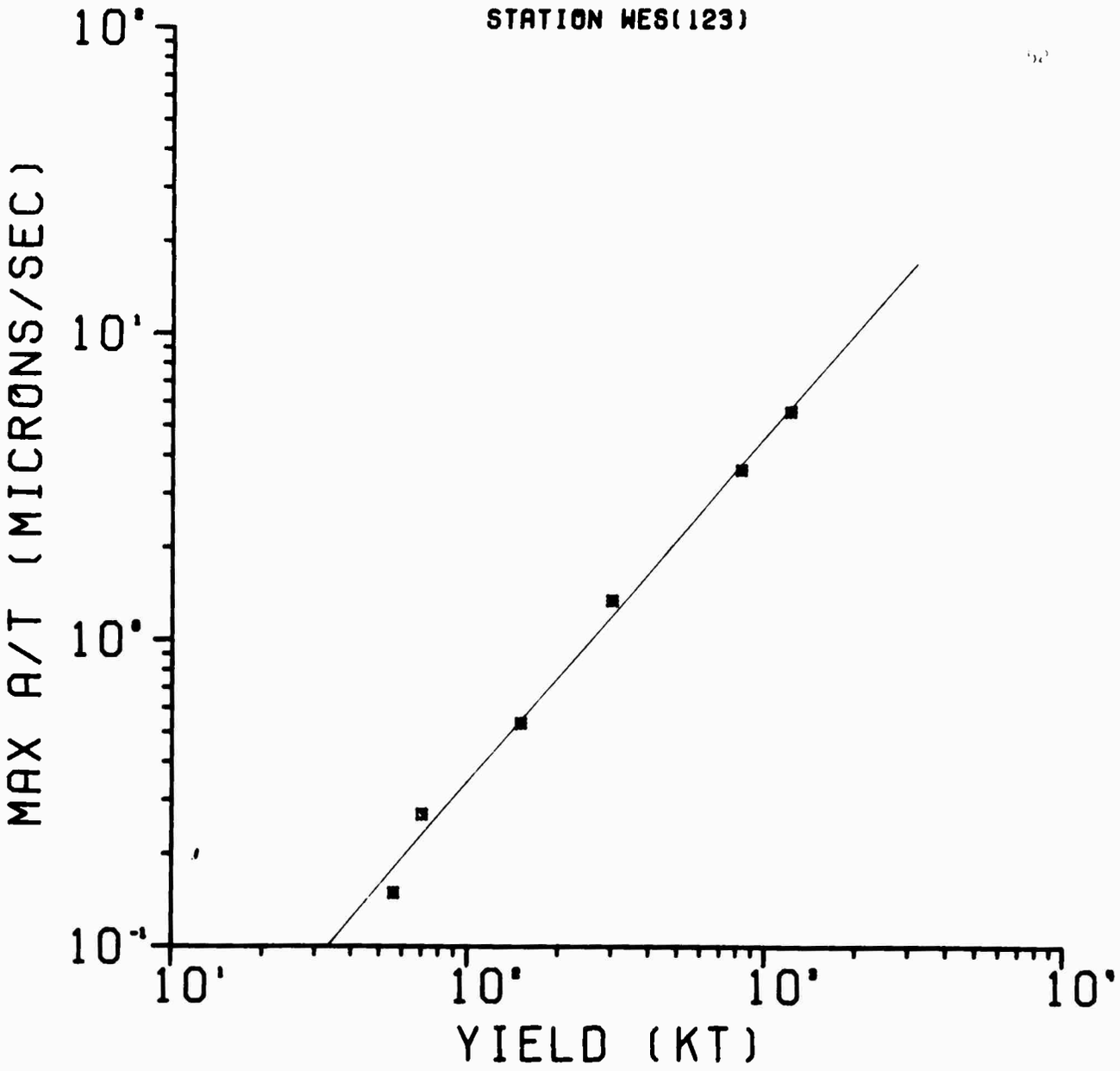

FIG 3.4

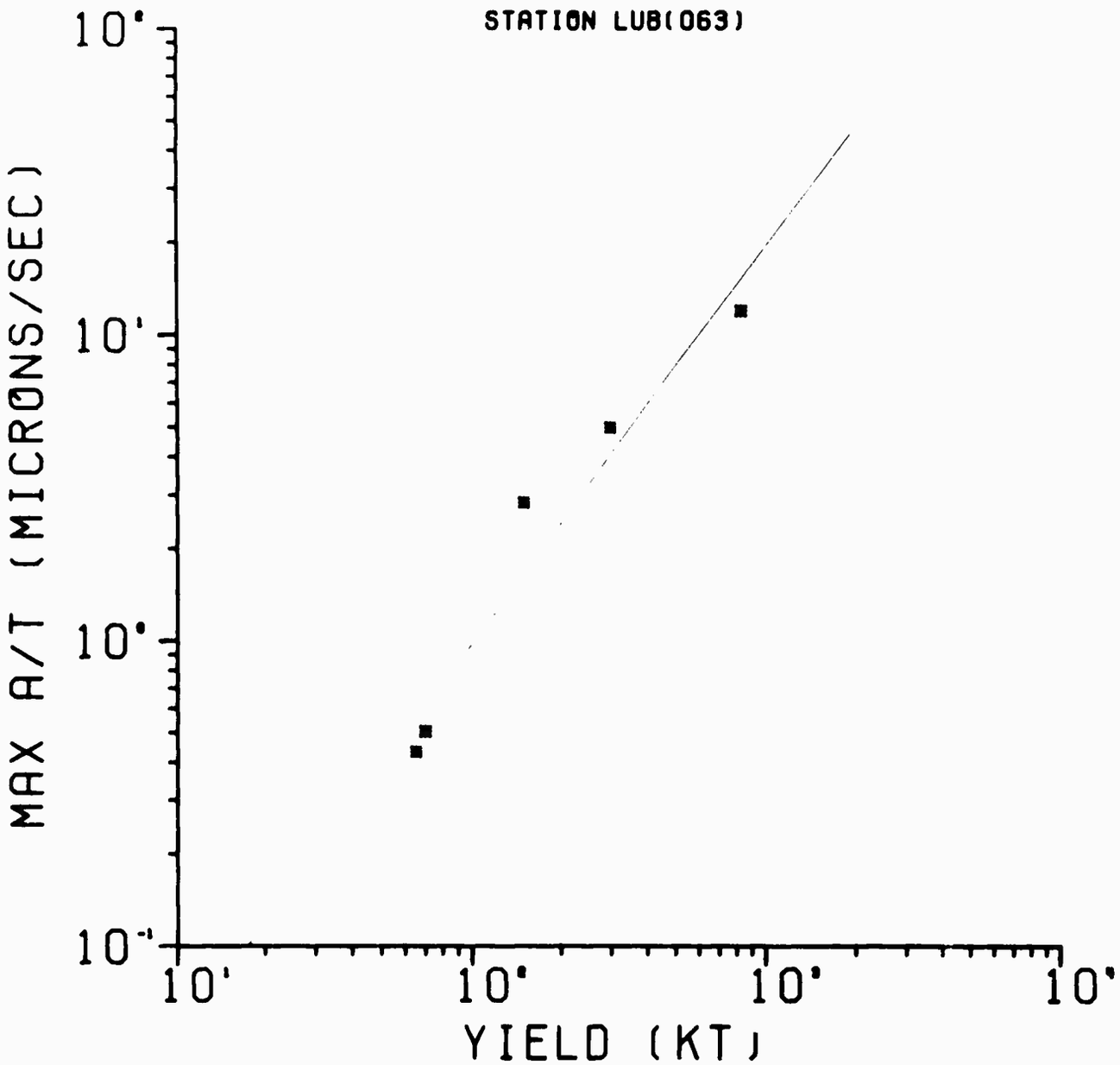
STATION LUB(063)
MAX A/T (MICRONS/SEC)
YIELD (KT)
10⁰
10⁻¹
10¹
10²
10³
10⁴

FIG 3.5

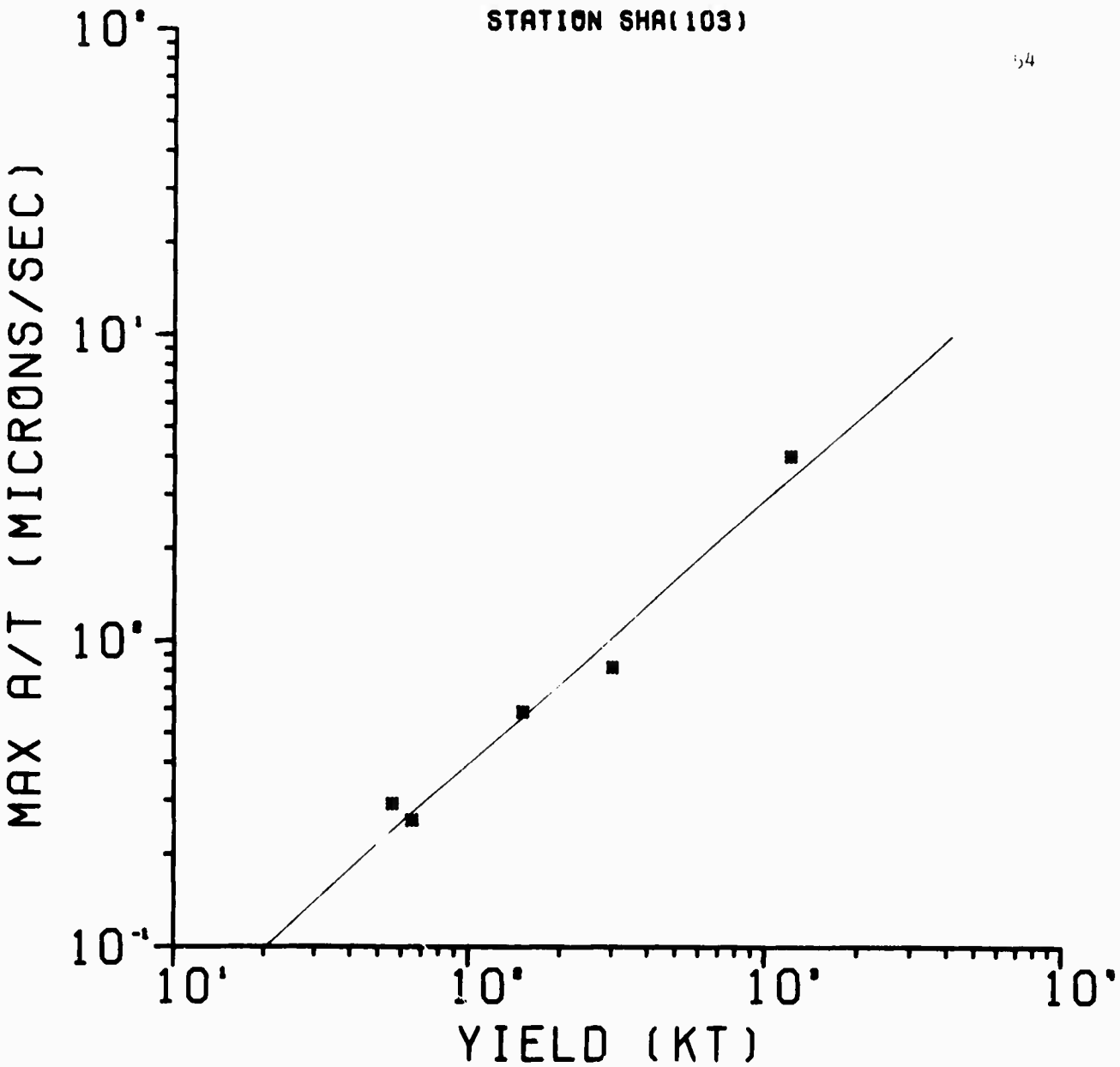
STATION SHA(103)
MAX A/T (MICRONS/SEC)
YIELD (KT)
10⁰
10⁻¹
10⁻²
10¹
10²
10³
10⁴

FIG 3.6

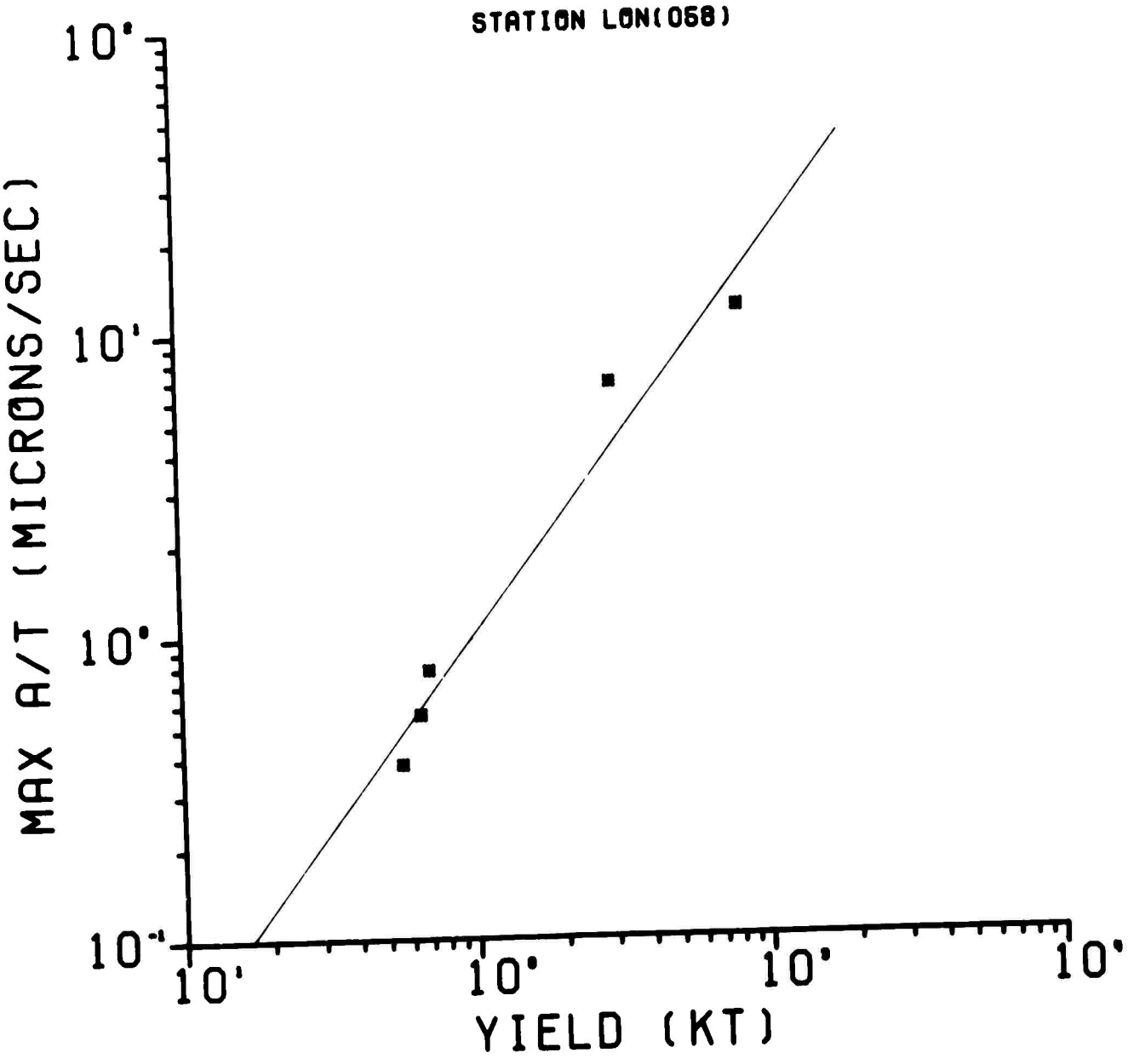

FIG 3.7

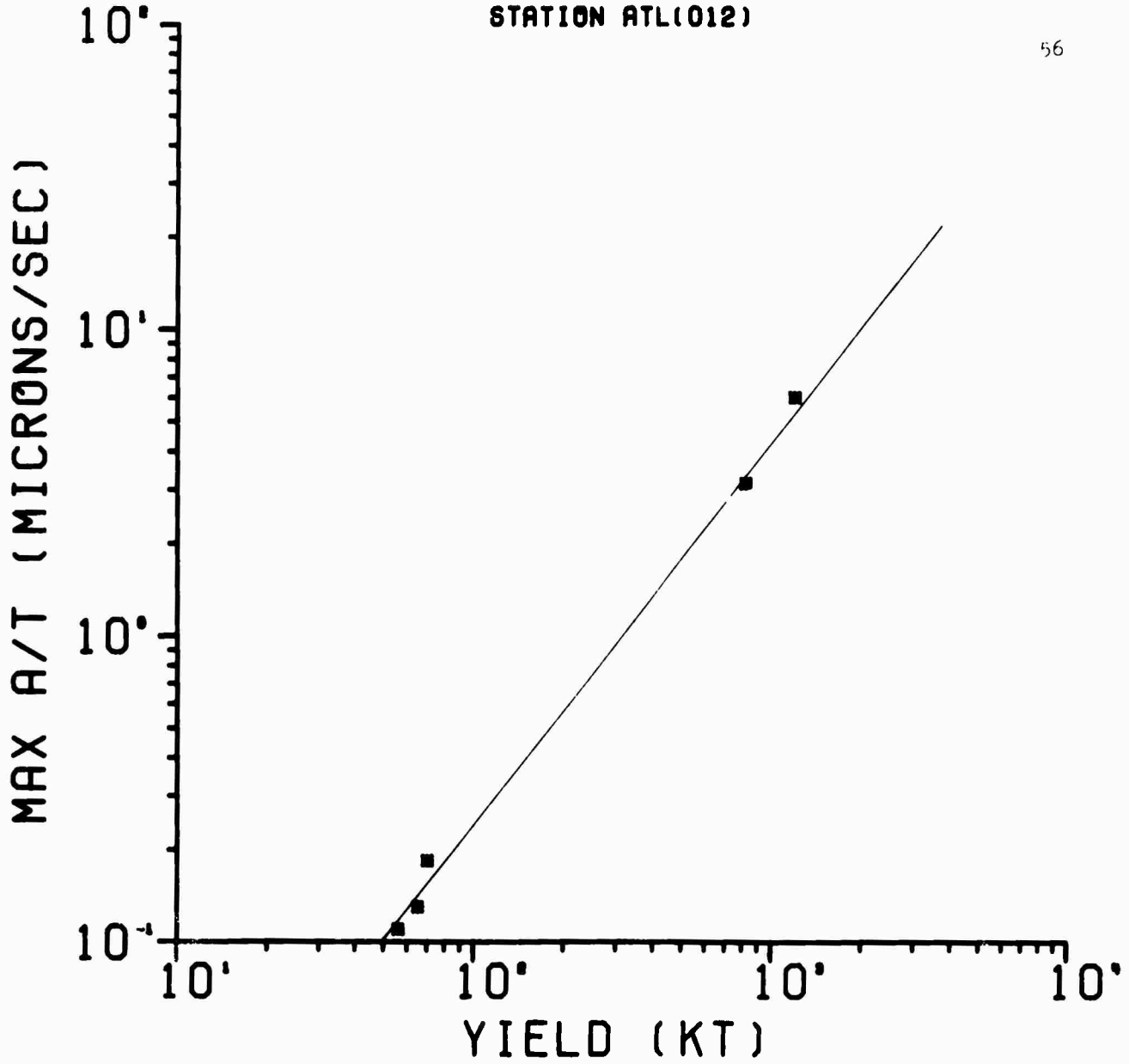
STATION ATL(012)
MAX A/T (MICRONS/SEC)
10²
10¹
10⁰
10⁻¹
10¹
10²
10³
10⁴
YIELD (KT)

FIG 3.8

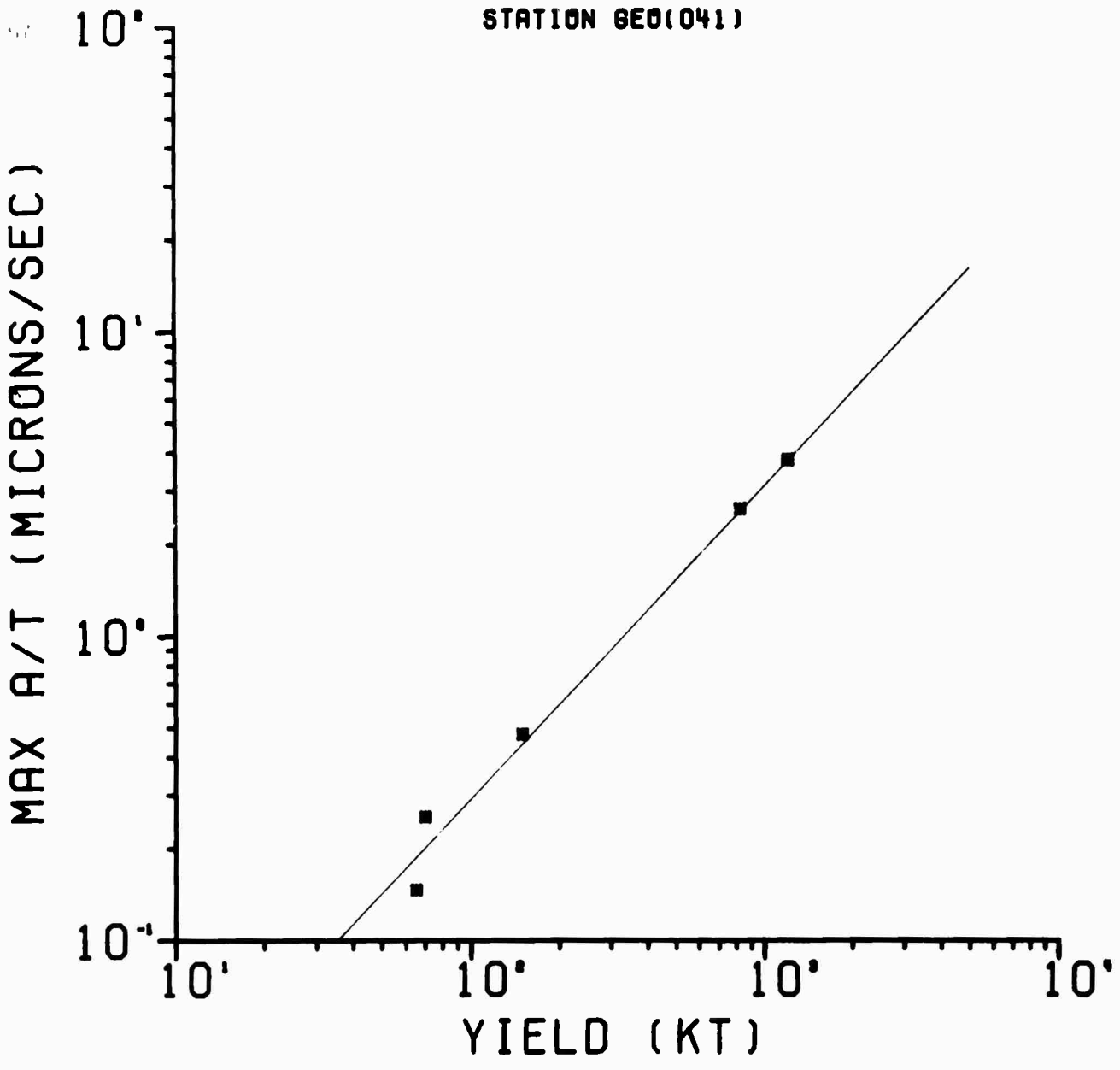
STATION GEO(041)
MAX A/T (MICRONS/SEC)
YIELD (KT)
10⁰
10¹
10⁰
10⁻¹
10¹
10²
10³
10⁴

FIG 3.9

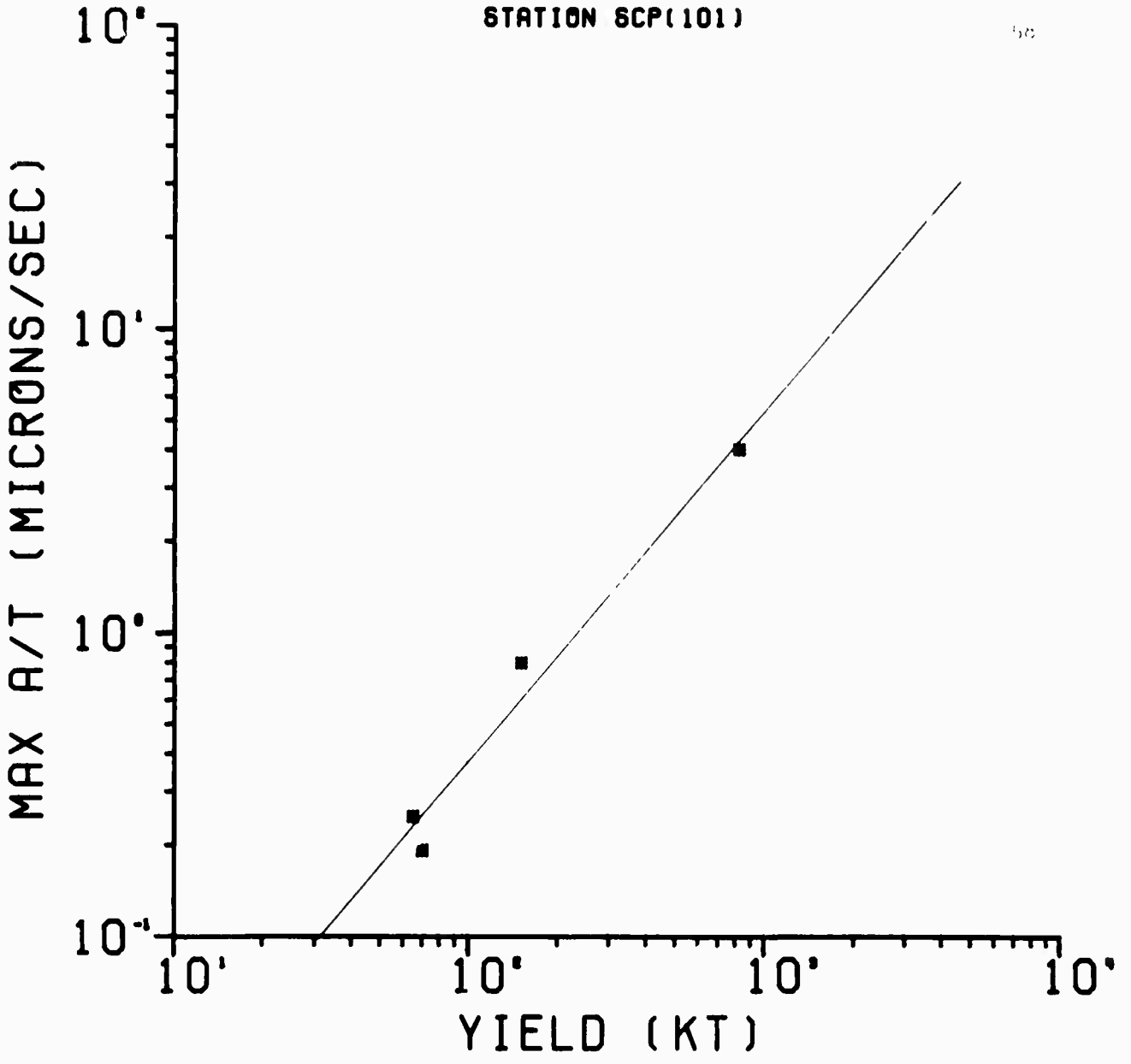
STATION SCP(101)
MAX A/T (MICRONS/SEC)
YIELD (KT)
10⁴
10³
10²
10¹
10⁻¹
10¹
10²
10³
10⁴

FIG 3.10

BLANK PAGE

4. Amplitude Equalization of P-wave Spectra from Underground Nuclear Explosions Recorded at Teleseismic Distances.

by Theron J. Bennett

Introduction

On the basis of body wave magnitude the twelve largest underground nuclear explosions to date were selected. It was later found that of these twelve only eight gave usable records on long-period instruments at epicentral distances greater than 20°. These events along with available information on times, coordinates, and assigned body wave magnitudes are presented in Table 1.

For each event, the long-period, vertical seismograms from all the stations in the U.S.C.G.S. World Wide Network were scanned and those with good signal-to-noise ratios were selected. The restriction of epicentral distances to ranges greater than 20°, in an effort to reduce crustal complications, does not leave many stations with good signal-to-noise ratios even for the very large events considered here. Those stations giving usable records are listed for each event in Table 1. These stations range in distance up to 80° for some events with a number of South American stations recording especially good signals from the Nevada Test Site explosions.

Method of Amplitude Equalization

The spectrum of the recorded P-wave signal can be represented, following the method of Ben-Menahem et al (1965),

as the product of the source spectrum and a series of transfer functions corresponding to various segments of the transmission path.

$$A(\omega) = H_{IN}(\omega)\, H_{RC}(\omega)\, H_{M}(\omega)\, H_{SC}(\omega)\, S(\omega) \qquad (1)$$

where H_{IN}, H_{RC}, H_M, and H_{SC} represent the transfer functions of the recording instrument, receiver crust, mantle, and source crust respectively.

The instrument response function following Kisslinger (1967) is given by:

$$H_{IN}(\omega) = \frac{m\,\omega^3}{\left\{\left[(\omega^2-\omega_n^2)(\omega^2-\omega_{n1}^2) - 4\zeta\zeta_1\omega_n\omega_{n1}(1-\sigma^2)\omega^2\right]^2 + 4\omega^2\left[\zeta_1\omega_{n1}(\omega_n^2-\omega^2) + \zeta\omega_n(\omega_{n1}^2-\omega^2)\right]^2\right\}^{1/2}} \qquad (2)$$

where ω_n and ω_{n1} are the natural (angular) frequencies of the seismometer and galvanometer respectively, m is a constant factor dependent on the peak magnification of the system, ζ and ζ_1 are damping factors, and σ^2 is the coupling factor. The values for these constants at stations in the World Wide System are provided by the U.S.C.G.S.

The transfer function for the receiver crust was determined using a computer program based on the Haskell-Thompson method for the crustal structures at each station provided by Teng (1968) and Steinhart and Meyer (1961). The response of the source crust for models of the Nevada and Aleutian test sites were found by applying the procedure developed by Fuchs (1965) for an explosive point source in a layered crust. A typical transfer function for the NTS crust model given in

Table 2 is presented in Figure 4.1 for a takeoff angle of 35°.

The mantle response (cf. Teng (1968)) is represented as the product of the frequency independent geometrical spreading and the anelastic attenuation which is a function of frequency:

$$H_n(\omega) = G \times \exp\left\{-\frac{\omega}{2}\int_{\text{ray path}} \frac{ds}{Q(r)V(r)}\right\} \qquad (3)$$

where ds is an element of length along the ray path, Q(r) is the intrinsic quality factor as a function of depth, and V(r) is the wave velocity as a function of depth.

The geometrical spreading was determined from an expression given by Bullen (1963):

$$G = \left\{\frac{1}{r_0^2 \sin\Delta\, \eta_0 (\tan^2 e_0 - \sin^2 e_0)^{1/2}} \left|\frac{d^2T}{d\Delta^2}\right|\right\}^{1/2} \qquad (4)$$

for a surface focus source where r_0 is the radius of the earth, Δ is the epicentral distance, T the travel time, $\eta_0 = r_0/v_0$ and e_0 is the angle of emergence of the ray at the surface which is given by $e_0 = \cos^{-1}\left\{\frac{v_0}{r_0}\frac{dT}{d\Delta}\right\}$. The travel time derivatives were obtained by fitting a polynomial over 5° segments of the Herrin P tables and performing the appropriate differentiations. This procedure is discussed in greater detail in the appendix.

The integral in the exponent of the anelastic attenuation factor of eq. 3 - viz. $\int_{\text{ray path}} \frac{ds}{Q(r)V(r)}$ - was evaluated by numerical integration for the Q model given in Table 3 and the Herrin velocity model. (See appendix for details).

Signal Processing

The P-wave signal for the long-period vertical record was digitized at 0.2 sec intervals over a time window of approximately 20 sec. It is believed that most of the P-wave signal energy has been included and any other phases such as PP which may arrive within the window are small in comparison to the P signal strength.

The mean and linear trend were removed from the data and a Hamming window applied. The results were then put into a Fast Fourier Transform computer program to obtain the amplitude spectrum, which is defined according to the norm:

$$F(\omega) = \int_{-\infty}^{\infty} f(t)\, e^{-i\omega t}\, dt \tag{5}$$

and its transform pair as:

$$f(t) = \frac{1}{2\pi} \int_{-\infty}^{\infty} F(\omega)\, e^{i\omega t}\, d\omega \tag{6}$$

Of course, in the case of discrete data these quantities take on analogous forms with finite sums replacing the integrals.

Next, the effects of transmission path were removed by inverting equation 2 and the amplitude spectra at the source determined for each event at each station.

Observations and Conclusions

A total of 75 P-wave signals from the eight events were processed in this manner. A typical amplitude spectrum for each, corrected only for instrument response, is presented in Figure 4.2. An example of the steps in the amplitude-

equalization procedure is shown in Figure 4.3, and the source spectra for the eight events of Figure 4.2 are presented in Figure 4.4. Amplitudes in all these figures are given in μ-sec. The spectra show the following features:

1. Most of the uncorrected spectra exhibit a broad, overall peak between frequencies of 0.1 Hz and 0.9 Hz. Most of the other fluctuations in the spectra appear to correlate better between events at a single station than between stations for a single event (cf. Figure 4.2). This would suggest that these variations are either due to differences in crust or upper mantle structures in the vicinity of the receivers or possibly the result of a radiation pattern in the source region. A similar phenomenon was noted by Filson (1970) using shorter period P-waves from Soviet explosions recorded at array stations.

2. Removal of the receiver crust seems to have little effect on the general appearance of the spectra though the overall level is reduced (cf. Figure 4.3).

3. Correction for the source crust has a more drastic effect on the shape of the curves. The trough at the low frequency end of the spectrum is greatly reduced and in many cases almost disappears. Also, the level of the curves at frequencies above this notch is cut by a factor of nearly ten (cf. Figure 4.3).

4. The most pronounced effect on both the shape and level of the spectra is produced by the mantle correction. The geometrical spreading adjustment changes the level of the

spectrum at a given station and correction for anelasticity introduces a linear trend in the semi-log plots of the amplitude spectra (cf. Figure 4.3). More dramatic is the general smoothing of the minor variations discussed under point 1 over the entire frequency band.

5. As one might hope, the amplitude spectra for a given explosion look more alike from station to station after application of the equalization procedure (cf. Figure 4.4). The similarity in the general level of the curves in the band 0.1 Hz to 0.8 Hz seems noteworthy.

6. In comparing the source spectra for different events recorded at different stations as in Figure 4.4, there is no obvious relation between the yield of the explosion and the level of the spectra. In Figure 4.4 it can be observed that throughout most of the frequency band the amplitudes for the Greeley source spectrum determined at Caracas are higher than those for the other events depicted despite the fact that the Greeley yield is only 825 KT compared with yields greater than 1000 KT for some of the other explosions.

7. Even when the source spectra for several explosions are compared at a single recording site, as in Figure 4.5, the relation of level and yield is still not apparent. In this case, the Halfbeak explosion with a yield of 300 KT shows up with nearly the same spectral level as the Boxcar event which had a yield four times as great.

8. In the spectra of Figure 4.5 minor peaks appear at the lower end of the frequency band for all of the NTS explosions

Neglecting for the moment Faultless which has some odd features, the spectra for the larger events such as Benham, Boxcar, and Greeley seem to exhibit multiple peaks between 0.1 Hz and 0.4 Hz while the spectra of the smaller events Halfbeak and Commodore show a better developed, single peak centered at about 0.2 Hz. Also the spectra for the larger events have minor troughs at a frequency of 0.7 Hz which do not show up for the smaller events. Similar features can be distinguished on many of the spectra at other stations.

9. At epicentral distances greater than about 25° the most notable features of the spectra are the trough near 0.1 Hz and the minor trough between 0.7 Hz and 0.8 Hz.

It is not known at this time whether these features or any other may be significant in analyzing near source characteristics of underground nuclear tests.

APPENDIX. Mantle Transfer Function

Geometrical Spreading. The most significant cause of amplitude diminution in body waves is geometrical spreading. The theory of geometrical spreading of spherical wave fronts is concisely presented in Bullen (1963). In a recent study by Duda (1970) calculations of geometrical spreading based on the Herrin P times and Jeffreys-Bullen S times were presented in conjunction with computations of body wave magnitude correction factors. In the present research some adjustments were made on the procedure used by Duda, and these changes along with other results which came up in connection with these refinements will be presented here.

The geometrical spreading can be calculated from the relation:

$$G(\Delta) = \frac{\eta_0}{r_0^2 \eta_1 \sin\Delta} \left\{ \eta_1^2 \tan^2 e_0 - \eta_0^2 \sin^2 e_0 \right\}^{-1/4} \left| \frac{d^2T}{d\Delta^2} \right| \qquad (A1)$$

where r_0 is the radius of the earth, Δ the epicentral distance, e_0 the angle of emergence of the ray at the earth's surface, $\eta_0 = r_0/v_0$, $\eta_1 = r_1/v_1$, v_0 the wave velocity at the surface, v_1 the wave velocity at the source depth, and r_1 the radial distance from the source to the center of the earth. Evaluation of $G(\Delta)$ by eq. A1 requires computation of the second derivative of the travel time. In the calculations carried out by Duda the first derivatives of the travel times $(dT/d\Delta)$ were taken to be the time differences between adjacent epicentral distances divided by the distance increment, and the second derivatives $(d^2T/d\Delta^2)$ were found similarly by taking the differences between values of the first derivative at adjacent points. This corresponds to taking the slope of a straight line between the two points to be the derivative. While this technique is good as a first approximation, it did result in some instability in the spreading curves computed by Duda, especially at short distances.

In the present analysis it was decided that a better approach might be to fit a polynomial over certain segments of the travel times and compute first and second derivatives from that. Thus it was assumed that the travel time could

be represented as:

$$T = a_0 + a_1 \Delta + a_2 \Delta^2 + a_3 \Delta^3 + \ldots + a_n \Delta^n$$

and the derivatives as:

$$\frac{dT}{d\Delta} = a_1 + 2 a_2 \Delta + 3 a_3 \Delta^2 + \ldots + n a_n \Delta^{n-1}$$

$$\frac{d^2T}{d\Delta^2} = 2 a_2 + 6 a_3 \Delta + \ldots + n(n-1) a_n \Delta^{n-2}$$

over some range of epicentral distances. The interval upon which the least squares fit was performed was arbitrarily chosen to be ten points which corresponds to a 5° segment of the Herrin tables. At first a second degree polynomial was fitted to the data, but it was later found that a third degree polynomial fit gave more consistent results when the travel times were calculated from the velocity model.

In Figure 4.6 the computations, based on this procedure, for ($dT/d\Delta$ vs Δ) and($d^2T/d\Delta^2$ vs Δ) are presented for P waves from a surface focus event. The angle of incidence at the surface as a function of epicentral distance, obtained from the relation:

$$i_0 = \sin^{-1}\left(\frac{v_0}{r_0}\frac{dT}{d\Delta}\right) \qquad (A2)$$

(where v_0 was taken as 6 km/sec, r_0 as 6371 km, and $dT/d\Delta$ has units of sec/radian), is also shown.

The geometrical spreading was then obtained using equation A1 and is presented in Figure 4.7 for a surface focus event. The amplitude at an epicentral distance of 80° was

taken as a reference and the spreading normalized on that value so that the results could be compared directly with Duda's curves. (Duda had chosen this distance as a reference because it corresponded to a range in which his calculations were most stable.)

In comparing the spreading computed here with that obtained by Duda, the most obvious difference is the improvement in stability as the new curve is relatively smooth over the entire epicentral distance range. The overall shape and level of Duda's curves are maintained.

Anelastic Attenuation. It has been clear from the earliest days of instrumental seismology that the frequency content of events recorded at near distances differs significantly from that of the same events recorded far away. It is now recognized that the mantle acts as a low-pass filter for teleseismic waves and this is caused primarily by anelastic behavior in the mantle.

In this research the procedure of Teng (1968) was used to evaluate the effect of anelastic behavior on the P-wave spectra. Teng had used the CIT11A velocity model in his analysis while in this study the Herrin model was used; it was therefore necessary to make some adjustments in the Q(r) model adopted by Teng.

In equation 3 it was noted that the effect of anelastic attenuation could be represented by a factor of the form:

$$\exp\left\{-\frac{\omega}{2}\int_{\text{ray}}\frac{ds}{Q(r)\,V(r)}\right\} = \exp\left\{-f\,t^{*}\right\} \qquad (A3)$$

The expression:

$$t^* \equiv \pi \int_{\text{ray path}} \frac{ds}{Q_\alpha(r)\,\alpha(r)} \qquad \text{(A4)}$$

where the α refers to P-waves, was evaluated numerically for several of the Q models suggested by Teng and a quantity called the differential attenuation as a function of Δ, normalized to an epicentral distance of 50°,

$$\delta A(\Delta) \equiv t^*(\Delta) - t^*(50^\circ) \qquad \text{(A5)}$$

was calculated for ray paths from an event with focal depth of 550 km. This quantity was then compared to observed differential attenuations given by Teng for two deep focus earthquakes in South America. As might be expected, since the velocities of the CIT 11A model and the Herrin model do not differ drastically, the adjustment in the Q(r) structure required to obtain a fit to the same attenuation data was not large. The best fit (cf. Figure 4.8) seemed to correspond to the model which Teng had suggested as an alternate. This model is shown in Table 3.

Using this Q model t* as a function of epicentral distance was calculated for a surface focus event. The results are shown in Figure 4.9. Then the expression

$$\exp\{-f t^*\}$$

giving the anelastic part of the mantle transfer function can be directly evaluated. To show how this affects the

spectra of P-waves at different epicentral distances, the mantle transfer function was computed taking into account only the anelastic behavior for distances of 5^{o}, 10^{o}, 20^{o}, and 50^{o}. The results are presented in Figure 4.10. The low pass filter character is evident.

References

Ben-Menahem, A., S. W. Stewart, and T. L. Teng (1965). A procedure for source studies from spectrums of long period seismic body waves, Bull. Seism. Soc. Am., 55(2), 203-235.

Bullen, K. E. (1963). An Introduction to the Theory of Seismology, Cambridge Univ. Press, Third Edition.

Duda, S. J. (1970). Travel times and body wave magnitude, Scientific Report No. 8, Air Force Contract AF 19(628)-5100, Saint Louis University.

Filson, J. R., (1970). On estimating explosive source parameters at teleseismic distances, Technical Note 1970-9, Air Force Contract AF 19(628)-5167, Lincoln Laboratory, Massachusetts Institute of Technology.

Fuchs, K. (1965). The transfer function for P-waves for a system consisting of a point source in a layered medium, Scientific Report No. 12, Air Force Contract AF 19(604)-7399, Saint Louis University.

Herrin, E., et al (1968) Seismological Tables for P phases, Bull. Seism. Soc. Am., 58(4), 1193-1352.

Kisslinger, C. (1967). Seismological Instrumentstion, IISEE Lecture Notes No. 2, International Institute of Seismology and Earthquake Engineering, Tokyo, Japan.

Steinhart, J. S., and R. P. Meyer (1961). Explosion studies of continental structure, Carnegie Inst., Wash., Publ. 622.

Teng, T. L.(1968). Attenuation of body waves and Q structure of the mantle, J. Geophys. Res., 73(6), 2195-2208.

Table 1

Event	Date	Time (GMT)	m_b	Location	Stations Analyzed
Benham (Ben)	12/19/68	16:30:00.0	6.3	37.232N 116.474W	ARE,BOG,CAR, FLO,NNA,OXF, QUI,SHA
Boxcar (Box)	4/26/68	15:00:00.0	6.3	37.295N 116.456W	AAM,ARE,BOG, CAR,COL,FLO, OXF,QUI,SHA
Commodore (Com)	5/20/67	15:00:00.0		37.130N 116.063W	FLO,LPS,OXF, SHA
Faultless (FLT)	1/19/68	18:15:00.0		38.625N 116.219W	AAM,ARE,ATL, BLA,BOG,CAR, COL,FLO,NNA, OXF,QUI,SHA, UNM,KRK
Greeley (GRE)	12/20/66	15:30:00.1	6.05-6.29	37.302N 116.408W	AAM,ARE,ATL, BLA,BOG,CAR, COL,FLO,LPS, NNA,OXF,QUI, SHA
Halfbeak (HLF)	6/30/66	22:15:00.0	6.02-6.04	37.316N 116.299W	AAM,BLA,LPS, OXF,SHA
Jorum (JOR)	9/16/69	14:30:00.0	6.2	37.314N 116.460W	ATL,BLA,COL, FLO,SCP,SJG, WES
Milrow (MIL)	10/2/69	22:06:00.0	6.5	51.417N 179.182E	ALQ,BLA,COL, DUG,FLO,HNR, JCT,LON,NDI, OXF,QUE,SHA, SHL,TUC

Table 2

NTS Crust Model

Layer Thickness D(km)	P-Vel α(km/sec)	S-Vel β(km/sec)	Density ρ(gm/cc)
2.14	3.24	1.86	2.20
0.36	4.40	2.50	2.40
2.50	5.10	2.60	2.50
20.00	6.10	3.50	2.70
10.00	7.00	4.00	3.00
-	8.00	4.60	3.30

Table 3

Mantle Q Model

Depth (km)	Q	Depth (km)	Q	Depth (km)	Q
0	450	1500	1000	2875	100
36	60	1700	1000		
50	75	1875	750		
70	75	2000	500		
150	75	2200	500		
530	75	2400	500		
750	100	2500	300		
950	250	2600	250		
1100	450	2700	200		
1300	550	2800	120		

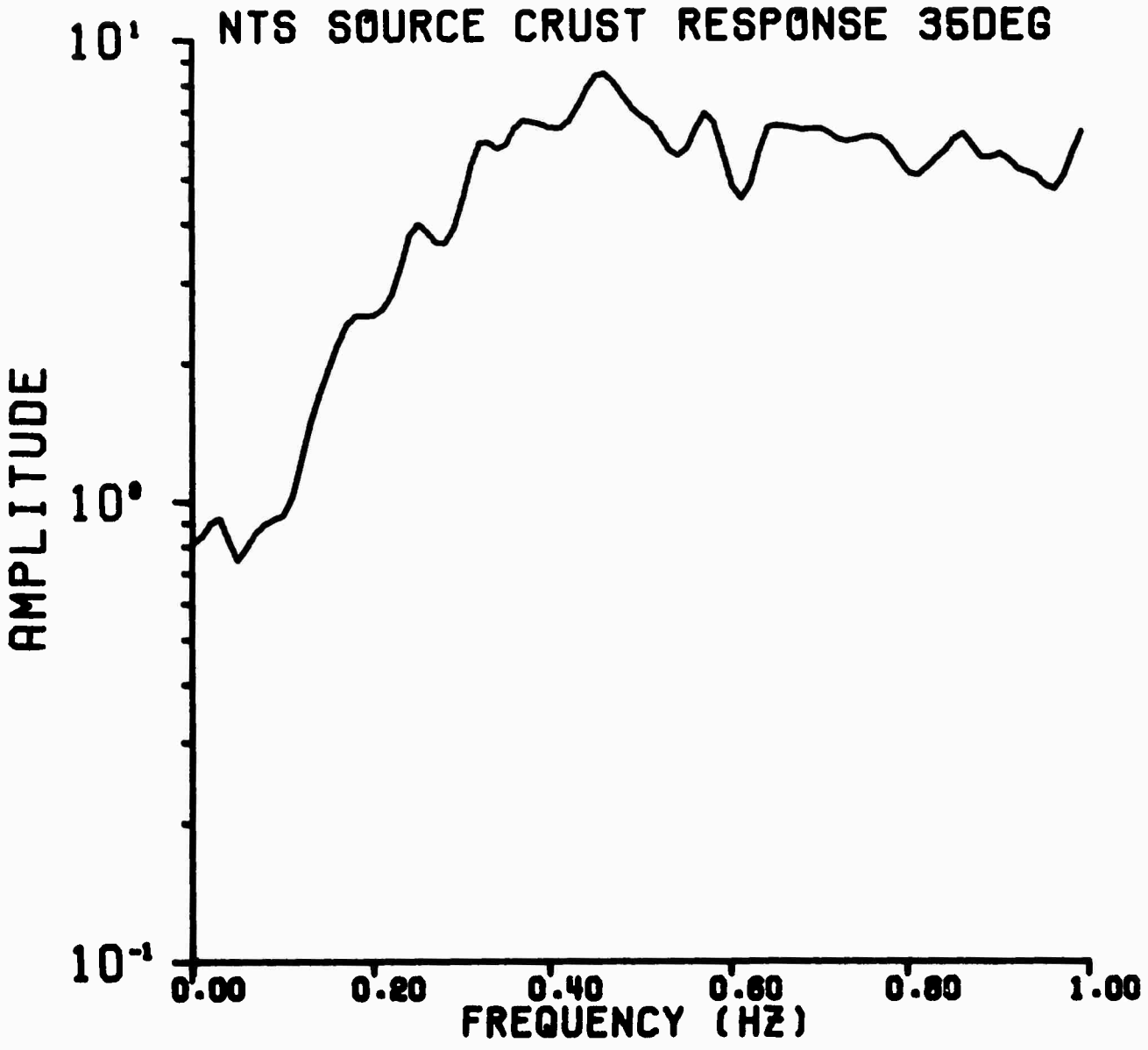
NTS SOURCE CRUST RESPONSE 35DEG
AMPLITUDE
10¹
10⁰
10⁻¹
0.00
0.20
0.40
0.60
0.80
1.00
FREQUENCY (HZ)

FIG 4.1

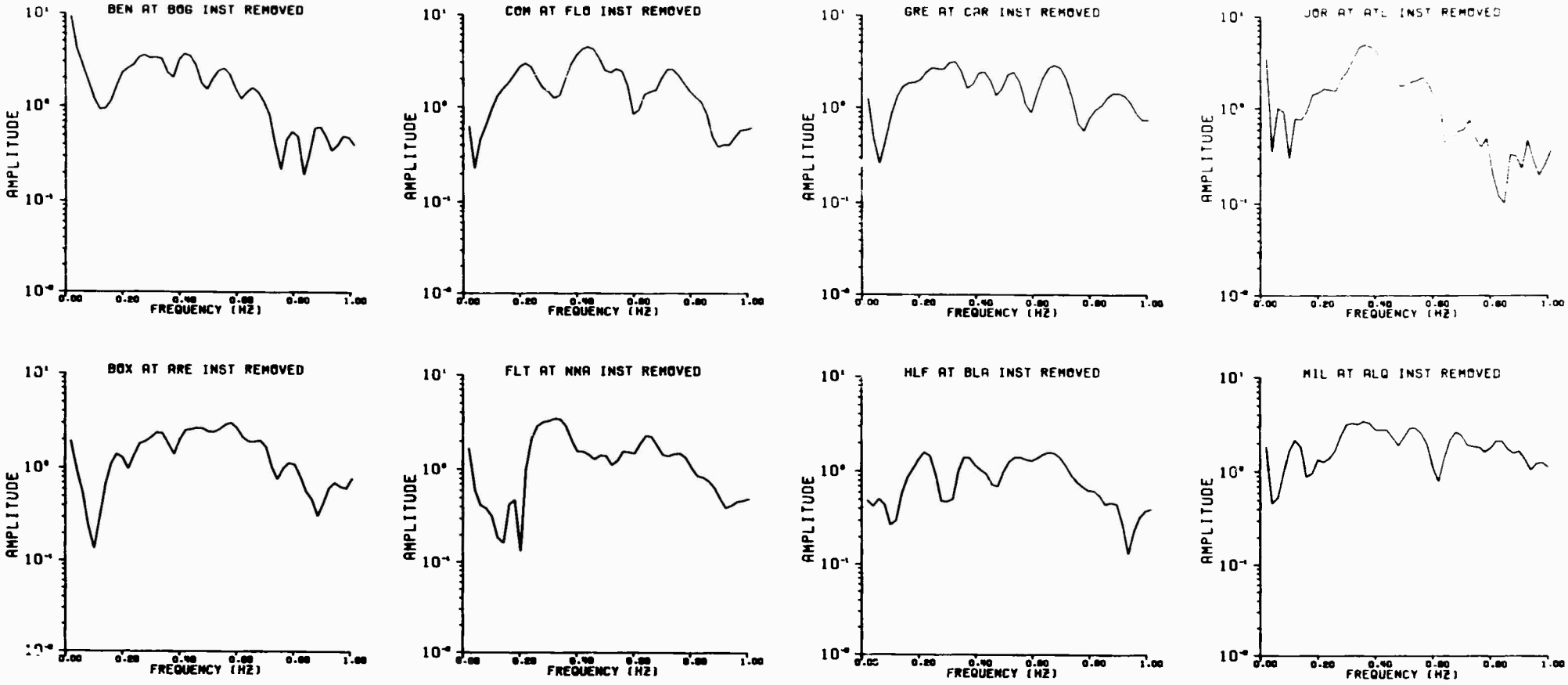
BEN AT BOG INST REMOVED
COM AT FLO INST REMOVED
GRE AT CAR INST REMOVED
JOR AT ATL INST REMOVED
BOX AT ARE INST REMOVED
FLT AT NNA INST REMOVED
HLF AT BLA INST REMOVED
MIL AT ALQ INST REMOVED
AMPLITUDE
FREQUENCY (HZ)

Fig 4.2

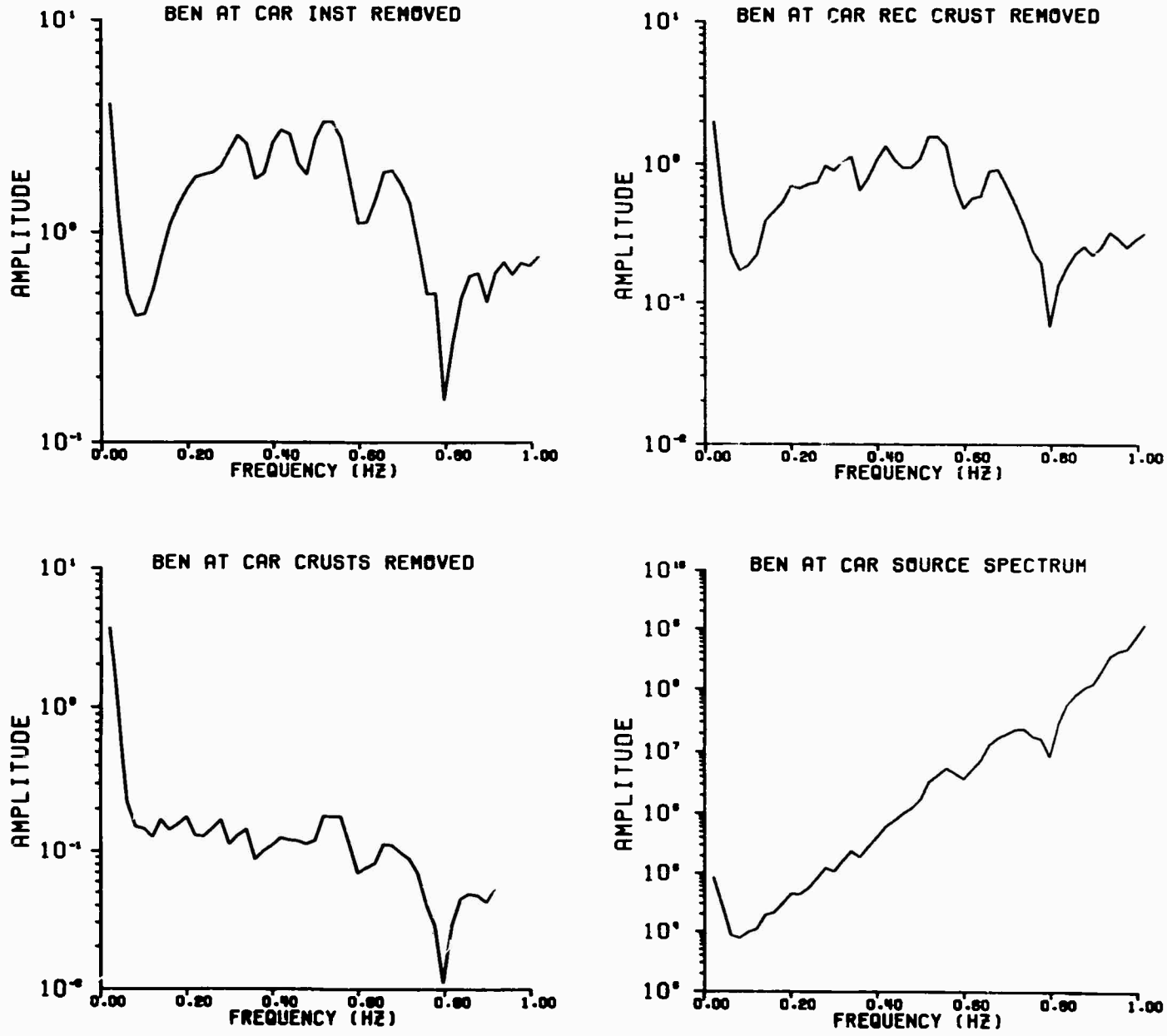
BEN AT CAR INST REMOVED
BEN AT CAR REC CRUST REMOVED
BEN AT CAR CRUSTS REMOVED
BEN AT CAR SOURCE SPECTRUM
AMPLITUDE
FREQUENCY (HZ)
0.00
0.20
0.40
0.60
0.80
1.00

FIG 4.3

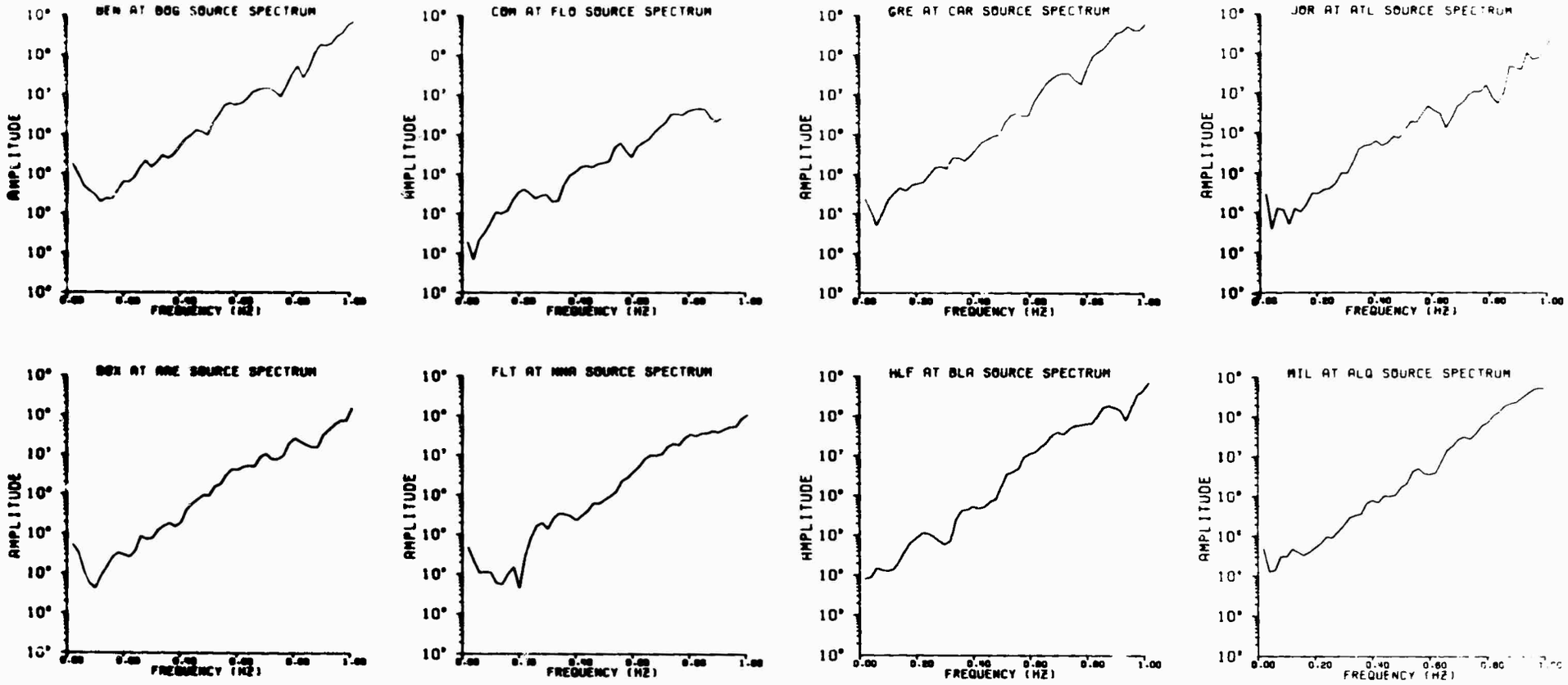
BEN AT BOG SOURCE SPECTRUM
COM AT FLO SOURCE SPECTRUM
GRE AT CAR SOURCE SPECTRUM
JOR AT ATL SOURCE SPECTRUM
BOX AT ANE SOURCE SPECTRUM
FLT AT NWA SOURCE SPECTRUM
HLF AT BLA SOURCE SPECTRUM
MIL AT ALQ SOURCE SPECTRUM
AMPLITUDE
FREQUENCY (HZ)

FIG 4.4

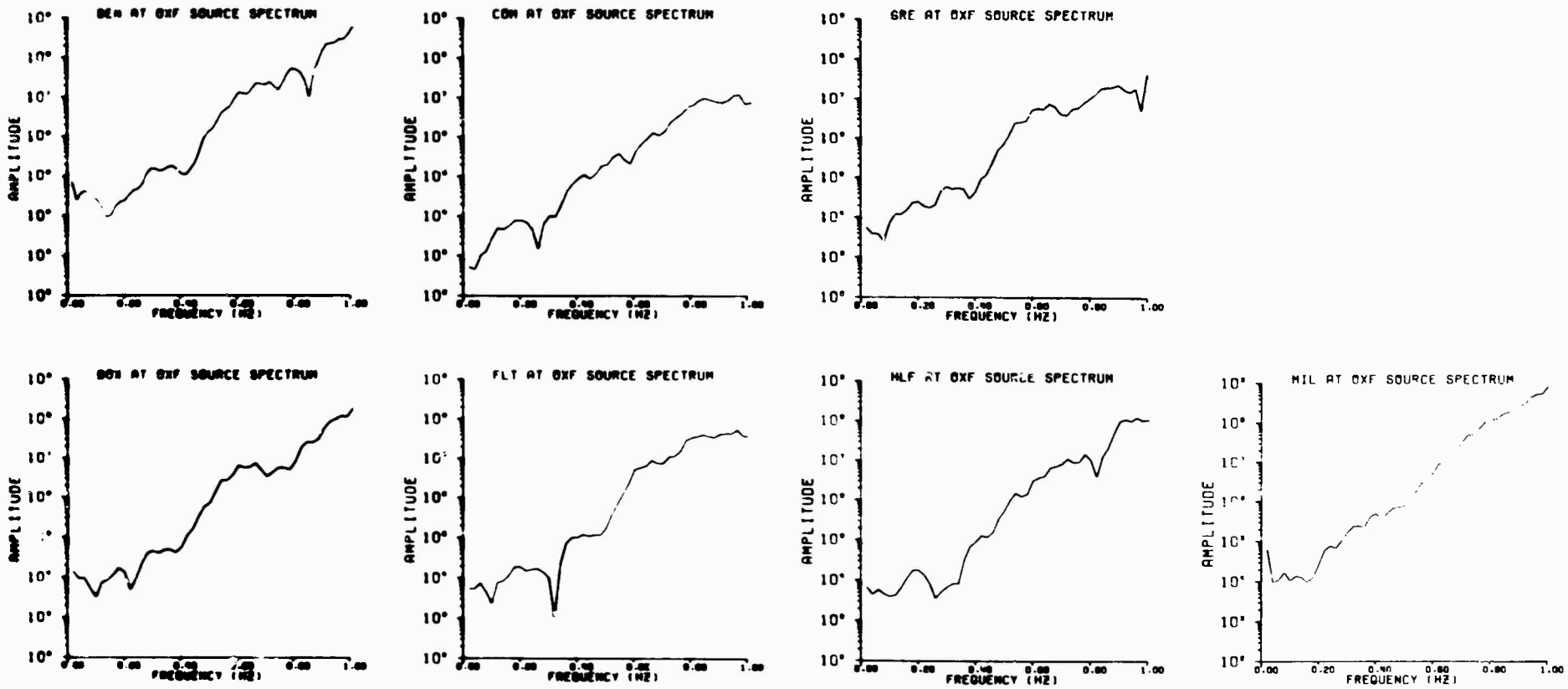
BEH AT OXF SOURCE SPECTRUM
CON AT OXF SOURCE SPECTRUM
GRE AT OXF SOURCE SPECTRUM
BOH AT OXF SOURCE SPECTRUM
FLT AT OXF SOURCE SPECTRUM
MLF AT OXF SOURCE SPECTRUM
MIL AT OXF SOURCE SPECTRUM
AMPLITUDE
FREQUENCY (HZ)
0.00
0.20
0.40
0.60
0.80
1.00

FIG 4.5

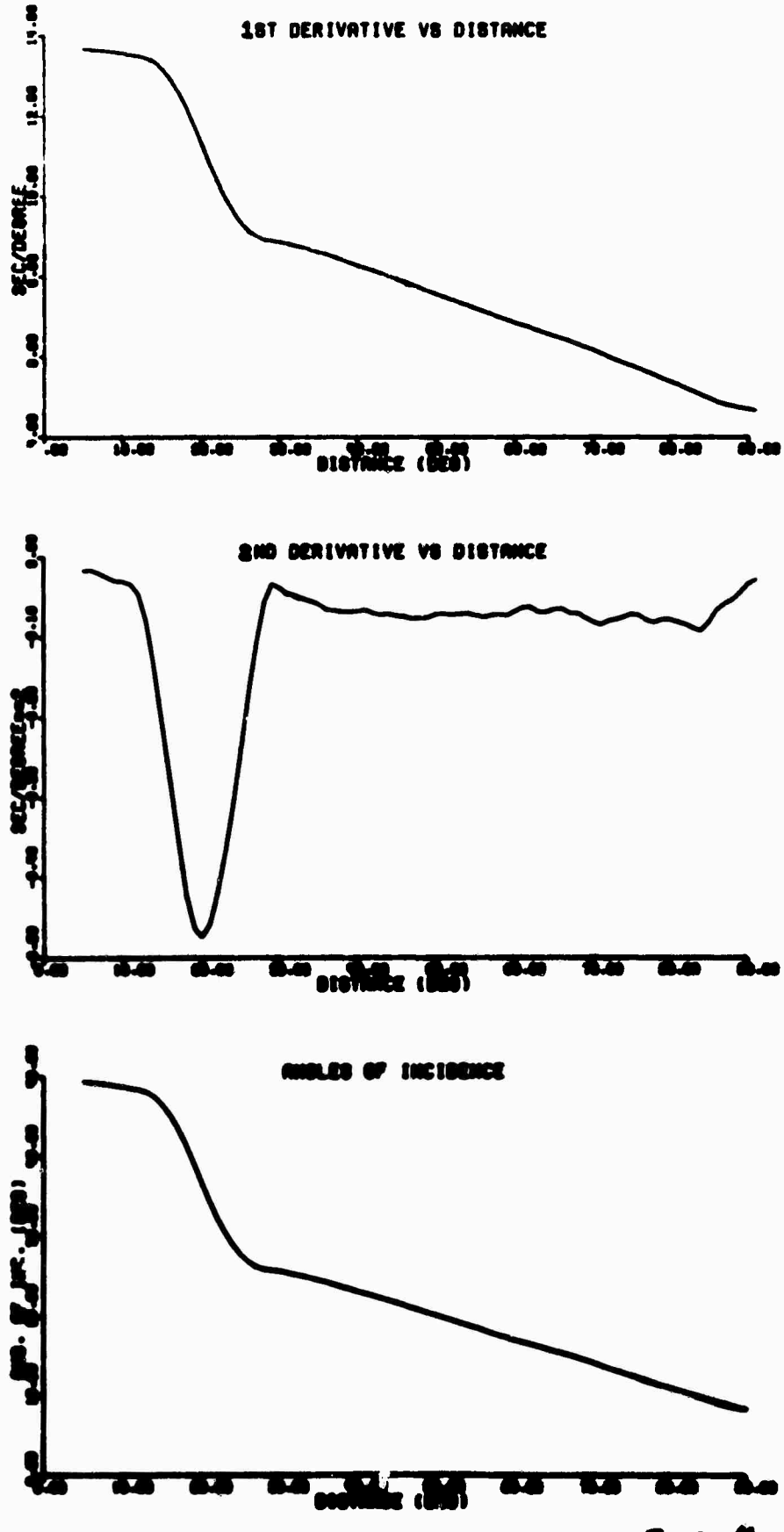
1ST DERIVATIVE VS DISTANCE
2ND DERIVATIVE VS DISTANCE
ANGLES OF INCIDENCE

FIG 4.6

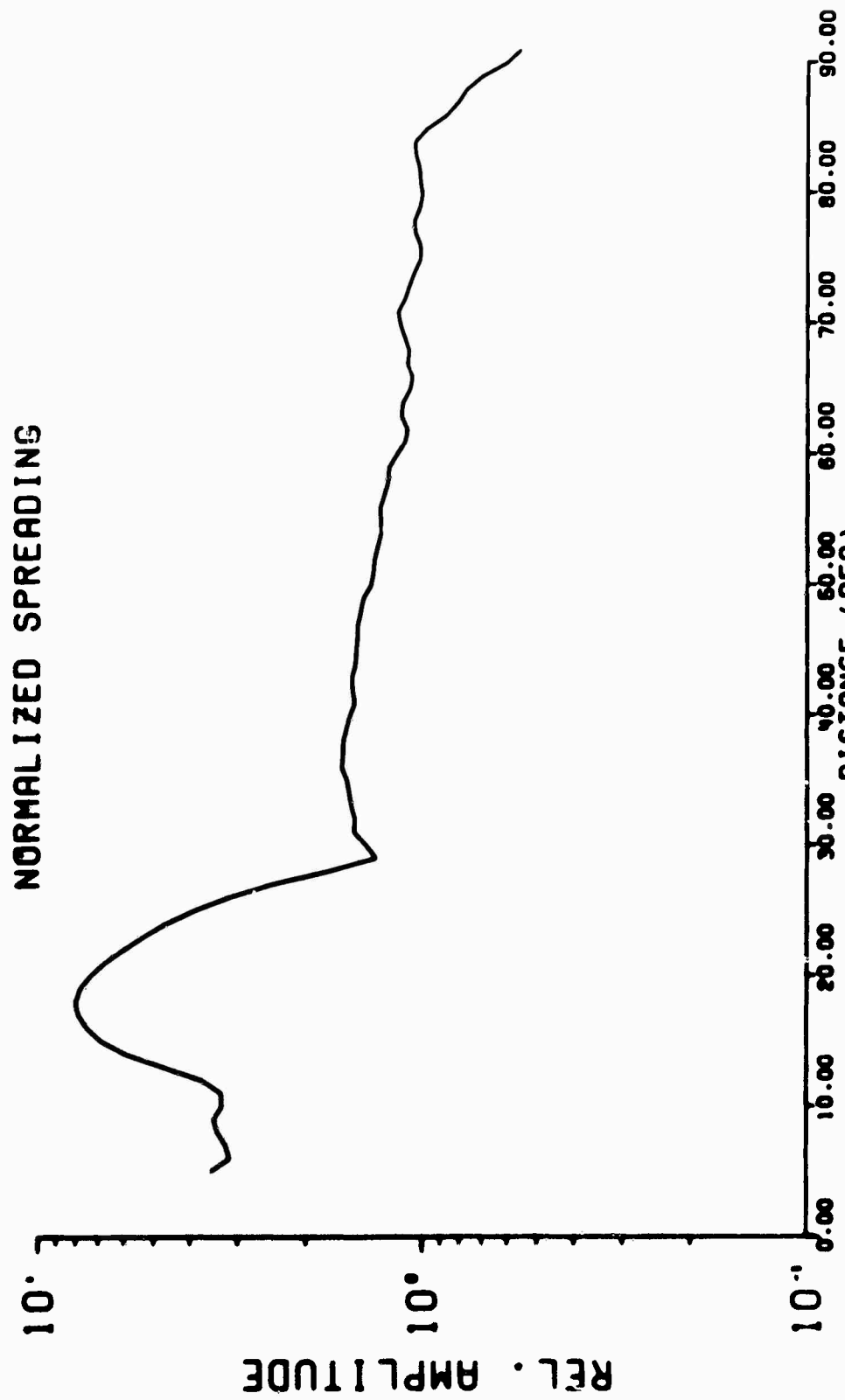
NORMALIZED SPREADINS
REL. AMPLITUDE
10'
10°
10⁻¹
0.00
10.00
20.00
30.00
40.00
50.00
60.00
70.00
80.00
90.00
DISTANCE (DEG)

FIG 4.7

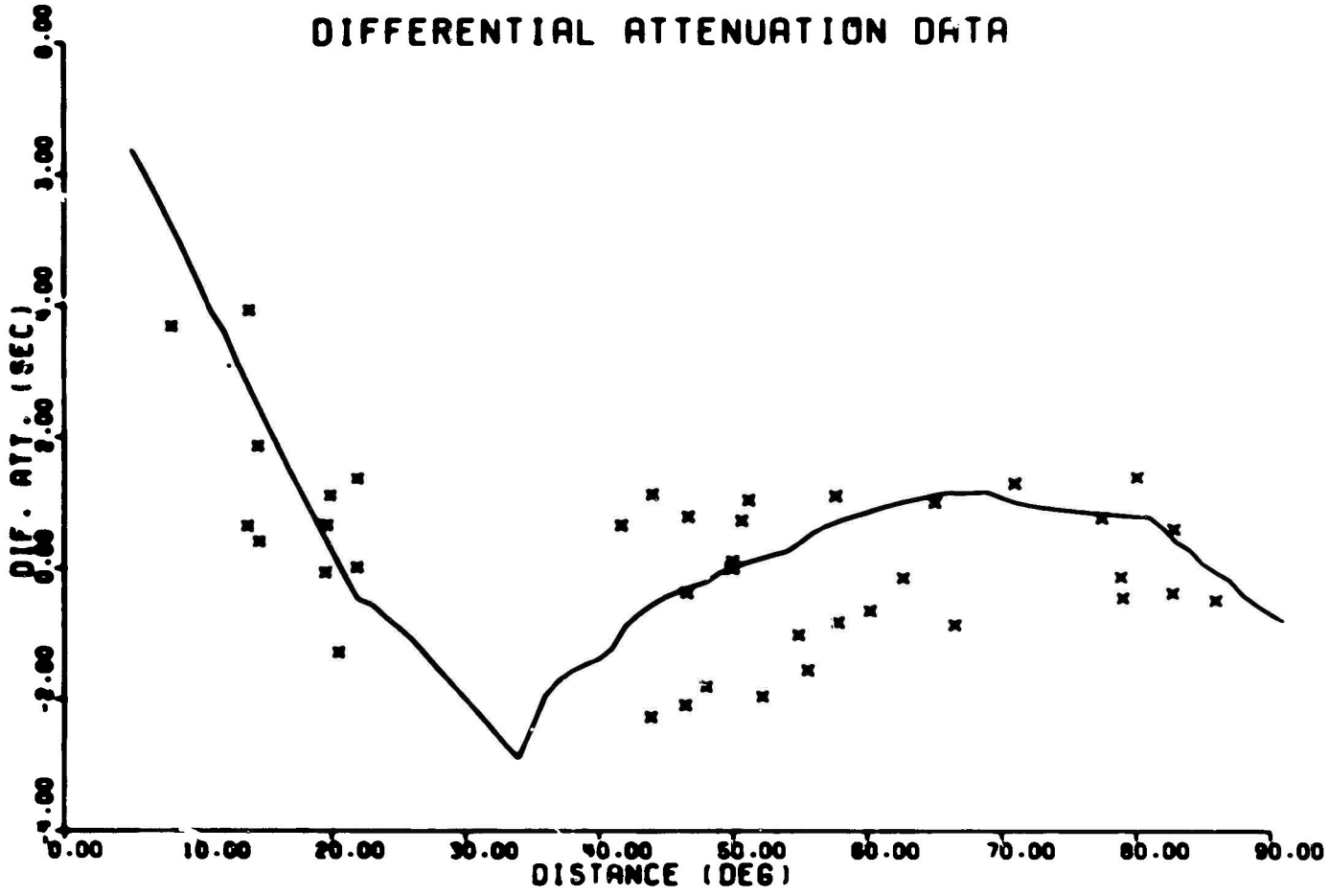
DIFFERENTIAL ATTENUATION DATA
DIF. ATT. (SEC)
3.00
0.00
-3.00
0.00
10.00
20.00
30.00
40.00
50.00
60.00
70.00
80.00
90.00
DISTANCE (DEG)

Fig 4.8

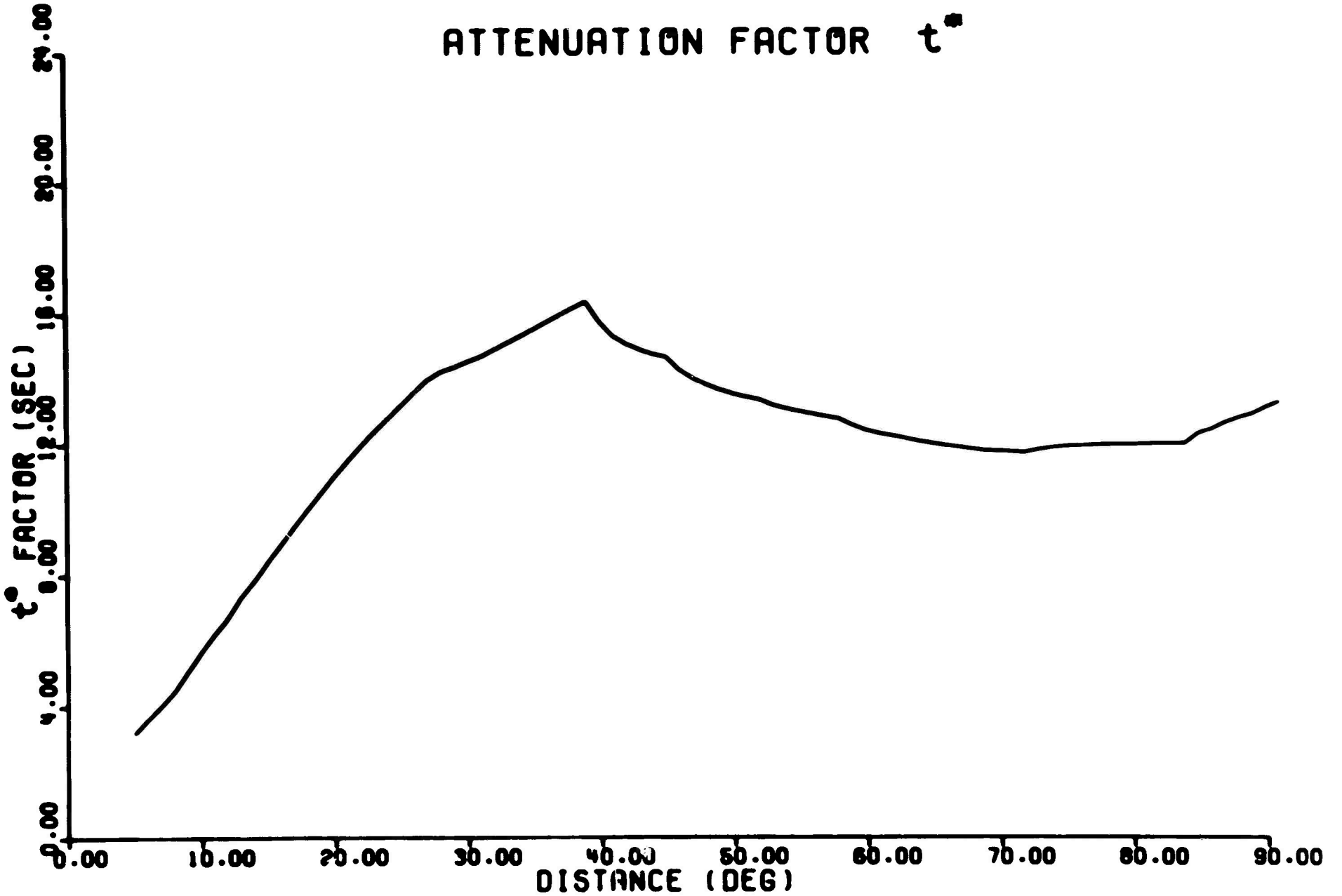
ATTENUATION FACTOR t*
t* FACTOR (SEC)
0.00
4.00
8.00
12.00
16.00
20.00
0.00
10.00
20.00
30.00
40.00
50.00
60.00
70.00
80.00
90.00
DISTANCE (DEG)

FIG 4.9

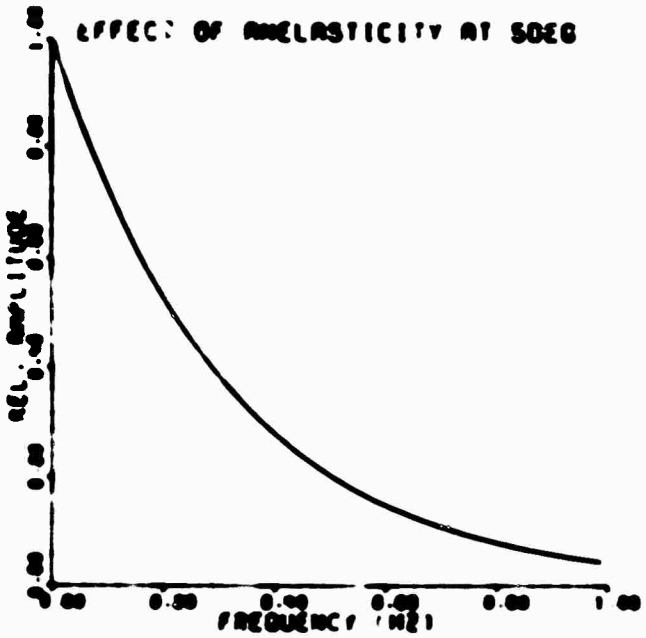
EFFECT OF ANELASTICITY AT 50EG
REL. AMPLITUDE
FREQUENCY (HZ)

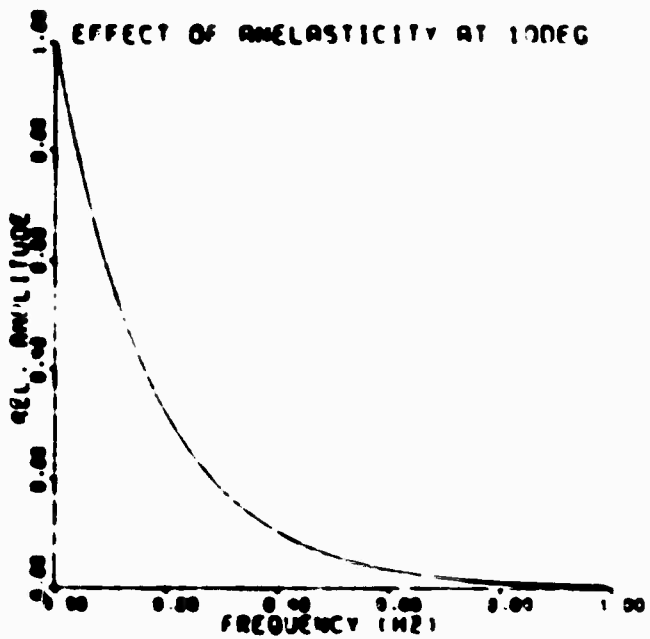
EFFECT OF ANELASTICITY AT 100EG
REL. AMPLITUDE
FREQUENCY (HZ)

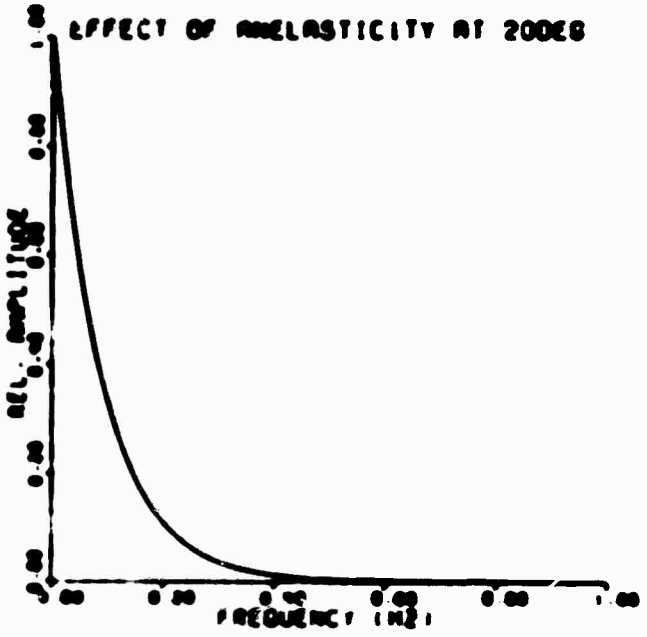
EFFECT OF ANELASTICITY AT 200EG
REL. AMPLITUDE
FREQUENCY (HZ)

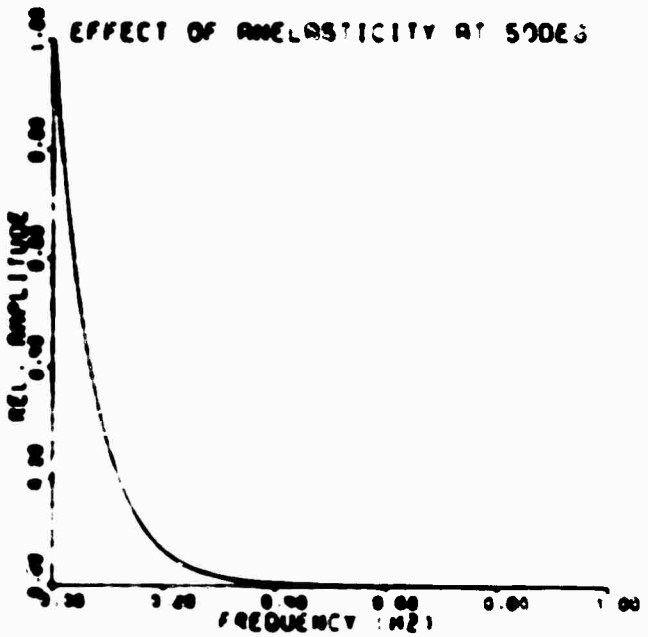
EFFECT OF ANELASTICITY AT 500EG
REL. AMPLITUDE
FREQUENCY (HZ)

FIG 4.10

Transmission in Crustal Layers

BLANK PAGE

5. The Effect of a Dipping Layer on P Wave Transmission.

Albert Rogers

Crustal inversion utilizing the amplitude spectra of P or S body waves makes possible the determination of the crustal parameters, depth and velocity contrast, beneath a single station with data from that station alone. It is, therefore, not only a very convenient way to measure qualities that are needed in other seismological studies, but it also provides a means of adding to basic knowledge about the crust. The method is particularly useful in remote areas of the earth where refraction and reflection surveys are difficult to conduct.

A number of researchers, Phinney (1), Fernandez (2,3,4) Leblanc (5), Hasegawa (6,7), Ellis and Basham (8), Castano (9), Ibrahim (10), and Utsu (11), have attempted to correlate the theoretical results predicted by the Haskell-Thomson formulation applied to body waves with body wave observed spectra. In some cases the lack of a correlation may imply the existence of a more complex model. Such complexities as anisotropy, anelasticity, and heterogeneity within the crustal system may significantly affect the amplitude response of body waves, introducing errors into the inversion process. The distortion of the transfer function may be great enough to make inversion impossible. The introduction of dip into one or more of the layers is one such complication.

In this study we examine the changes produced in the transfer function for P waves passing through a dipping layer. Two aspects are considered: the errors due to dip introduced into the crustal depth determination when the layer is erroneously assumed to be horizontal; and, the applicability of a ray theory embodying dip to improve the accuracy of the depth determination as well as to find the dip beneath the station.

We assume a single dipping layer, that is, a wedge, overlying a half-space. Plane P waves are incident from below the layer, and the diffracted waves that are generated at the vertex of the wedge are ignored. The difficulties associated with finding the normal mode solution make a first approach involving analogue seismic models and ray theory very attractive.

The ray theory we have developed is a computational scheme for summing the plane wave P and SV potentials subject to the boundary conditions expressed by Knott's equations and Snell's law. We have used the theory to determine the vertical and horizontal displacements for the multiple reflection solution for a dipping layer. In the following discussions the model study transfer function is defined as the ratio of the vertical displacement at the top of the layer to the total incident P displacement at the base of the layer. For the crustal study the transfer function is defined as the ratio of the vertical transfer function to the horizontal transfer function.

Matching of the observational transfer function to the theoretical may be accomplished by eye or analytically. When matching by eye the theoretical transfer function is plotted on log-log paper in dimensionless frequency Hf/v, where H is the depth beneath the station, v is the layer velocity, and f is frequency. One such curve represents the theoretical transfer function for any layer depth and velocity, for a given velocity contrast, angle of incidence, and angle of dip. The observational curve is plotted on log-log paper of the same cycle size. The curves are then superimposed and translated without rotation until a fit is observed. The depth is determined by reading from the axes any two corresponding values of Hf/v and f, and assuming a value for the layer velocity.

A more objective method was developed using the correlation coefficient and the mean square deviation defined by (1):

$$\text{Correlation coeff} \equiv r_{ij} \equiv \frac{\sum_{\alpha=1}^{N}(y_{i\alpha}-\bar{y}_i)(y_{j\alpha}-\bar{y}_j)}{\left[\sum_{\alpha=1}^{N}(y_{i\alpha}-\bar{y}_i)^2\sum_{\alpha=1}^{N}(y_{j\alpha}-\bar{y}_j)^2\right]^{1/2}}$$

$$\text{Mean sq. dev.} \equiv S_{ij}^2 \equiv \frac{1}{N}\sum_{\alpha=1}^{N}(y_{i\alpha}-y_{j\alpha})^2 \qquad (1)$$

where y_i equals the theoretical transfer function and y_j equals the observational transfer function. The correlation coefficient is computed about the mean $\bar{y}$, and normalized by the standard deviation so that it is primarily a measure of the degree of equality in shape of the two variables y_i and y_j. The mean square deviation chiefly determines the degree of

equality in amplitude between the two curves.

The mean square deviation was computed after fitting the two transfer functions by eye and normalizing them at corresponding values in the range of the peak seismograph magnification.

In order to analytically shift the two transfer functions past one another in the search for the best fit, they were linearly interpolated at intervals of .01 log frequency and log dimensionless frequency. The correlations were determined for earthquake data for lag values measured in kilometers between 15 km and 90 km. This is less than $\pm$ 15% of the total lag measured from the zero lag position. The model data lag values varied between 16 and 30 mm, which is less than $\pm$ 7% of the total lag. The number of independent points used in the region of maximum fit varied from 40 to 50 for the earthquake data and was equal to 23 for the model data.

In the evaluation of the ray theory we have studied the effects on the earthquake transfer function of variations of velocity contrast, depth, angle of emergence, angle of dip, and spectral resolution. The transfer functions have been evaluated for a Poisson's ratio of .25 and a density ratio of .83.

Figure (5.1a) shows the earthquake transfer function for velocity ratios of .9, .8, and .7. It is apparent that increasing the contrast increases the level of the peaks but does not appreciably alter the shape of the curves. What

differences are present are due to the fact that the curves have unavoidably been smoothed in a slightly different manner. The nature of the program for obtaining the curves also makes it inconvenient to obtain values at exactly the same intervals of dimensionless frequency. These transfer functions were evaluated for 10° of dip and 60° angle of emergence.

Figure (5.1b) shows the transfer function for two values of depth with a dip 10° and an angle of emergence 126°. It is clear that changes in depth produce no changes in the shape or level of the transfer function. Any changes which are present can be explained by the argument given above. Likewise, we could expect there to be no change in the transfer function level or shape had only the layer velocity been changed with contrast velocity.

Variations of the angle of incidence reveal that the level of the transfer function increases without major character change as the angle of incidence varies from 50° to 60°. There is a major character change between 60° and 100° as wave propagation goes from up to down dip. As the angle of incidence varies from 100° to 130° the level of the transfer function decreases without major character change.

We used the correlation coefficient to determine the theoretical error resulting from fitting a 0° dip theoretical transfer function to 0°, 5°, 10°, 15°, 20°, 25°. Equivalently, transfer functions plotted in frequency were shifted past the 0° transfer function plotted in dimensionless frequency and the correlation and mean square deviation were determined.

The values are given in Table 1 for the up and down dip cases. For waves incident at 60° the correlation coefficient goes through a minimum at 60°. There ceases to be any measurable fit as the dip varies from 60° to 75°. "No fit" indicates that all values of the correlation fluctuate around zero or some lower value with no well defined maximum. The mean square deviation increases rapidly in the region 0° to 10°, is constant near 10° and 15°, and begins to increase again beyond 15°. The depth values are determined at points of maximum correlation, and it is evident that error in the depth determination is less than 5% in all cases and less than 2.5% for dips less than or equal to 10°. For waves incident at 120° the correlation coefficient goes through a minimum or region of no fit at 15° and again at 25°. The mean square deviation increases continuously as the dip increases. The error in the value of the depth varies from 2% to 7%. This indicates that in most instances the depth of the layer may be determined within 7% by matching to the transfer function for a horizontal layer even though the layer may have dips up to 20°. However, the degree of correlation may be small or zero in some cases. It is this fact that may permit the determination of the dip as well as the depth.

It is useful to study the value of the correlation coefficient from a statistical viewpoint. We may test whether the value of r_{ij} differs significantly from zero or whether two r_{ij} values differ significantly from each other. We may also determine confidence limits of the correlation in the

population. If we test the null hypothesis H_0 that the theoretical transfer functions compared above are uncorrelated, that is drawn from a normal bivariate population with $\rho r_{ij} = 0$, against the alternative hypothesis H that they are positively correlated, it is found that a positive correlation exists in all cases except for the instances of no fit. If the value of $r_{ij} \geq .214$ (this number applies only to these theoretical curves), H is accepted at the 95% level of significance. A value of r_{ij} this large due to chance would occur only once in twenty times if the sample is drawn from a population with $\rho r_{ij} = 0$.

It is more informative, perhaps, to test if the measured values of the correlation are taken from a population of high correlation, say $\rho r_{ij} = .9$. The 95% confidence limits given in Table 1 indicate that only the 5° correlations (including the 0° cases) for both angles of emergence could have been taken from a population of high correlation. In all other cases we would be forced to accept the alternative hypothesis of low correlation. The Haskell-Thomson model yields statistically significant correlations when dips less than 5° are present. For dips greater than 5° their model does not give significant correlations, and in some cases the correlation is low or zero. Theoretically, even in cases of low correlation, the depth may be determined within 7%.

In the theoretical studies of the spectral resolution we measured the effect on the transfer function of applying a Hamming window of 80, 40, and 20 sec length to theoretical

seismograms. Windows as short as 20 sec have no effect on the accuracy of the depth determination for a 50 km crust. However, a short window may smooth the transfer function enough to make a dip determination impossible.

The analogue model study was conducted in an effort to investigate under controlled laboratory conditions the accuracy of the crustal inversion process. It also provided a test of the ray theory. The experiments were designed for the measurement of the vertical transfer function for three values of dip, 5°, 7.5°, 10°, and for vertically incident waves. To what extent the model results apply to crustal transfer functions is unknown; however, subsequent analysis reveals that conclusions based on the model results are entirely comparable to the conclusions reached using the theoretical crustal transfer functions.

For the experiments we used a two dimensional model, Figure (5.2), with a 1/8 inch thick aluminum alloy half-space and a Plexiglas layer. The model was actually constructed with the solid-solid interface horizontal and the dip in the free edge of the layer. The depth from the receiver to the half-space, measured along the normal to the free surface, was constant for all three cases. For the free surface to represent a horizontal plane, as in the real earth, the receiver was displaced from the model vertical by an angle equal to the angle of dip. These two steps insured that the amplitude response that was observed reflected only changes in the angle of dip. The lower receiver measured the source

function and was the same distance from the source as the source was from the base of the layer beneath the receiver.

The two centimeter layer thickness beneath the receiver was chosen as a compromise. If the layer depth were much shallower, the major spectral peaks and troughs would become widely spaced and shift to high frequencies (based on the formula for normal incidence to a horizontal layer). The source function would illuminate few or none of the peaks and troughs in such a spectrum. On the other hand, if the layer depth were made much greater, the peaks and troughs would become so closely spaced that they could not be resolved by the available spectral resolution. In addition, the two-way travel time increases and few multiples would be observed before interfering phases from the sides of the model arrive.

Capacitive receivers were used, and silver acetylide explosive charges served as the energy source. When properly formed, these charges yielded a simple broad-band signal, 5 kHz to 300 kHz, that adequately illuminated the layer amplitude spectrum.

A comparison between the theoretical and observed model transfer function is plotted in Figure (5.3). The degree of fit appears "best" in the 5° and 10° cases. The 7.5° results are not as significant due to the interference of antisymmetric modes. This problem was overcome for the 5° and 10° experiments. The regions of significant deviation are below 50 kHz as evidenced by an increase in amplitude and shift to lower

frequency in relation to the theoretical. However, the ray theory is not valid in this frequency band, since the wavelengths are 2 to 15 times the layer thickness. Above 160 kHz there is a distinct frequency dependent shift of the observed peaks and troughs towards frequencies lower than the theoretical. This is accounted for by the occurrence of geometrical dispersion and the breakdown of two-dimensionality in the model. The condition for destructive interference for normal incidence to a horizontal layer is given by,

$$f \propto V/4H$$

and, therefore, a change in velocity produces a proportional change in the frequency of interference.

$$\Delta f \propto \Delta V/4H$$

or

$$\Delta V/f = \Delta V/V$$

Comparing the observed and experimental for 5° reveals that the trough at 230 kHz (theoretical) appears at 211 to 216 kHz, a proportional decrease in percentages of 6-8%. The phase velocity of a 1/8" thick Plexiglas layer at 230 kHz is determined from the equation (after Tolstoy and Usdin (12)):

$$\frac{\tan\left[\left[1-c^2/\beta^2\right]^{1/2} kh/2\right]}{\tan\left[\left[1-c^2/\alpha^2\right]^{1/2} kh/2\right]} = \frac{4\left[1-c^2/\alpha^2\right]^{1/2}\left[1-c^2/\beta^2\right]^{1/2}}{\left[2-c^2/\beta^2\right]^2}$$

The zero frequency limit of the phase velocity is

$$c = a\sqrt{\mu/\rho} = 1.63 \text{ mm}/\mu\text{s}$$

The principle root of the transcendental equation using the model constants and 230 kHz is c = 1.60 mm/μs. This represents a decrease in the velocity of 6%.

The correlation coefficient technique was employed to analytically measure the error in the depth determination as well as to study the feasibility of measuring the dip. Table (2) shows the results of comparing each of the experimental spectra to their corresponding theoretical spectra. Only the values up to 160 kHz were used in order to exclude the effect of geometrical dispersion. As was observed by eye, the degree of fit is better in the 5° and 10° spectra according to the measured values of the correlation coefficient and the mean square deviation. The measured depths of the layers beneath the receiver were 20.0 mm, 20.3 mm, and 20.5 mm, for the 5°, 7.5°, and 10° layers respectively. The measurements include the epoxy bonding layer as well as the foil used as one plate of the receiver pickup. The values of depth determined using the correlation coefficient are in error by about $\pm$ 1%. An error of this size may be made in measuring the depth; in addition, the correlation was computed in intervals of .46 mm, and, therefore, the depth may be in error by $\pm$ .23 mm or approximately $\pm$ 1%. It is evident that the depth of a layer may be determined to a high degree of accuracy in a controlled experiment even though the correlation may be small. This conclusion is in agreement with previous theoretical results.

A set of WWSSN earthquake records were chosen and analyzed in order to determine the practicability of applying these results to the real earth. Long period records were chosen even though portions of the spectral band violate the regions of validity of the ray theory (wavelength much longer than the layer thickness). The frequencies used were .0125 cps. to .6 cps which represent wavelengths varying from 10 to 1/5 the layer thickness. Table (3) gives all the pertinent earthquake statistics.

The theoretical transfer functions were evaluated using the required angle of incidence, a fixed velocity contrast of .6, and a fixed density contrast of .83. Table (4) contains the results of comparing theoretical to observed transfer functions for dips of 0° through 30° in 5° increments for two earthquakes recorded at Antofagasta. Two features clearly stand out. First, the correlation coefficients have double valued maxima, and second, the correlation goes through a minimum at 10°. The double values are due to the "periodic" nature of the transfer function. Comparing the two regions of fit by eye indicates the fit for the smaller depth to be best. Geologically, the smaller depth seems more likely since Antofagasta is on the Chilean coast about 120 km from the trench axis. However, there is some evidence suggesting the larger depth based on refraction and gravity surveys. This evidence will be discussed further, subsequently. The fact that the value of the correlation coefficient goes through a minimum at 10° was also noted

in Table (1) where two theoretical transfer functions were compared. Those functions are also the theoretical curves for Antofagasta. This indicates that the increase in the value of the correlation above 10° cannot be associated with actual dips that large. Furthermore, the confidence intervals indicate that for the earthquake of 17/01/67, the 0° and 5° spectra represent a significantly better fit at the 95% level than do any other cases. The confidence intervals also indicate that we cannot statistically differentiate between 0° and 5° of dip; however, we may accept the values as "indicators" of the true dip. The 5° case appears to be slightly more significant when both the correlation and mean square deviation are taken into account for both earthquakes. This result agrees with the "best" fit by eye. The values of the depth that are obtained for 5° of dip are 47.2 km and 45.0 km. The mean is 46.1 with a standard deviation of $\pm$ 1.5 km. The final fit that is obtained for both earthquakes is shown in Figure (5.4).

The results for earthquakes recorded at Nana, La Paz, and Arequipa are given in Table (5). The correlation coefficients and the 95% confidence intervals for NNA reveal that the 0° and 5° theoretical curves do not correlate positively with the observational spectrum. Positive correlations do exist for 10°, 15°, and 20° of dip with the maximum occurring at 15°, although the maximum is not significantly different than the other values at the 95% level. Taking into account both the correlation coefficient and the mean

square deviation, the best fit is for a layer dipping 15° SE and a depth of 74.7 km. Figure (5.5) shows the chosen fit.

Positive correlations are found for LPB; however, the degree of visual correlation shown in Figure (5.5) is poor. In the case of ARE there are no positive correlations and the visual fit is also poor. Hence no conclusions regarding these data will be drawn. Both of these stations are at high elevations, and it is likely that the crustal structure beneath them is complex.

The crustal depth determined at Antofagasta is in good agreement with results of refraction data slightly to the northeast. Aldrich et al (13) give a value of 46 km based on a one layer crust, with velocity 6.0 km/sec. There are indications of a two layer crust with a second layer velocity of 7.0 km/sec and total crustal thickness of 56 km. Our data possibly have two interpretations as well, since a fit was also obtained for a 57.3 km crust. Study of two layer transfer functions (Fernandez (14)) indicate that for some velocity ratio and depth combinations it is possible that the transfer function became "doubly periodic" in relation to the one layer transfer function. That is, for each peak in the one layered transfer function, there are two in the two layered case. Therefore, in fitting a one layered theoretical transfer function to a two layered observational spectrum, two matches may actually be possible.

Gravity data interpreted by Lomnitz (15) near Antofagasta also support a larger value, near 55-60 km.

The dip of the Moho near both the Peruvian and Chilean coasts is between 5^{o} and 10^{o} using data and interpretation of Fisher and Raitt (16), Woolard (17), and Tatel and Tuve (18). Lomnitz (15) north-south gravity profile in Chile indicates a crust dipping gently (approx. $1/2^{o}$) to the north leading to crustal depths of 70 km beneath northern Chile and southern Peru. Our 75 km depth determination at Nana indicates that a deep crust extends into northern Peru as well. Geologically, we may expect a deep crust at Nana, since it is located at the foot of the Andes about 240 km from the trench axis - twice as far as Antofagasta is from the trench axis.

References

1. Phinney, R. A. (1964). Structure of the earth's crust from spectral behavior of long-period body waves, Journ. Geophys. Res., 69, 2997-3018.

2. Fernandez, L. M. (1967). Master curves for the response of layered systems to impressional seismic waves, Bull. Seism Soc. Am., 57, 515-543.

3. Fernandez, L. M. and J. Careaga (1966). The thickness of the crust in central U.S. and LaPaz, Bull. Seism. Soc. Am., 56, 711-741.

4. Fernandez, L. M., J. Careaga and G. Da Silva (1968). Influence of a slipping crust on the spectrum of "P" seismic waves, paper presented at the AGU Annual Meeting, 1966, Washington, D.C. (abstracted in Trans. Am. Geophys. Union, 49, No. 2, 1968).

5. Leblanc, Gabriel (1966). Spectral analysis of short-period first arrivals of April 13, 1963 Peruvian earthquake, Ph.D. thesis, Pennsylvania State University.

6. Hasegawa, H. S. (1969). A study of the effect of the Yellowknife crustal structure upon the coda of teleseismic events, Geophys. J. R. Astro.Soc. 18, 159-175.

7. Hasegawa, H. S. (1970). Short-period P-coda characteristics in the eastern Canadian Shield, Bull. Seism. Soc. Am., 60, 859-868.

8. Ellis, R. M. and P. W. Basham (1968). Crustal characteristics for short-period P waves, Bull. Seism. Soc. Am., 58, 1681-1700.

9. Castano, Juan C. (1967). The determination of crustal thickness in Central America from the spectra of dilatational body waves, M.S. thesis, St. Louis University.

10. Ibrahim, Abou-Bakr K. (1969). Determination of crustal thickness from spectral behavior of SH waves, Bull. Seism. Soc. Am., 59, 1247-1258.

11. Utsu, T. (1966). Variations in spectra of P waves recorded at Canadian Arctic seismograph stations, Can. J. Earth Sci., 3, 597-621.

12. Tolstoy, I. and B. Usdin (1953). Dispersive properties of stratified elastic and liquid media: a ray theory, Geophysics, 18, 493-512.

13. Aldrich, L. O., H. E. Tatel, M. A. Tuve, and O. W. Wetherill (1958). The earth's crust, Carnegie Inst., Wash. Year Book 57, 104-111.

14. Fernandez, L. M. (1965). The determination of crustal thickness from the spectrum of P waves, St. Louis University, Scientific Report No. 13, Contract AF 19(604)-7399.

15. Lomnitz, C. (1962). On Andean structure, J. Geophys. Res., 67, 351-363.

16. Fisher, Robert L. and Russell W. Raitt (1962). Topography and structure of the Peru-Chile trench, Deep-sea Research, 9, 423-443.

17. Woollard, G. P. (1960). Seismic crustal studies during the IGY. Part II: Continental Program, Trans. Am. Geophys. Un. 41, 351-355.

18. Tatel, H. E. and M. A. Tuve (1958). Seismic studies of the Andes, Trans. Am. Geophys Un. 39, 580-582.

Table 1

	Corr. Coeff.	95% Correlation Confidence Limits		Mean Sq. Dev.	Normalizing - Theo.	Factor Observ.	Depth (km)
			54° Updip				
0°vs0°	1.000	1.0	1.0	.000	1.0	1.0	50.0
" " 5°	.964	.974	.990	.001	"	"	51.2
" " 10°	.391	.170	.577	.028	"	"	48.9
" " 15°	.574	.390	.719	.027	"	"	52.3
" " 20°	.668	.580	.780	.039	"	"	51.2
" " 25°	No fit	--	--	--	"	"	--
			126° Downdip				
0°vs0°	1.000	1.0	1.0	.000	1.0	1.0	50.0
" " 5°	.901	.845	.937	.004	"	"	48.9
" " 10°	.725	.560	.820	.009	"	"	46.7
" " 15°	No fit	--	--	--	"	"	--
" " 20°	.309	.074	.507	.042	"	"	53.6
" " 25°	No fit	--	--	--	"	"	--

Table 2

5°vs5°	.726	.451	.875	.074	5.957	5.102	20.20 mm
7.5°vs7.5°	.249	-.174	.595	.223	6.969	2.948	20.20 mm
10°vs10°	.393	-.017	.690	.178	4.719	3.223	20.67 mm

Table 3

Sta.	Date	Lat.	Long.	Origin Time (GMT)	Depth (km)	Epicentral Distance (deg)	Mag. (COS)	Azimuth Epi. to Sta.
ANT	17/01/67	27.4S	63.3W	01 07 54.3	588	7.4	5.6	298.6°
ANT	05/03/65	27.0S	63.3W	14 32 19.2	573	7.2	5.5	295.8°
ARE	09/09/67	27.7S	63.1W	10 06 44.1	578	13.6	5.8	323.5°
LPB	23/08/68	22.0S	63.5W	22 36 51.3	537	7.0	5.8	320.6°
NNA	09/09/67	27.7S	631.W	10 06 44.1	578	13.6	5.8	317.8°

Table 4

ANT 17/01/67

	Corr. Coeff.	95% Correlation Confidence Limits		Mean Sq. Dev.	Normalizing Factor Theo.	Obsery.	Depth (km)
0° vs observ.	.715	.538	.835	.117	1.038	1.100	46.3
"	.699	-	-	.160	"	"	56.7
5° "	.666	-	-	.120	"	"	47.2
5° "	.674	-	-	.164	"	"	56.7
10° "	no fit	-	-	-	"	"	-
15° "	.199	-.099	.464	.183	"	"	46.1
15° "	.313	-	-	.264	"	"	59.4
20° "	.295	-	-	.190	"	"	47.2
20° "	.382	.10.	.609	.267	"	"	59.4
25°&30° obs.	no fit	-	-	-	"	"	-

ANT 05/03/65

0° vs observ	.309	-	-	.046	2.185	1.146	46.1
0° "	.361	-	-	.039	"	"	59.4
5° "	.332	-	-	.042	"	"	45.0
5° "	.366	-	-	.038	"	"	58.0
10° "	.333	-	-	.054	"	"	43.0
15° "	.438	-	-	.053	"	"	49.4
20° "	.410	.167	.625	.042	"	"	45.0
25°&30° obs	no fit	-	-	-	"	"	-

Table 5

	Corr. Coeff.	95% Correlation Confidence Limits		Mean Sq. Dev.	Normalizing Factor Theo.	Normalizing Factor Observ.	Depth (km)
NNA							
0° vs observ.	.239	-	-	.054	1.974	1.750	76.5
5° "	.282	-.010	.524	.052	"	"	74.7
10° "	.464	-	-	.051	"	"	74.7
15° "	.482	.219	.680	.051	"	"	74.7
20° "	.478	-	-	.059	"	"	77.1
25°&30°obs	no fit	-	-	.059	"	"	-
LPB							
0° vs observ	.360	-	-	.027	.920	.700	41.1
0° "	.323	.033	.564	.025	"	"	82.0
5° "	.345	-	-	.030	"	"	40.1
5° "	.335	-	-	.028	"	"	80.1
10° "	.453	-	-	.031	"	"	78.3
15° "	.468	-	-	.036	"	"	78.3
20° "	.477	.213	.675	.050	"	"	60.1
25°&30°obs	no fit	-	-	-	"	"	-
ARE							
0° vs observ	.207	-	-	.034	1.949	1.474	63.6
5° "	.195	-	-	.035	"	"	62.2
10° "	.243	-	-	.031	"	"	53.3
15° "	.242	-	-	.035	"	"	54.6
20° "	-.243	-.053	.500	.044	"	"	53.9
25°&30°obs	no fit	-	-	-	"	"	-

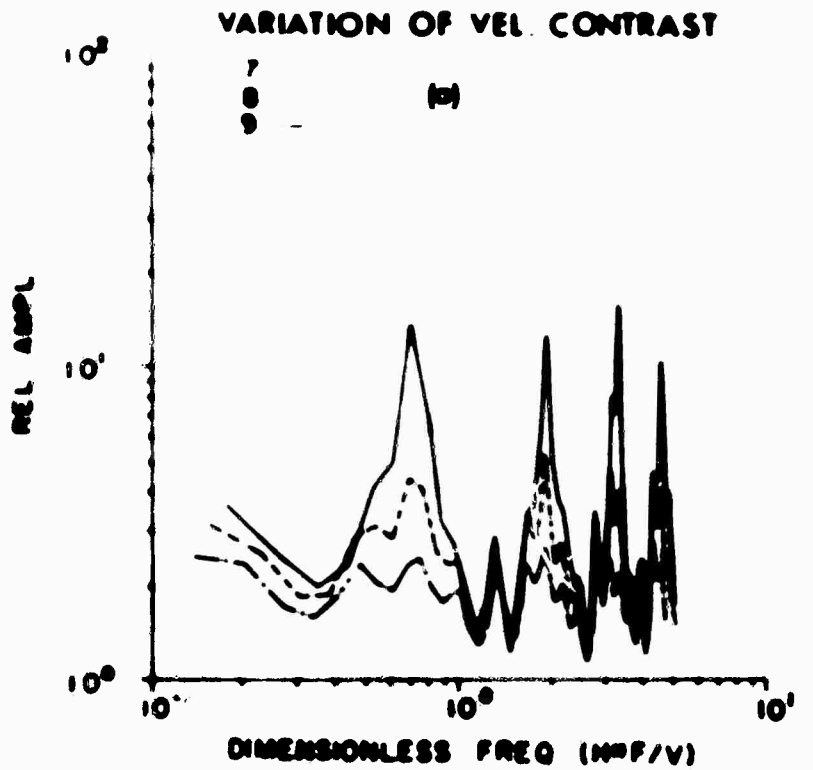
VARIATION OF VEL. CONTRAST
(a)
REL AMPL
DIMENSIONLESS FREQ (H=F/V)

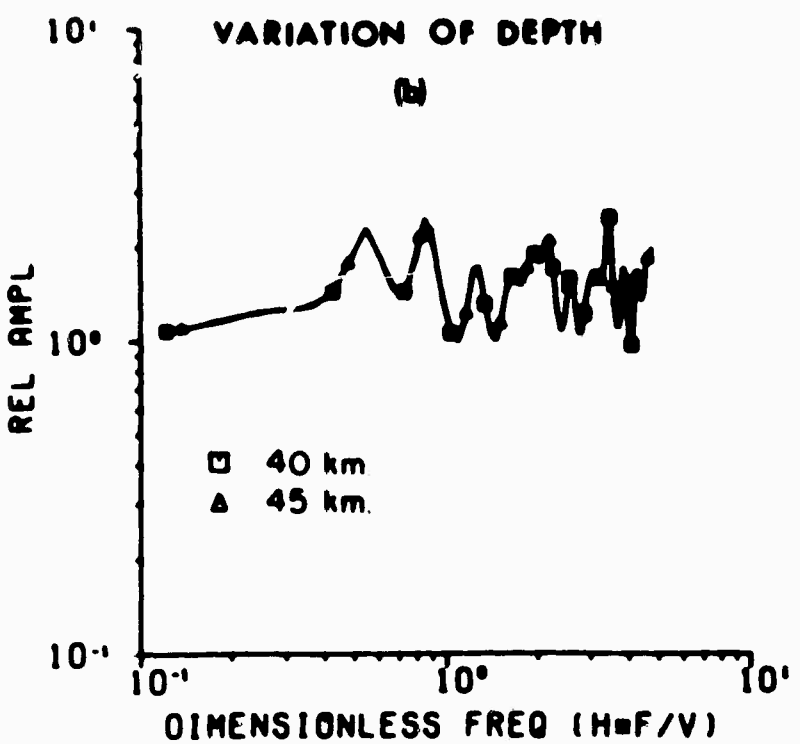
VARIATION OF DEPTH
(b)
REL AMPL
40 km
45 km
DIMENSIONLESS FREQ (H=F/V)

FIG 5.1

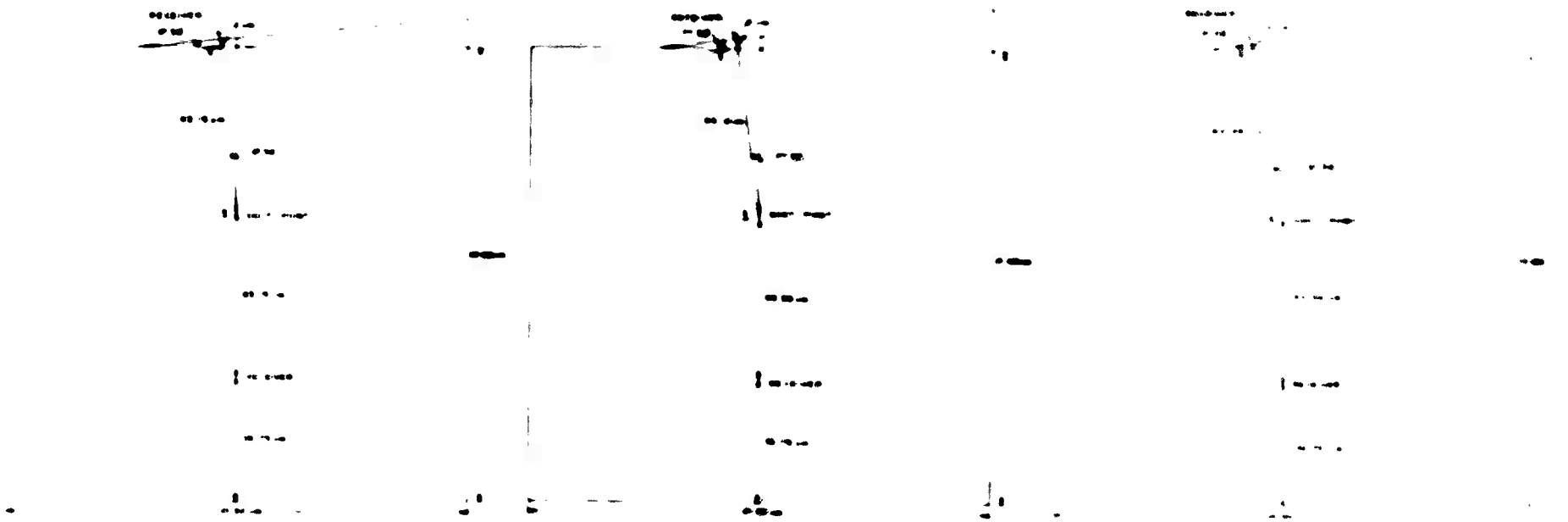

Fig 52

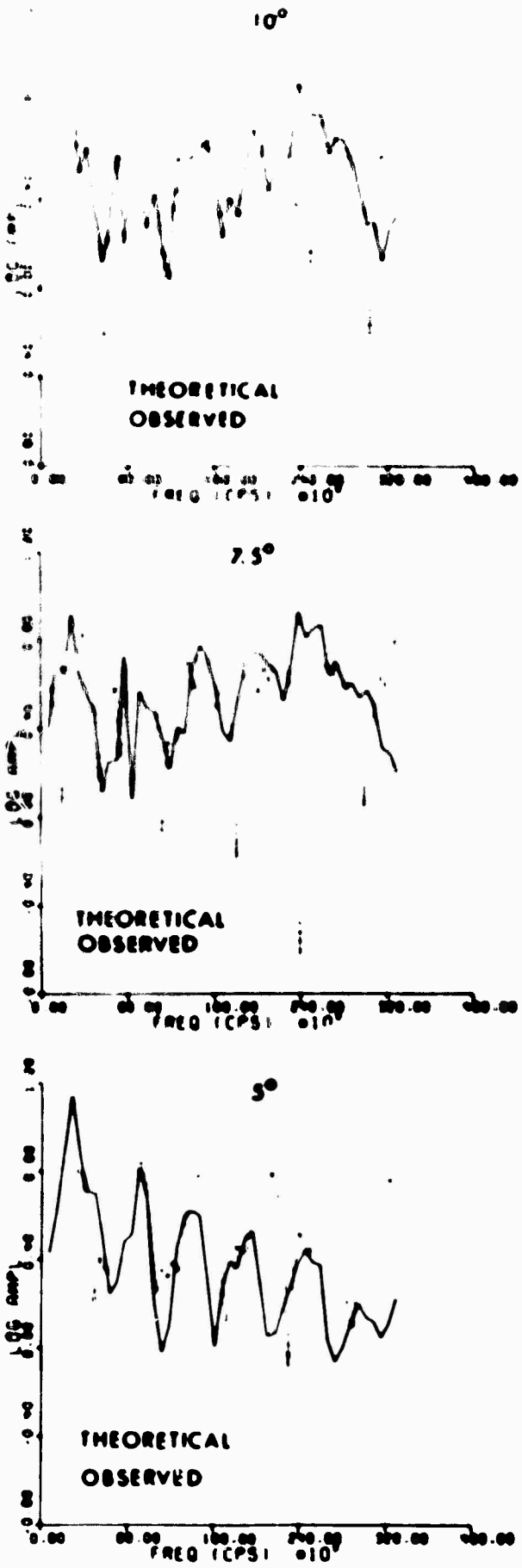
10°
THEORETICAL
OBSERVED
FREQ (CPS)
7.5°
THEORETICAL
OBSERVED
FREQ (CPS)
5°
THEORETICAL
OBSERVED
FREQ (CPS)

FIG 5.3

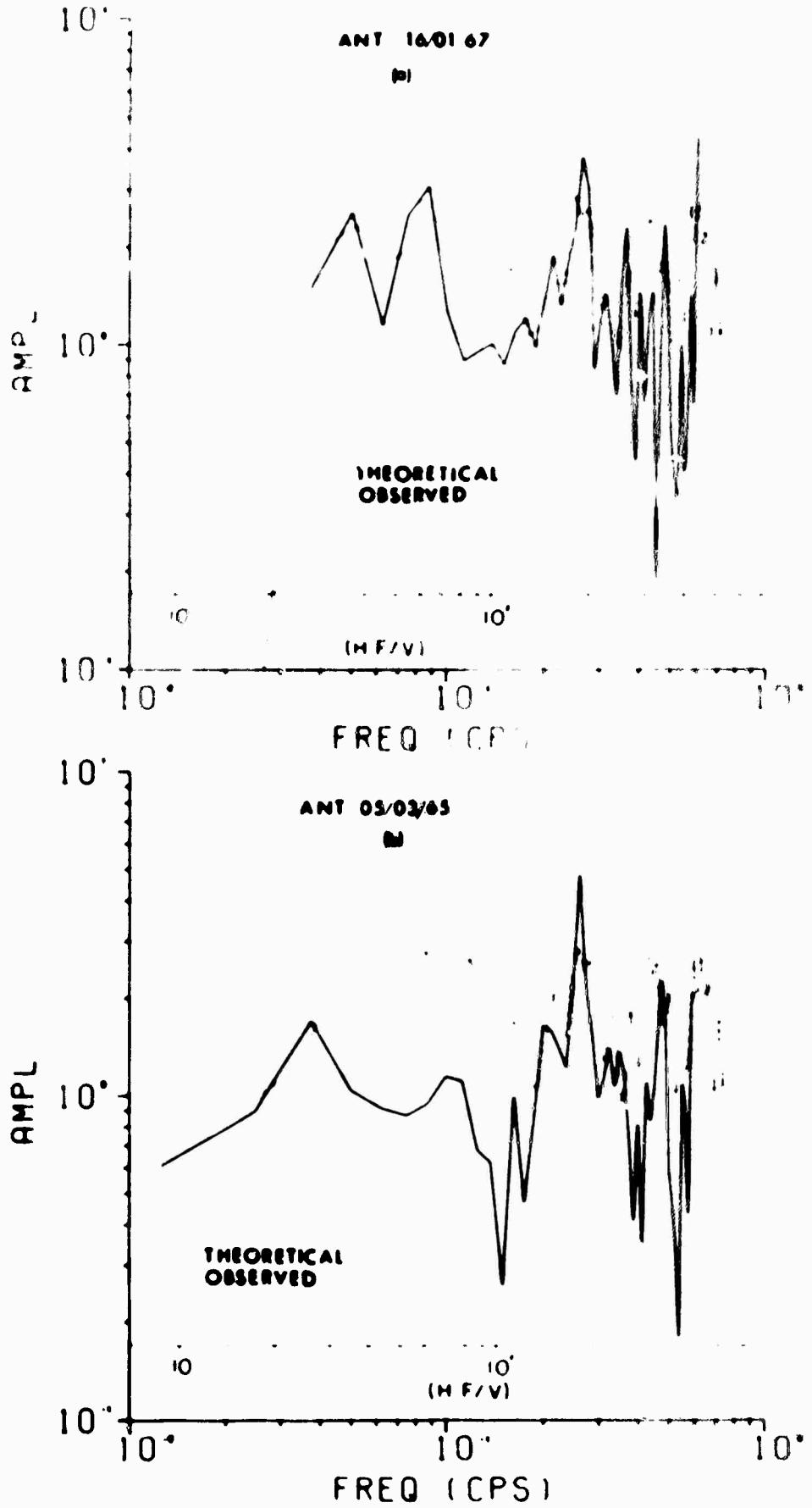
ANT 16/01 67
(P)
THEORETICAL
OBSERVED
(H F/V)
FREQ (CPS)
ANT 05/02/65
(M)
AMPL
THEORETICAL
OBSERVED
(H F/V)
FREQ (CPS)

FIG 5.4

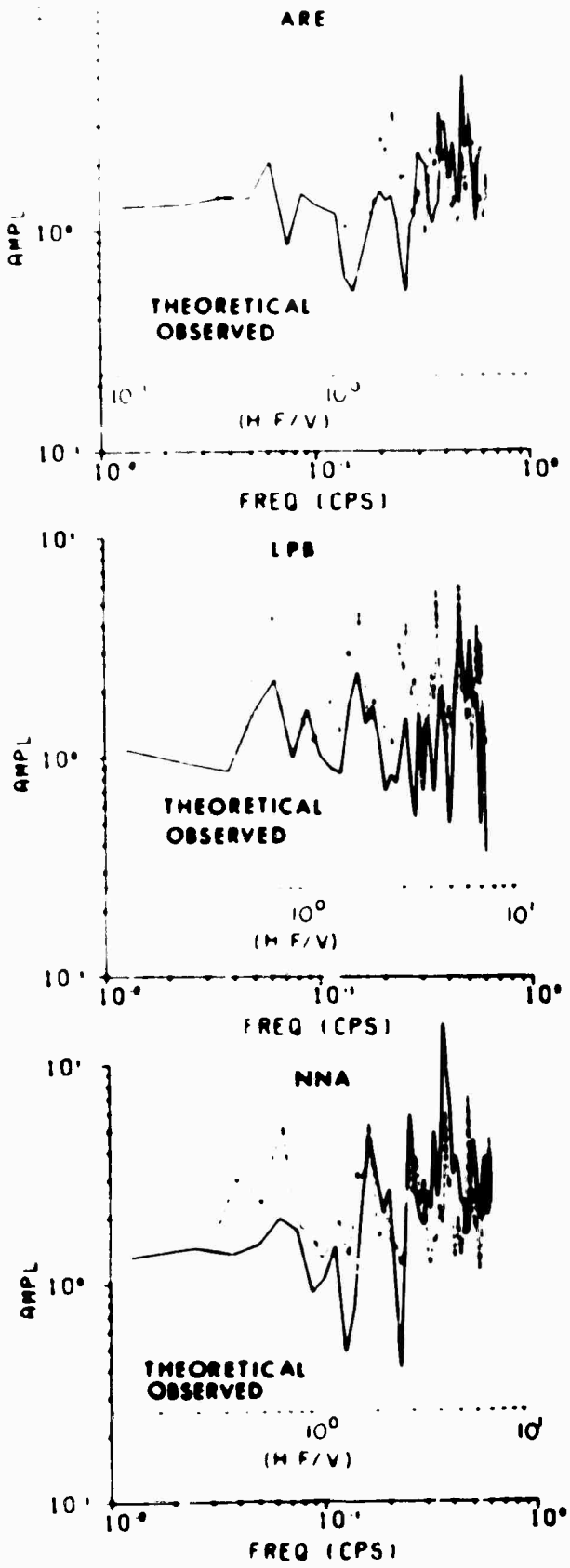
ARE
AMPL
10°
THEORETICAL
OBSERVED
10⁻¹
10⁰
(H F/V)
10⁻¹
10°
10⁻¹
10°
FREQ (CPS)
LPB
AMPL
10°
THEORETICAL
OBSERVED
10°
10¹
(H F/V)
10⁻¹
10°
10⁻¹
10°
FREQ (CPS)
NNA
AMPL
10°
THEORETICAL
OBSERVED
10°
10¹
(H F/V)
10⁻¹
10°
10⁻¹
10°
FREQ (CPS)

FIG 5.5

Tectonic Strain Release and Test Monitoring

BLANK PAGE

6. Geological Factors Affecting Triggering and a Model of Aftershock Production.

by Carl Kisslinger

It is known that when an explosion is fired in a solid medium under stress, the resulting seismic signal is altered from that produced by a similar explosion in an unstressed medium. With reference to the specific problem of monitoring underground explosions, the important question is whether this alteration of the signal can make the detection, location, or identification of the event more difficult. The principal concern is whether the concurrent release of tectonic strain energy at the time of the explosion can sufficiently alter the seismic signal to make application of identification criteria less certain. A closely related question is whether it might be possible to intentionally place an explosion in a tectonic environment in which a large release of tectonic strain by faulting would occur, i.e. a large earthquake would be triggered intentionally, as an evasion technique.

An ambient field stress field will affect the seismic signal through several mechanisms. Of these, the least important for the present problem is the introduction of a small amount of velocity anisotropy because of the stress dependence of the elastic moduli. More important is the control exerted by the ambient stress on the generation of tensile fractures. In a homogeneous isotropic unstressed

material, the tensile fractures that mark the outer limits of non-elastic behavior will be distributed more or less uniformly around the shot cavity, with essentially the same length, so that the basic spherical symmetry of the source is not markedly disturbed. If, however, an appreciable prestress is present, tensile cracks in a few directions will grow to considerable length. Prestress is not the only condition that can result in preferential fracturing. Planes of weakness resulting from depositional processes will have a similar effect, especially in surficial materials.

A propagating tensile fracture is a source of seismic waves and these will be superimposed on the primary signal from the explosion. This is one mechanism by which S waves are generated directly by the explosion (Kisslinger, et al, 1961). The energy for these waves is derived from the expanding explosion products and the role of the ambient stress is primarily that of determining the direction of crack propagation.

Finally, prestress will result in the production of a seismic signal due to release of stored elastic strain energy in response to the shot. One way in which this will occur is as a result of the sudden creation of an enlarged cavity in the medium. Another, potentially more dramatic, is the occurrence of slip on fault surfaces in response to the explosive loading.

It is this last effect, the triggering of a tectonic earthquake by the explosion, that is most likely to cause

difficulty in applying discrimination criteria. However, a concurrent earthquake can cause difficulty only if it generates seismic waves comparable in energy to those produced by the explosion itself. An earthquake with magnitude equal to or exeeeding the seismic magnitude of the explosion has not yet been triggered, but because earthquakes generate wave types and put energy in frequency bands that are not strongly excited by explosions, there is evidence from the seismic signals of earthquake generation.

Geological Factors Affecting Triggering.

Our attention has been directed to the question of the circumstances under which triggering will occur and the environmental factors that determine the extent of the faulting.

Of the numerous questions raised by the available field observations of explosion-induced faulting, one of the most interesting is whether the extent of faulting scales with the yield of the explosion. The alternative is that the action is one of triggering such that once the yield exceeds some threshold, rupture begins and its extent is determined by the ambient stress and strength of the material and is independent of the yield. McKeown and Dickey (1969) have published data for Pahute Mesa that shows a straightforward relation of fault length to yield. This dependence, when combined with the absence of aftershocks on these faults, indicates that the prestress is well below that at which slip would occur naturally and the slippage is driven by

the stress pulse from the explosion. However, the occurrence of appreciable slip and of some aftershocks, especially after Benham, is evidence that a sizable tectonic stress field is present in the rocks of Pahute Mesa.

The fact that Boxcar, Benham, Handley and Jorum all produced visible surface faulting of about the same extent, but only Benham produced large numbers of aftershocks has not been explained. A possible explanation is inherent in a model of the local structure that was suggested by Cummings (1968), Figure 6.1. He modelled the Timber Mountain caldera as a hole in a homogeneous elastic plate under uniform tension. He used this model to account for the orientation of the numerous faults that intersect the caldera boundary, including those in the neighborhood of the events under discussion. Though the model is undoubtedly too simple, it does account for the orientation of the faults fairly well and is a credible representation of the situation.

In this model, the large events on Pahute Mesa are located roughly along the line at right angles to the direction of regional tension. Benham is at about 1.3 caldera radii from the center, and the other shots, Boxcar, Jorum, Handley, and Greeley are at about 2 radii from the center. Because the effects of the hole in a prestressed plate are quite localized, this model calls for a maximum tensile stress and a maximum shear stress at Benham about 1.5 times those at the more northern sites, Figure 6.2. The gradients in stress are greater at Benham than at the other places

also. For each kilobar of regional tensile load, the maximum tensile stress is 1.82 kb at Benham (almost twice the applied load) and 1.22 kb at the northern site. The corresponding values of maximum shear stress are 0.73 kb and 0.47 kb, respectively. The stress gradients at Benham are, for the tensile stress 0.15 bar/meter per kilobar of regional stress, and for the maximum shear stress, 0.07 bar/meter. At the northern sites the corresponding gradients are about one-fifth the value at Benham. Of course, local inhomogeneities may cause localized stress gradients over short distances that are much greater than these.

A further point in support of the applicability of this model is the fact that the numerous Benham aftershocks are concentrated along a trajectory whose direction is predicted by Cumming, for which there was no surface fault, but which connected known segments of faults. Also, the late aftershocks, beginning 22 days after the event are largely concentrated to the south, inside the caldera boundary.

In the absence of more information about the in situ stress and the strength of the faults it is not possible to judge if a stress increase of fifty percent is enough to account for the difference in response at Benham and the other shots.

Further evidence of a difference in Benham and Boxcar related to tectonic strain release is found in the relative excitation of SV and SH waves by the two explosions. The horizontal component of SV as observed at 11 stations in

the Western Hemisphere is close to the same for the two events. SH amplitudes, on the other hand, are uniformly three to four times larger for the Benham event than for Boxcar, with about the same period.

Milrow raised some interesting questions, in that it produced so few afterevents in a setting that is known to be highly seismic. The absence of aftershocks later than cavity collapse (Engdahl and Tarr, 1970) and evidence of the long-term tectonic stability of Amchitka Island (Morris, 1970; Anderson, 1970) indicate that the rocks of that island are under less stress than those of the Basin and Range Province. One inference is that the island is mechanically decoupled from the active seismic region in which it is embedded. Anderson interprets "the deformation of the surficial rocks of the central Aleutian Ridge as related to volcanism and plutonism, and as such the deformation does not reflect in a first order sense the regional compressional stress across the arc."

The strain energy released in the Milrow aftershocks almost certainly came from the static strain field produced by the explosion and subsequently relieved by the collapse.

Thus, the prompt release of tectonic strain by an explosion is governed by a number of factors that can be evaluated in the field but have not been adequately treated yet. These include the magnitude and orientation of the regional stresses and the stress concentrations in the neighborhood of the shot caused by the local geology. The

occurrence of an unstable rupture that would give rise to a large earthquake seems to require that the explosion take place near a fault that is stressed almost to the point of failure. In this event the identification of the signal as coming from an explosion might be very difficult.

It has been recognized that surface wave magnitudes from NTS events are systematically larger, relative to m_b, than those for explosions in Central Asia, Novaya Zemlya and the Sahara. For example, for a large Novaya Zemlya event, m_b = 6.5, the ratio m_b : M_s is 1.30. The average for two Central Asia events, m_b = 6.0 and 5.5, the ratio is 1.52. For one Sahara event, m_b = 5.7, the ratio is 1.32. For events Greeley and Boxcar the ratios are both 1.18. O. Nuttli has determined shear wave magnitudes and found for these events that the shear body wave magnitude is close to M_s for all sites, the ratios m_{shear} : M_s ranging from 1.02 to 1.13. The relatively high values for both M_s and m_{shear} for NTS events have been interpreted as due to the contribution of tectonic strain release. The contribution to the shear wave magnitude from the SH component is very small for most of the events examined. A detailed study of the Benham shear wave magnitude is still to be done.

Aftershock Excitation.

In collaboration with J. T. Cherry, Jr., of Livermore Radiation Laboratory, Livermore, California, a mechanism by which an underground explosion may trigger a swarm of small

earthquakes has been investigated. The effect to be explained is the permanent alteration of the tectonic environment in the zone usually considered to respond elastically to the explosive loading. A non-elastic effect must be produced beyond the usually defined zone of cracking, crushing, etc., one that causes small earthquakes to occur over an extended period of time.

The suggested mechanism is the interaction of elastic shear waves proceeding outward from the region around the explosion with localized gradients in the ambient tectonic stress field. As a result of the interaction a field of small slipped areas or dislocation loops is formed and the continued action of the ambient field on these dislocations results in the swarm of earthquakes. The shear waves may proceed directly from the explosion or be produced by reflection of compressional waves at the free surface or other boundaries. The stress concentrations are the result of either material inhomogeneities or the effect of preexisting cracks in the medium, which is in equilibrium in an ambient regional stress field.

Our appeal to the role of local stress concentrations follows closely the hypotheses of Droste and Teisseyre (1959, 1960) and of Mogi (1962) regarding the preparation of a region for earthquakes and aftershocks.

The equations of motion for an elastic medium under initial stress are derived by Biot in The Mechanics of Incremental Deformation. If the body forces and initial stress

are all zero, we have the usual equations of motion. For the body forces zero and the initial stresses constant, Biot has shown that P and S waves can propagate in the medium and that the velocities depend on the amount of the initial stress, and an initially isotropic medium is in general not isotropic under the ambient stresses.

If the body forces are zero and if the coordinate axes are taken as the principal axes of the ambient stress, but the ambient stress intensity is permitted to vary, the two equations are coupled through the shear strain term, which involves the stress gradients as coefficients. Although the solution of the resulting equations is very difficult, it can be easily seen by substitution that a pure plane shear wave propagating parallel to one of the coordinate axes is not a possible solution. For example, a plane shear wave travelling parallel to the y axis, displacement parallel to the x axis, must be accompanied by a particle acceleration parallel to the y axis. A pure compressional wave, on the other hand, can exist!

Physically, the stress gradient acts analogously to the tension in a stretched string, resulting in an equivalent spring that converts a displacement into an acceleration. Because the stress gradient is a multiplier of the strain in the equation, a small strain can produce a large acceleration if the stress gradient is large, and a change in sign of the stress gradient will change the sign of the acceleration. Large stress gradients are easily produced over the short

distance in a modest stress field in the neighborhood of small inhomogeneities.

We propose then that as a shear wave passes through a zone in which a strong stress gradient changes sign, a resultant tensile stress may act momentarily, reducing the effective pressure, and slip may occur under the action of the ambient stress. The slipped areas created in this may become the nuclei for growth of the dislocations under the action of the ambient field, in the manner proposed by Droste and Teisseyre.

The Benham aftershock swarm exhibits features that may be explained by this mechanism. Fig. 6.3 shows the epicenters and the hypocenters, on a vertical radial plane, of the first 19 aftershocks reported by Hamilton and Healy (1969). These are only a small sample of the many events during the first six hours after Benham, but they show that early aftershocks occurred at three to six kilometers from the shot, and, in fact, outline the zone of most of the activity for the first three weeks after the event. The mechanism by which the region was primed for the aftershocks acted quickly and did not move out slowly from the explosion site.

Fig. 6.4 is a hypocenter plot of all 668 events located by the USGS through April 18, 1969, on a single plane. Superimposed are two rays: one defines the deepest ray for a P to S conversion by surface reflection for which more than half the reflected energy is in the form of S waves for an idealized medium. All rays above this one out to large angles of

incidence at the surface exhibit this property. The ray appears to form a rough lower envelope to the activity. The velocity model used by the USGS was used in drawing this ray.

The other ray represents an SV wave taking effect about 35° to the vertical at the source. This is the angle at which a beam of energetic S waves should radiate from a horizontal depth force without moment and was selected on the basis of a model of a near-surface explosion proposed by Gupta and Kisslinger in 1966. This ray also passes along the lower bound of the activity. For either source of S-waves, the cut-off of activity below about 5.5 km may then be an effect of the sharp velocity contrast at 5 km depth. The circled points are hypocenters of late events in the swarm, mostly south of the regional swarm regions.

The distribution of the aftershocks shown by Hamilton and Healy (1969) raises the question of why the events are distributed as they are. The absence of activity to the east suggests, under the present hypothesis, that the main fault, which did slip at shot time, effectively decoupled shear waves from the eastern zone. The concentration of events between previously mapped fault segments suggests that the swarm has acted to complete the formation of a linear subsurface fracture. If so, the swarm has some similarities to natural earthquake swarms, for example that in Matsushiro, Japan. There a great swarm accompanied the formation of a new fault, according to Japanese geologists, activity died out in the original active zone as it did in Benham, and

in later stages of the swarm the activity expanded outward into fresh material.

The limited evidence indicates that moderate to strong earthquakes occur on preexisting faults, and no case is known to the author in which a great earthquake was accompanied by the formation of a new fault in virgin material. It may be that the formation of a new fault is normally accompanied by an earthquake swarm, perhaps initially microearthquakes, though the converse is by no means indicated, that is, that all swarms are associated with fault formation.

References

Anderson, R. E., Tectonic Setting of Amchitka Island, Alaska, USGS-474-75, U. S. Geological Survey: Denver, Colorado, 1970.

Cummings, D., Mechanical Analysis of the Effect of the Timber Mountain Caldera on Basin and Range Faults, Jour. Geophys. Res., 73(8): 2787, 1968.

Droste, S. and R. Teisseyre; the Mechanism of Earthquakes in Terms of the Dislocation Theory," Science Reports of Tohoku University, ser. 5, Geophysics, vol. 11, no. 1, pp. 55-71, 1969.

Engdahl, E. R., and A. C. Tarr, Aleutian Seismicity - Milrow Seismic Effects, CGS-746-102, U. S. Coast and Geodetic Survey: Rockville, Maryland, 1970.

Kisslinger, C., E. J. Mateker, Jr., and T. V. McEvilly, SH Motion from Explosions in Soil, Jour. Geophys. Res. 66(10):3487-3496, 1961.

McKeown, F. A., and D. D. Dickey, Fault Displacements and Motion Related to Nuclear Explosions, Bull. Seis. Soc. Am., 59(6): 2253-2270, 1969.

Mogi, K., On the Time Distribution of Aftershocks Accompanying the Recent Major Earthquakes in and Near Japan, Bull. Earthquake Res. Inst., Tokyo University, vol. 40: 107-124, 1962.

Morris, Robert H., A Preliminary Study of Relict Marine Terraces of the Western Aleutian Islands, Alaska, USGS-474-62, U. S. Geological Survey: Denver, Colorado, 1970.

Figure Captions

Figure 6.1 Model of Pahute Mesa - Timber Mountain caldera tectonics after D. Cumming. σ is the regional tensile stress. Nuclear events are designated: H - Handley, J - Jorum, G - Greeley, Bo - Boxcar, Be - Benham. The dashed curves are predicted orientations of faults.

Figure 6.2 Variation of maximum tensile stress, σ_1, and maximum shear stress, S, with distance to the north from the caldera boundary. Distance is in terms of caldera radii.

Figure 6.3 Epicenters (left) and hypocenters of the first 19 Benham aftershocks listed by the USGS. Body wave magnitudes are in parentheses.

Figure 6.4 Hypocentral plot of Benham aftershocks through April 18, 1969. The solid ray is a P to S conversion at the smallest angle of incidence for which more than one-half the reflected energy is in the shear wave. The dashed ray represents the direction of the maximum amplitude of SV waves generated by the horizontal component of the explosive loading for a near-surface source.

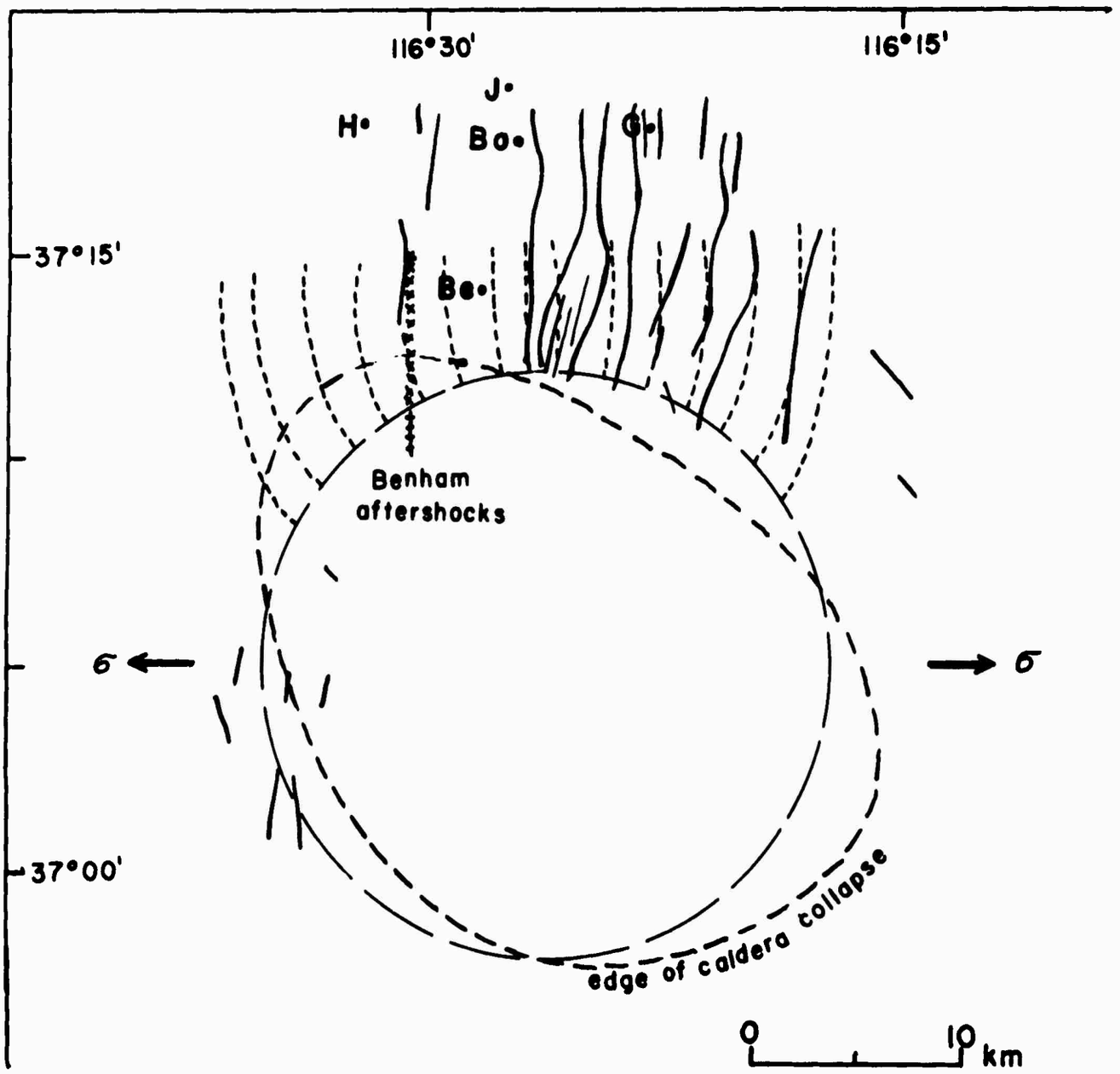

adapted from Cummings (1968)

Fig. 6.1

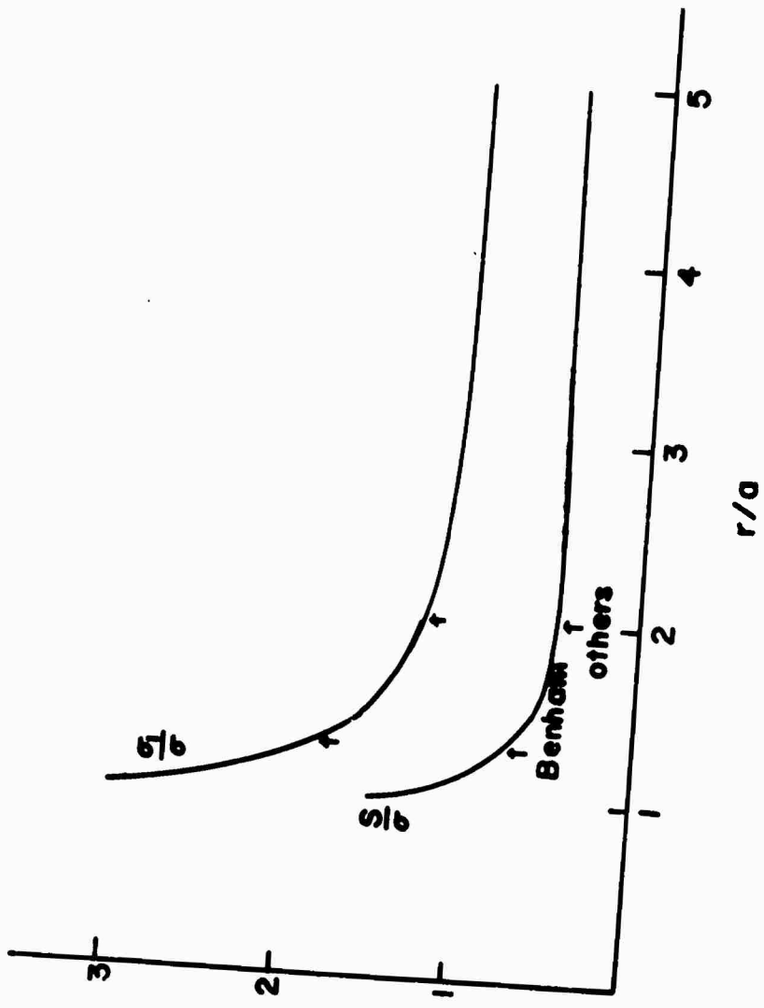

Fig. 6.2

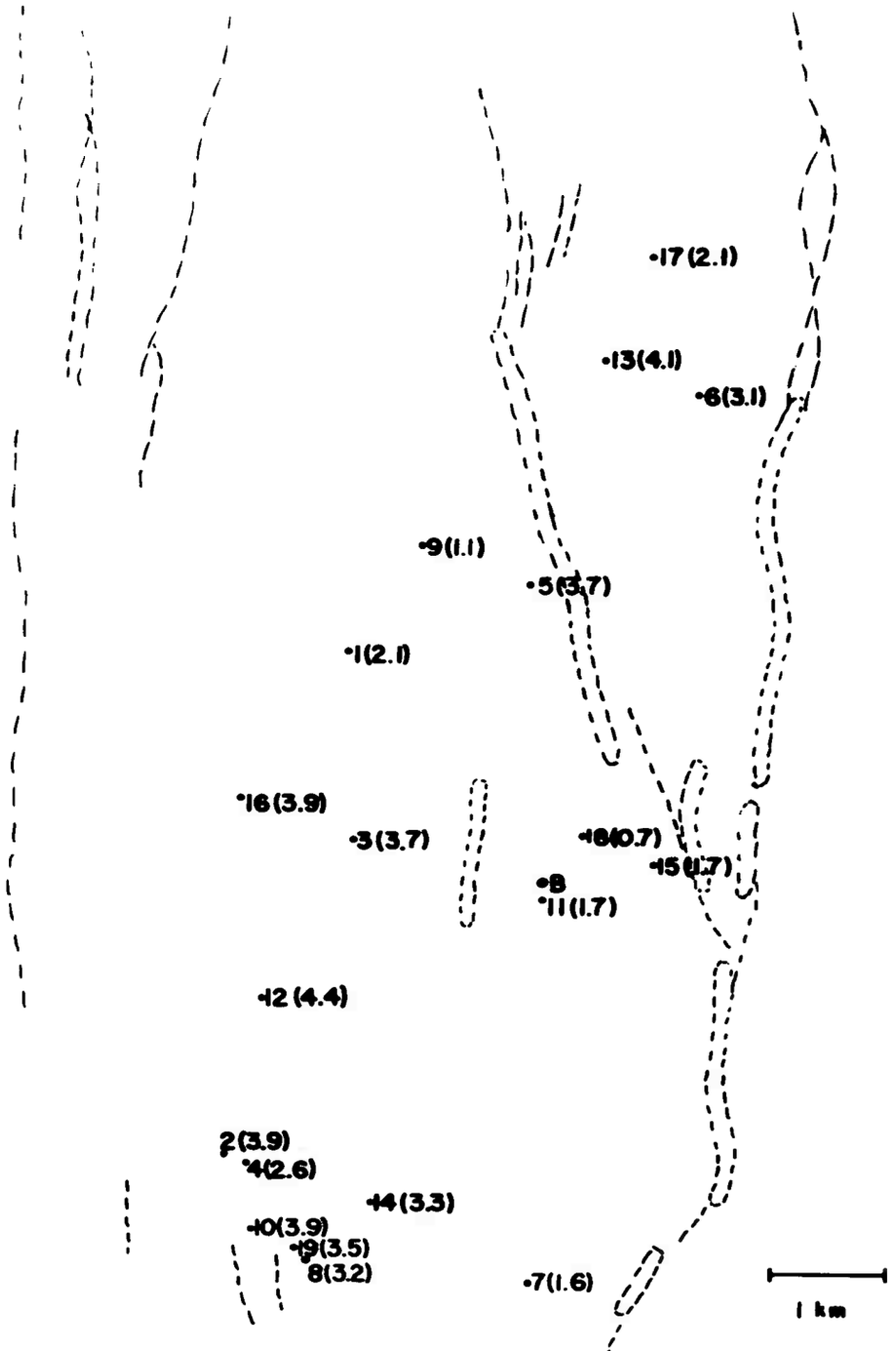
17(2.1)
13(4.1)
6(3.1)
9(1.1)
5(3.7)
1(2.1)
16(3.9)
3(3.7)
18(0.7)
15(1.7)
8
11(1.7)
12(4.4)
2(3.9)
4(2.6)
14(3.3)
10(3.9)
9(3.5)
8(3.2)
7(1.6)
1 km

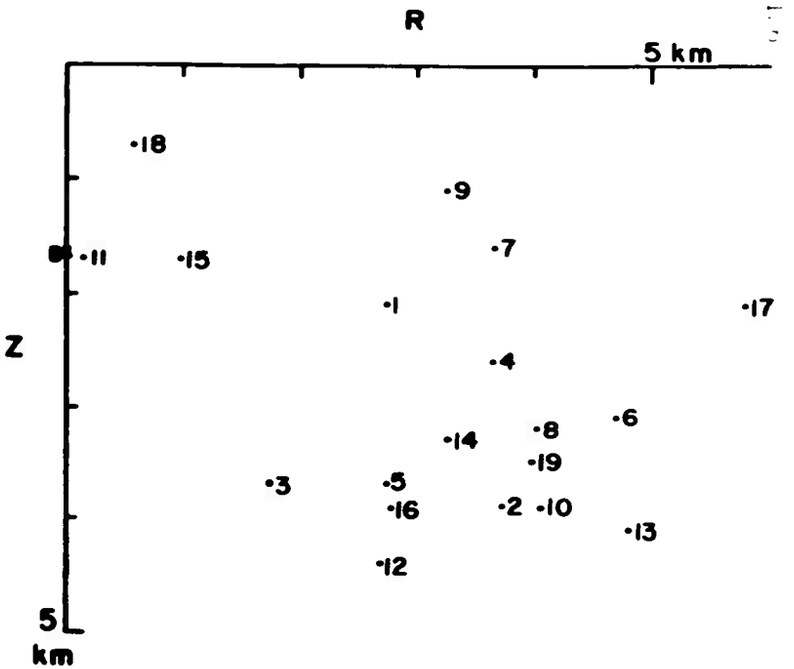
R
5 km
Z
5
km
18
9
11
15
7
1
17
4
6
14
8
19
3
5
16
2
10
13
12

Fig. 6.3

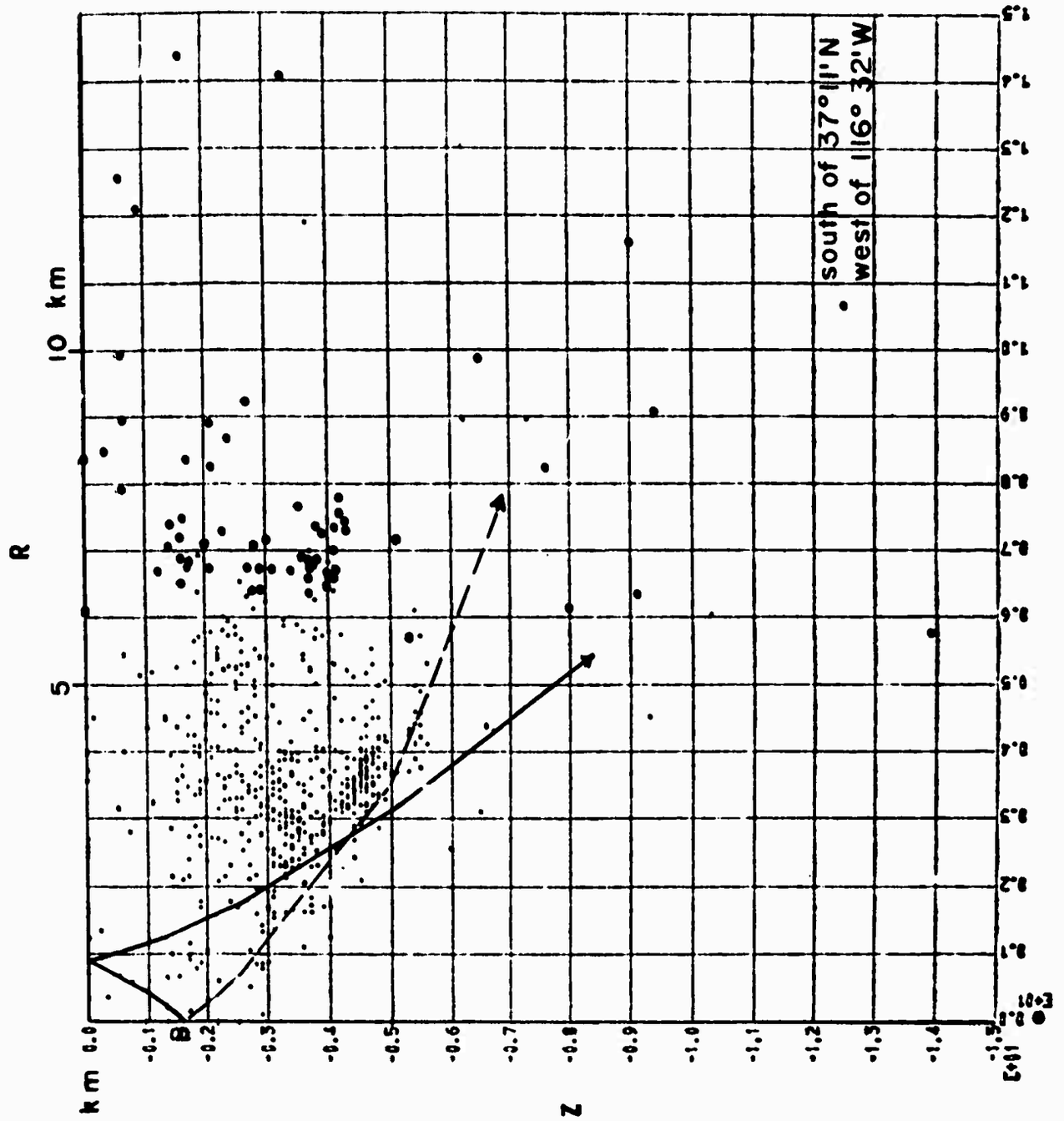
R
10 km
5
km
0.0
-0.1
B
-0.2
-0.3
-0.4
-0.5
-0.6
-0.7
-0.8
-0.9
-1.0
-1.1
-1.2
-1.3
-1.4
Z
south of 37°11'N
west of 116° 32'W
ALL DATA PLOTTED

Fig. 6.4

7. P Pulses from Earthquakes Triggered by Explosions.

Rene Rodriguez

Introduction

The purpose of this research was to determine in the time domain the influence of an earthquake triggered by explosions into the final P pulse shape. Two kinds of sources were considered to act in a region, namely: an explosive source, and a tectonic source (moving fault) triggered by the arrival of a signal from the explosion.

a) Explosive Source. An explosive point source in an homogeneous, isotropic media can be represented by three mutual perpendicular couples of equal point forces without moment (Fuchs, 1966). The total effect can be represented by a superposition of the three couples, because of the linear dependence between displacements and forces. This is equivalent to considering the explosion and its effects only in the elastic zone, where the infinitesimal strain theory is valid (Kisslinger, 1963). From Nakano (1923), the displacements due to an explosive point source were calculated and they are: in cartesian coordinates:

$$\underline{u}_P = \frac{\kappa \varepsilon}{4\pi \rho r^4 v_p^3}\left\{ (x^3 + y^2x + z^2x)\,\underline{i} + (x^2y + y^3 + z^2y)\,\underline{j} + (x^2z + y^2z + z^3)\,\underline{k} \right\} \dot{F}\left(t - \frac{R}{v_p}\right) \qquad (1)$$

in polar coordinates:

$$\underline{u}_{Pr} = \frac{\kappa \varepsilon}{4\pi \rho R v_p^3}\, \underline{e}_r\, \dot{F}\left(t - \frac{R}{v_p}\right) \qquad (2)$$

where v_p = compressional wave velocity

R = distance between source and receiver

ρ = density of the media

$\kappa\varepsilon$ = equivalent moment of the couple (strength of the explosive source)

$\hat{e}_r$ = radial unit vector.

b) Tectonic Source. A moving double couple is utilized to model an extending source. Following Berckhemer (1966), consider the fault plane in the xz plane and a double couple acting at the origin O (Fig. 7.1). Let B be a point on the focal plane given by it cartesian coordinates. Let the force per unit area $\underline{K}$ be acting over the surface element $d\xi\, d\zeta$, then the resultant force will be given by

$$d\underline{K} = \underline{K}\, d\xi\, d\zeta \qquad (4)$$

Let the receiver A be at a distance r from the source, very large compared with the diameter 2r' of the focal area. The rays from all the source elements to A will nearly be parallel. This approximation can be justified if

$$r'^2 \ll \lambda_{min}\, r$$

where is the wave length.

If the focal process starts at the origin O, the stress release at any other point such as B will start after a delay time

$$t_0 = t_f(s) \qquad (5)$$

where $t_f(s)$ = time due to the fracture process.

The delay time at the receiver A will be:

$$t_o = t_f(\xi) - \frac{r - \xi \cdot e_r}{v} \qquad (6)$$

where:

$$e_r = \frac{r}{r}$$

$$\xi = \gamma_1 i + \gamma_2 j + \gamma_3 k$$

$$\gamma_1 = \frac{x}{r} = \cos\theta$$

$$\gamma_2 = \frac{y}{r} = \sin\theta \sin\phi$$

$$\gamma_3 = \frac{z}{r} = \sin\theta \cos\phi$$

$$r = (x^2 + y^2 + z^2)^{1/2}$$

$v = v_p$ for P waves $\qquad$ $v = v_s$ for S waves

In each source element a double couple acts. Integration over the total focal plane leads to the resulting pulse of the displacement at A. From the expressions given by Nakano (1923) the displacement at A will be

$$u_{pr} = \frac{\kappa \varepsilon \sin 2\theta \cos\phi}{4\pi \rho r v_p^3} e_r \int_c^a \int_d^b \dot{f}\left(t - t_o'(\xi)\right) d\gamma\, d\gamma \qquad (9)$$

$$u_{s\theta} = \frac{\kappa \varepsilon \left\{\cos^2\theta + \sin^2\theta \cos^2\phi (1 - 4\cos^2\theta)\right\}^{1/2}}{4\pi \rho r v_s^3} e_\theta \int_c^a \int_d^b \dot{f}\left(t - t_o'(\xi)\right) d\gamma\, d\gamma \qquad (10)$$

where Up stands for P waves, Us for S waves, a, b, c, d, are the dimensions of the fault and e_θ is the tangential unit vector.

The composite source.

Consider an isotropic, homogeneous media. Let the explosion be detonated at a certain time t_1. Waves spreading radially will travel around the explosive source in all directions. It is assumed as a working model that as soon as the

first wave front from the explosion reaches the fault area in one point, this will be the starting point for the triggering; this will occur after a delay time (Fig. 7.2)

$$t = \frac{M}{v_p} \tag{11}$$

where M is the distance between the explosion and fault.
Any other point in the fault such as B will start releasing energy after a time delay

$$t = \frac{M}{v_p} - t_f(s) \tag{12}$$

At this point if we consider the fracture process to be linear (unilateral or bilateral) propagating in + x direction

$$t_f(s) = \frac{x}{c} \tag{13}$$

where C = fracture velocity.
Then the total time delay from the explosion to any point on the fault will be:

$$t = \frac{M}{v_p} - \frac{x}{c} \tag{14}$$

Meanwhile direct waves from the explosion traveling thru the medium will reach the receiver after a time delay:

$$t = \frac{R}{v_p}$$

and waves from the fault after a time:

$$t = \left(\frac{M}{v_p} + \frac{x}{c} + \frac{r - (x\cos\theta + y\sin\theta\cos\phi)}{v} \right) = \tau_u \tag{15}$$

when the fracture process is unilateral or

$$t - \left(\frac{M}{v_p} + \frac{\gamma}{c} + \frac{r + (\xi \cos\theta + \eta \sin\theta \cos\phi)}{v} \right) \quad . \quad \tau_a^r \qquad (16)$$

when it is bilateral.

V = Vp for P waves V = Vs for S waves

Then the total displacement due to the composite source at the receiver A will be

$$\underline{u}_p = \frac{K_1 \varepsilon_1}{4\pi \rho R v_p^3} \underline{e}_{r_1} \dot{F}\left(t - \frac{R}{v_p}\right) + \frac{K\varepsilon \sin 2\theta \cos\phi}{4\pi \rho r v_p^3} \underline{e}_\phi \int_c^a \int_d^b \dot{f}\left(\tau_u^r\right) d\xi\, d\eta \qquad (17)$$

$$\underline{u}_s = \frac{K\varepsilon \left\{ \cos^2\theta + \sin^2\theta \cos^2\phi \left(1 - 4\cos^2\theta\right) \right\}^{1/2}}{4\pi \rho r v_p^3} \underline{e}_\theta \int_c^a \int_d^b \dot{f}\left(\tau_u^s\right) d\xi\, d\eta \qquad (18)$$

If we assume further that the radius of the composite source r" is very small compared with the distance, which can be satisfied if

$$r^2 \ll \lambda_{min} r \quad , \qquad (19)$$

then the displacements can be written as:

$$u_p = \frac{K_1 \varepsilon_1}{4\pi \rho R v_p^3} \dot{F}\left(t - \frac{R}{v_p}\right) + \frac{K\varepsilon \sin 2\theta \cos\phi}{4\pi \rho r v_p^3} \int_c^a \int_d^b \dot{f}\left(\tau_u^r\right) d\xi\, d\eta \qquad (20)$$

$$u_s = \frac{K\varepsilon \left\{ \cos^2\theta + \sin^2\theta \cos^2\phi \left(1 - 4\cos^2\theta\right) \right\}^{1/2}}{4\pi \rho r v_s^3} \int_c^a \int_d^b \dot{f}\left(\tau_u^s\right) d\xi\, d\eta \qquad (21)$$

for unilateral fracture, and

$$u_p = \frac{K_1 \varepsilon_1}{4\pi \rho R v_p^3} \dot{F}\left(t - \frac{R}{v_p}\right) + \frac{K\varepsilon \sin 2\theta \cos\phi}{4\pi \rho r v_p^3} \int_c^a \int_d^b \dot{f}\left(\tau_a^r\right) d\xi\, d\eta \qquad (22)$$

$$u_s = \frac{K\varepsilon\{\cos^2\theta + \sin^2\theta\cos^2\phi(1-4\cos^2\theta)\}^{1/2}}{4\pi\rho r v_p^3}\int_c^a\int_d^b \dot{f}(\tau_s^s)\,d\xi\,d\tau \qquad (23)$$

for bilateral fracture.

For the final evaluation of the displacements an assumption about the time function for P and S wave forms at the source has to be made.

1. Time function for the explosive source.

Two kinds of functions will be assumed:

Type 1 Explosion (EX). The displacements at large distance corresponding to step in pressure at the source is given by (Kisslinger, 1963)

$$u = u_1 e^{-\alpha\tau}\sin\omega_0\tau$$

which is a damped sinusoidal motion propagating radially with angular frequency ω_0 where:

$$\tau = t - t_0 \qquad (24)$$

$$\alpha = \frac{m\,\omega_0}{(m+m^2)^{1/2}} \qquad (25)$$

$$\omega_0 = \frac{2v_p(m+m^2)^{1/2}}{a_1(1+2m)} \qquad (26)$$

a_1 = radius of the cavity

$m = \frac{\mu}{\lambda}$ = ratio of shear modulus to Lame's constant.

Assuming for the earth that Poisson's ratio is 0.25, m = 1 and for Vp = 7 km/sec

$$\omega_0 = \frac{14\sqrt{2}}{3}\,\frac{1}{a_1}$$

$$\alpha = \frac{14}{3}\,\frac{1}{a_1}$$

For a very large cavity radius, for example a = 1 km

$$\omega_0 = 6.6 \text{ 1/sec}$$

$$\alpha = 4.66 \text{ 1/sec}$$

$$f_{req.} = 1.05 \text{ Hz}$$

The corresponding normalized displacement for this type of time function is plotted in Figure 7.3 taking α as a parameter.

Type 2 Explosion (EX). A step-like function at the source will be assumed as a second type of time function for an explosion of the form:

$$u = u_1 \tau e^{-\alpha\tau} \qquad (27)$$

where will be evaluated by comparison during the numerical evaluation of the pulses. This type of function is similar to the pressure function calculated by Toksoz (1967) from surface wave studies of the Benham nuclear explosion. The value of 1.5 for in the time function seems to fit best the observed Love wave spectrum.

Plots of the normalized displacement for different alpha's are shown in Figure 7.4.

2. Time function for the tectonic source.

Various kinds of wave forms have been proposed by many different authors. Bollinger (1967) gives a list of the P wave forms used most often:

Boxcar	$B(\tau)\begin{cases}1 & 0<\tau<h\\ 0 & \tau>h,\ \tau<0\end{cases}$	
Step function	$U(\tau)\begin{cases}1 & \tau>0\\ 0 & \tau<0\end{cases}$	
Damped sinusoid	$e^{-\beta\tau}\sin\beta\tau$	(28)
$\frac{\sin\beta\tau}{\beta\tau}$	$\frac{\sin\beta\tau}{\beta\tau}\,U(\tau)$	

From spectral studies of body waves by Ben-Menahem et al (1965), the gross structure of the source time function was found to be of the form:

$$(1 - e^{-\beta\tau})\, H(\tau)$$

$$\text{with} \qquad 0 \leq \frac{1}{\beta} \leq 10 \tag{29}$$

Studies on the observed surface waves by Ben-Menahem and Toksoz (1963 a,b) and Stauder and Hirasawa (1965), show that the time function at the source can be expressed by a step-like function. According to their results the following particular form can be assumed for the time function:

$$f(\tau) = \begin{cases} 1 - e^{-\beta\tau} & \tau \geq 0 \\ 0 & \tau < 0 \end{cases} \tag{30}$$

or in dimensionless time form

$$f(T) = \begin{cases} 1 - e^{-QT} & T \geq 0 \\ 0 & T < 0 \end{cases} \tag{31}$$

where

$$\text{and} \qquad T = \frac{v_s \beta}{b} \qquad Q = \frac{b\beta}{v_s} \tag{32}$$

b = fault length

V_s = S wave velocity

Wave forms of P waves are plotted considering Q as a parameter (Fig. 7.5). Ben-Menahem and Toksoz presented the value of $\beta = 1/22$ from surface waves of the 1952 Kamchatka earthquake. Stauder and Hirasawa present a corresponding value

for Q = 10. From the considerations of Stauder and Hirasawa, Q may be considered to be almost constant for any earthquake rather than constant, because it seems to take a longer time to release the stored strain energy in a larger source, than in a smaller one.

In the present paper two kinds of time functions will be assumed for P waves:

Type 1 Fault (FAU). A damped sinusoid.

$$f(\tau) = e^{-\beta\tau} \sin \beta\tau \tag{33}$$

will be assumed for P wave forms from earthquakes, where the value of β will be chosen by comparison during the numerical computations of seismic pulses.

Type 2 Fault (FAU). A step-like function for the source function as given by Ben-Menahem (1963 a,b) and Hirasawa and Stauder (1965)

$$f(\tau) = \begin{cases} 1 - e^{\beta\tau} & \tau > 0 \\ 0 & \tau < 0 \end{cases} \tag{34}$$

The reason for assuming this time function instead of a more complete one, for example that given by Ben-Menahem, et al (1965), is because we want to gain simplicity for the evaluation of the integral over the fault area, which for the case of a function involving Heaviside function cannot be evaluated analytically as we wish.

Models.

Theoretical studies by Berckhemer and Jacob (1965), Savage (1965, 1966), Stauder and Hirasawa (1965) show that a unilateral fracture process has more influence on seismic pulses than bilateral faulting. By the nature of the problem, unilateral faulting seems the more suitable process to model a triggered earthquake although bilateral faulting is also possible. Because we are interested in seeing the influence of triggered earthquakes on seismic pulses from nuclear explosions, a unilateral fracture process will be assumed in the development of the final displacement formulas.

Model 1. Type 2EX + Type 1FAU (Fig. 7.6)

$$\dot{F}(\tau) = \tau\, e^{-\alpha\tau}$$
$$f(\tau) = e^{-\beta\tau} \sin\beta\tau \qquad (35)$$

With these two time functions, expressions for the displacements corresponding to formulas (20) and (21), after integration over the fault area, becomes:

$$u_p = D_1 \tau_1 e^{-\alpha\tau_1} + D_2 \left\{ -e^{-\beta\tau_2}[\sin\beta\tau_2 + \cos\beta\tau_2] + e^{-\beta\tau_3}[\sin\beta\tau_3 + \cos\beta\tau_3] + e^{\beta\tau_4}[\sin\beta\tau_4 + \cos\beta\tau_4] - e^{\beta\tau_5}[\sin\beta\tau_5 + \cos\beta\tau_5] \right\} \qquad (36)$$

$$u_s = D_3 \left\{ -e^{-\beta\tau_6}[\sin\beta\tau_6 + \cos\beta\tau_6] + e^{-\beta\tau_7}[\sin\beta\tau_7 + \cos\beta\tau_7] + e^{-\beta\tau_8}[\sin\beta\tau_8 + \cos\beta\tau_8] - e^{-\beta\tau_9}[\sin\beta\tau_9 + \cos\beta\tau_9] \right\} \qquad (37)$$

Where

$$D_1 = \frac{K_1 \varepsilon_1}{4\pi \rho r v_p^3} \quad , \quad D_2 = \frac{K \varepsilon \cos\theta}{4\pi \rho r v_p^2 \left(\frac{1}{c} - \frac{\cos\theta}{v_p}\right) \beta} \quad , \quad D_3 = \frac{K \varepsilon \left\{\cos^2\theta + \sin^2\theta \cos^2\phi \left(1 - 4\cos^2\theta\right)\right\}^{1/2}}{8\pi \rho r v_s^2 \sin\theta \cos\phi \left(\frac{1}{c} - \frac{\cos\theta}{v_p}\right) \beta} \tag{38}$$

$$\tau_1 = t - \frac{R}{v_p} \qquad \tau_6 = t - \left(\frac{M}{v_p} + \frac{r}{v_s} - \frac{a \sin\theta \cos\phi}{v_s}\right)$$

$$\tau_2 = t - \left(\frac{M}{v_p} + \frac{r}{v_p} - \frac{a \sin\theta \cos\phi}{v_p}\right) \qquad \tau_7 = t - \frac{M}{v_p} - \frac{r}{v_s}$$

$$\tau_3 = t - \left(\frac{M}{v_p} - \frac{r}{v_p}\right) \qquad \tau_8 = \tau_6 - b\left(\frac{1}{c} - \frac{\cos\theta}{v_s}\right)$$

$$\tau_4 = t - \left(\frac{M}{v_p} + \frac{r}{v_p} + b\left(\frac{1}{c} - \frac{\cos\theta}{v_p}\right) - \frac{a \sin\theta \cos\phi}{v_p}\right) \qquad \tau_9 = \tau_7 - b\left(\frac{1}{c} - \frac{\cos\theta}{v_s}\right)$$

$$\tau_5 = t - \left(\frac{M}{v_p} + \frac{r}{v_p} + b\left(\frac{1}{c} - \frac{\cos\theta}{v_p}\right)\right) \tag{39}$$

V = Vp for P waves and V = Vs for S waves.

Model 2. Type 1EX + 1FAU (Fig. 7.6)

$$\dot{F}(\tau) = e^{-\alpha\tau} \sin\omega_0 \tau$$
$$f(\tau) = e^{-\beta\tau} \sin\beta\tau \tag{40}$$

With the same configuration as Model 1 the integrated expressions corresponding to formulas (20) and (21) with the time functions assumed are:

$$u_p = D_1 e^{-\alpha\tau_1} \sin\omega_0 \tau_1 + D_2 \left\{ - e^{-\beta\tau_2} \left[\sin\beta\tau_2 + \cos\beta\tau_2\right] + \right.$$
$$+ e^{-\beta\tau_3} \left[\sin\beta\tau_3 + \cos\beta\tau_3\right] + e^{-\beta\tau_4} \left[\sin\beta\tau_4 + \cos\beta\tau_4\right]$$
$$\left. - e^{-\beta\tau_5} \left[\sin\beta\tau_5 + \cos\beta\tau_5\right] \right\} \tag{41}$$

$$u_s = D_3 \left\{ - e^{-\beta\tau_6} \left[\sin\beta\tau_6 + \cos\beta\tau_6\right] + e^{-\beta\tau_7} \left[\sin\beta\tau_7 + \cos\beta\tau_7\right] + \right.$$
$$\left. + e^{-\beta\tau_8} \left[\sin\beta\tau_8 + \cos\beta\tau_8\right] - e^{-\beta\tau_9} \left[\sin\beta\tau_9 + \cos\beta\tau_9\right] \right\} \tag{42}$$

Where D1, D2 and D3 are the same as in Model 1.

Model 3. Type 1EX + Type 2FAU (Fig. 7.6)

$$\dot{F}(t) = e^{-\alpha\tau} \sin\omega_0\tau \qquad (43)$$

$$\dot{f}(\tau) = (1 - e^{-\beta\tau})$$

Using again the same configuration of Model 1 the integrated expressions corresponding to formulas (20) and (21) with the time functions assumed are:

$$u_p = D_1 e^{-\alpha\tau_1} + D_2 \left\{ e^{-\beta\tau_2} - e^{-\beta\tau_3} - e^{-\beta\tau_4} + e^{-\beta\tau_5} \right\} \qquad (44)$$

$$u_s = D_3 \left\{ e^{-\beta'\tau_6} - e^{-\beta'\tau_7} - e^{-\beta'\tau_8} + e^{-\beta'\tau_9} \right\} \qquad (45)$$

$\tau_1, \tau_2, \ldots\ldots, \tau_9$ are given by formula (39)

Where again D1, D2, and D3 are the same as in Model 1.
It is noticed that whatever the time function is, we have the same time delays, namely

$$\begin{aligned}
T_1 &= \frac{R}{v_p} \\
T_2 &= \frac{H}{v_p} + \frac{r}{v_p} - \frac{q \sin\theta \cos\phi}{v_p} \\
T_3 &= \frac{H}{v_p} + \frac{r}{v_p} \\
T_4 &= \frac{H}{v_p} + \frac{r}{v_p} + b\left(\frac{1}{c} - \frac{\cos\theta}{v_p}\right) - \frac{q \sin\theta \cos\phi}{v_p} \\
T_5 &= \frac{H}{v_p} + \frac{r}{v_p} + b\left(\frac{1}{c} - \frac{\cos\theta}{v_p}\right)
\end{aligned} \qquad (46)$$

for P waves, and

$$T_6 = \frac{M}{v_p} + \frac{r}{v_s} - \frac{a \sin\theta \cos\phi}{v_s}$$

$$T_7 = \frac{M}{v_p} + \frac{r}{v_s}$$

$$T_8 = \frac{M}{v_p} + \frac{r}{v_s} + b\left\langle \frac{1}{c} - \frac{\cos\theta}{v_s} \right\rangle - \frac{a \sin\theta \cos\phi}{v_s}$$

$$T_9 = \frac{M}{v_p} + \frac{r}{v_s} + b\left\langle \frac{1}{c} - \frac{\cos\theta}{v_s} \right\rangle$$

for S waves.

The sense of the first (direct) motion from the explosion will always be up if the positive sign is taken in the direction of Z axis. The second arrival will correspond to the P wave triggered by the explosion due to the contribution of T2 or T3, whichever is minimum. Of course if

$a \sin\theta \cos\phi < 1$ T2 is minimum, or if

$a \sin\theta \cos\phi > 1$ T3 is minimum, depending in either case on the values of θ and ϕ. This minimum value also will determine the polarity of the second arrival for a given constant distance, because the difference in sign between T2 and T3. The difference between T2 and T3 is strongly dependent on the width of the fault considering that θ, ϕ, and Vp are fixed, that is:

$$\left| |T_2| - |T_3| \right| = \left| \frac{a \sin\theta \cos\phi}{v_p} \right| \qquad (47)$$

On the other hand, because the difference in sign a reverse in polarity will occur after the contribution of the third

term (one-fourth of a complete cycle), therefore the theory predicts a possible way of estimating the width of the fault independent of the assumption for the time function, if, of course, in practice this second arrival could be identified with accuracy from actual records.

A third spike is expected due to the contribution of T4 or T5, whichever is minimum, where the length of the fault plays an important role. This arrival will correspond to the stopping phase (Savage 1965, 1966). The same analysis can be made for the S wave generated at the fault.

Numerical Calculations.

Fortran programs have been written to evaluate the displacements at the receiver for all three models and variable parameters such as distance, relative orientation of the sources, relative strength, etc.

Model 1.

These programs calculate the P and S pulses at the receiver due to the composite source for different parameters, namely:

a) r = distance between fault-explosion to station

b) Θ and ϕ related the orientation of the station with respect to the fault

c) M = distance between explosion and fault

d) Θ_1 and ϕ_1 related the orientation of the explosion with respect to the fault

e) b = length of the fault.

At the beginning values of $\alpha = 0.5$ and $\beta = 0.1$ were assumed arbitrarily, considering only that the rise and decay for the

explosive source should be faster than for the propagating fault. All the early results for Model 1 correspond to these two values. It then became clear that these coefficients were critical, and various attempts to calculate the order of these have been made. Attempts to relate these coefficients to the magnitude and distance and the time of duration of observed pulses were unsuccessful. More successful was an attempt to relate α with β directly, equating the theoretical displacements due to an explosive point source acting alone and the displacement due to a double couple of equivalent strength. The numerical values obtained have been used to calculate the values as shown in Fig. 7.7. As predicted by the theory, the first arrival corresponds to the direct pulse from the explosion, the second to the triggered earthquake, the third is the stopping phase from the earthquake, and the fourth the S arrival. The difference in frequency content between the pulse from the explosion alone and that corresponding to the fault is striking. In these calculations the following values for the different parameters were taken:

α = 5.0

β = 0.7

Strength of the tectonic source $K_{\varepsilon_2 w_2} = 10^{23}$ dyn-cm

Distance fault-station r = 100 km

Distance explosion-fault M = 15 km

Fault length b = 10 km

Strength of the explosive source $K_{\varepsilon_1 w_1} = 10^{26}$ dyn-cm

$\theta = 30^{\circ}$ $\phi = 120^{\circ}$

$\theta_1 = 150^{\circ}$ $\phi_1 = 30^{\circ}$

Fig. 7.8 is the same as Fig. 7.7 but with strength of the explosive source decreased to 10^{25} dyn-cm.

Model 2.

The program for this model calculates the displacement due to a composite source as assumed in Model 2. Displacements have been calculated using the expressions derived by Kisslinger (1963) and by amplitude equalization. As in Model 1 we have the four spikes and more or less equal frequency content. In this case also the same parameters of Model 1 have been used (Fig. 7.9).

Model 3.

This program calculates the displacement due to a composite source as assumed in Model 3. The value of α, as suggested by the theoretical and observational calculations of Kisslinger, was taken as 4.66, which corresponds to a very large cavity radius (1 km). Beta again was calculated by amplitude equalization. In this model the arrivals observed in Models 1 and 2 are clearly seen. The frequency content is slightly different from those models, probably because of different values of the coefficients used. This model, not only theoretically but also experimentally seems to fit better the actual physical problem (Fig. 7.10).

Currently we are trying to improve the Fortran programming to obtain separately first pulses only from the explosion and

from the triggered earthquake, as well as the combination of both. This will give a better picture of what we are intending to do. After this, the next step will be to analyze the relative importance of each one of the parameters used in the theory into the final P pulses. Further on all the theoretical P pulses calculated will be convolved with the crust-seismograph response to determine the actual theoretical seismogram. In this sense a convolution Fortran program has been already written and the response for the WWSSN seismograph and crust response has been already obtained in digital form, taking the models given by Ben-Menahem.

Also, some practical applications of this theory will be applied. For this purpose, P waves from the Boxcar nuclear explosion are being analyzed, where very peculiar kinks in the first cycle have been found at some of the standard stations. What those kinks mean physically we are not in a position to say yet; however, on the basis of a better understanding of the theory, perhaps we will be able to answer this very interesting question.

The analysis developed here can easily be extended to the case in which the triggering occurs at the time of arrival of an S-wave proceeding from the explosion. The details of this extension will depend on the model chosen for the generation of these S-waves, e.g. by reflection, by crack formation, etc.

References

Ben-Menahem, A. and M. N. Toksoz (1963a). "Source Mechanism from Spectrums of Long-Period Seismic Surface Waves, 2. The Kamchatka Earthquake of November 4, 1952," Journ. Geophys. Res. 68:5207-5222.

Ben-Menahem, A. and M. N. Toksoz (1963b). "Source Mechanism from Spectra of Long-Period Seismic Surface Waves, 3. The Alaska Earthquake of July 10, 1958," Bull. Seism. Soc. Am., 53:905-919.

Ben-Menahem, A., S. W. Smith and T. Teng (1965). "A Procedure for Source Studies from Spectrums of Long-Period Seismic Body Waves," Bull. Seism. Soc. Am., 55:203-236.

Berckhemer, H. and K. H. Jacob (1965). "Synthetic Seismic Pulses from Propagating Faults," Universitat Frankfurt/Main, Sci. Rpt. No. 1 AF 61 (052)-801, 31 pp.

Bollinger, G. A. (1967). "Determination of Earthquake Fault Parameters from Long-Period P Waves," Ph. D. Thesis, St. Louis University, 126 pp.

Fuchs, K. (1965). "The Transfer Function for P-Waves for a System Consisting of a Point Source in a Layered Medium," St. Louis University, Sci. Rpt. No. 292, AF 19(604)-7399, 48 pp.

Hirasawa, T. and Wm. Stauder (1965). "On the Seismic Body Waves from a Finite Moving Source," Bull. Seism. Soc. Am., 55: 237-262.

Kisslinger, C. (1963). "The Generation of the Primary Seismic Signal by a Contained Explosion," University of Michigan, VESIAC Rpt. 4410-48-X, 85 pp.

Nakano, H. (1923). "Notes on the Nature of the Forces which Give Rise to the Earthquake Motions," Seis. Bull. Centr. Meteor. Observ., Japan, 1:92-120.

Savage, J. C. (1965). "The Effect of Rupture Velocity upon Seismic First Motions," Bull. Seis. Soc. Am., 55:263-275.

Savage, J. C. (1966). "Radiation from Realistic Model of Faulting," Bull. Seis. Soc. Am., 56:577-592.

Toksoz, M. N. and K. Clermont (1967). "Radiation of Seismic Waves from the Bilby Explosion," ARPA No. 624, Proj. Vela Uniform. 17 pp.

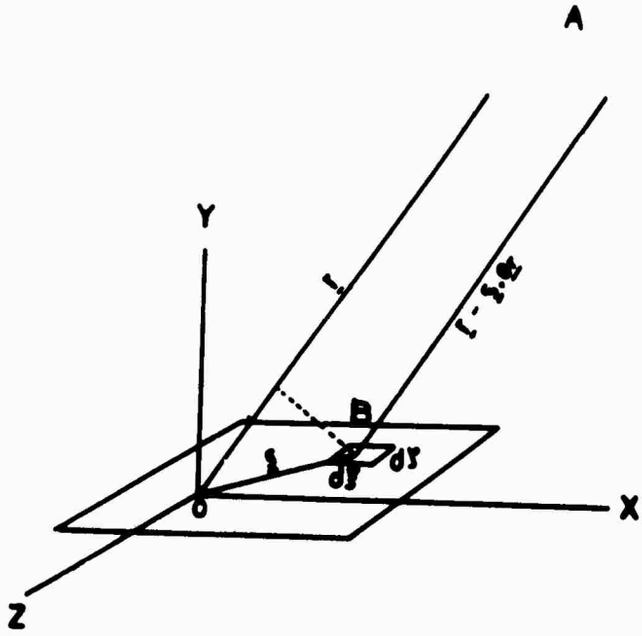

$\underline{r} = x\underline{i} + y\underline{j} + z\underline{k}$

fig 7.1

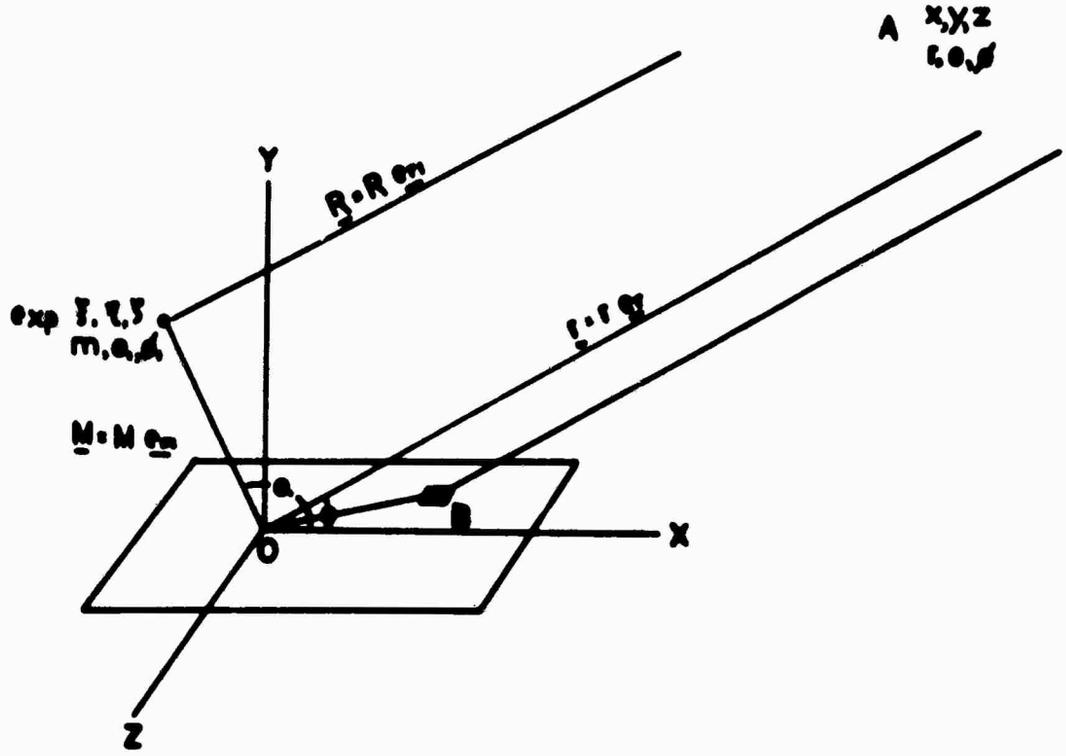

fig 7.2

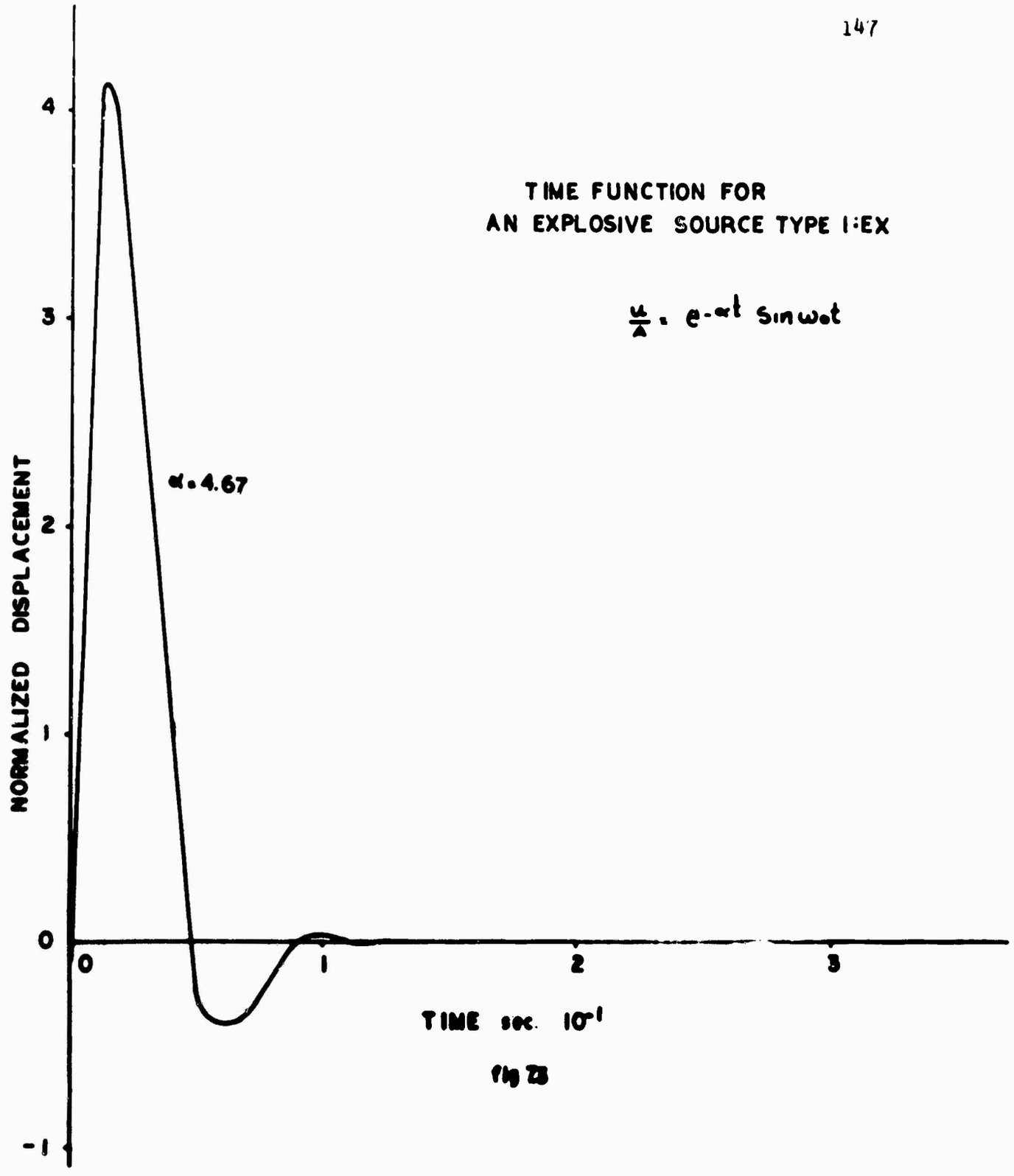
TIME FUNCTION FOR
AN EXPLOSIVE SOURCE TYPE 1:EX
$\frac{u}{A} = e^{-\alpha t} \sin \omega_0 t$
NORMALIZED DISPLACEMENT
4
3
2
1
0
-1
α = 4.67
0
1
2
3
TIME sec. 10^{-1}

fig 28

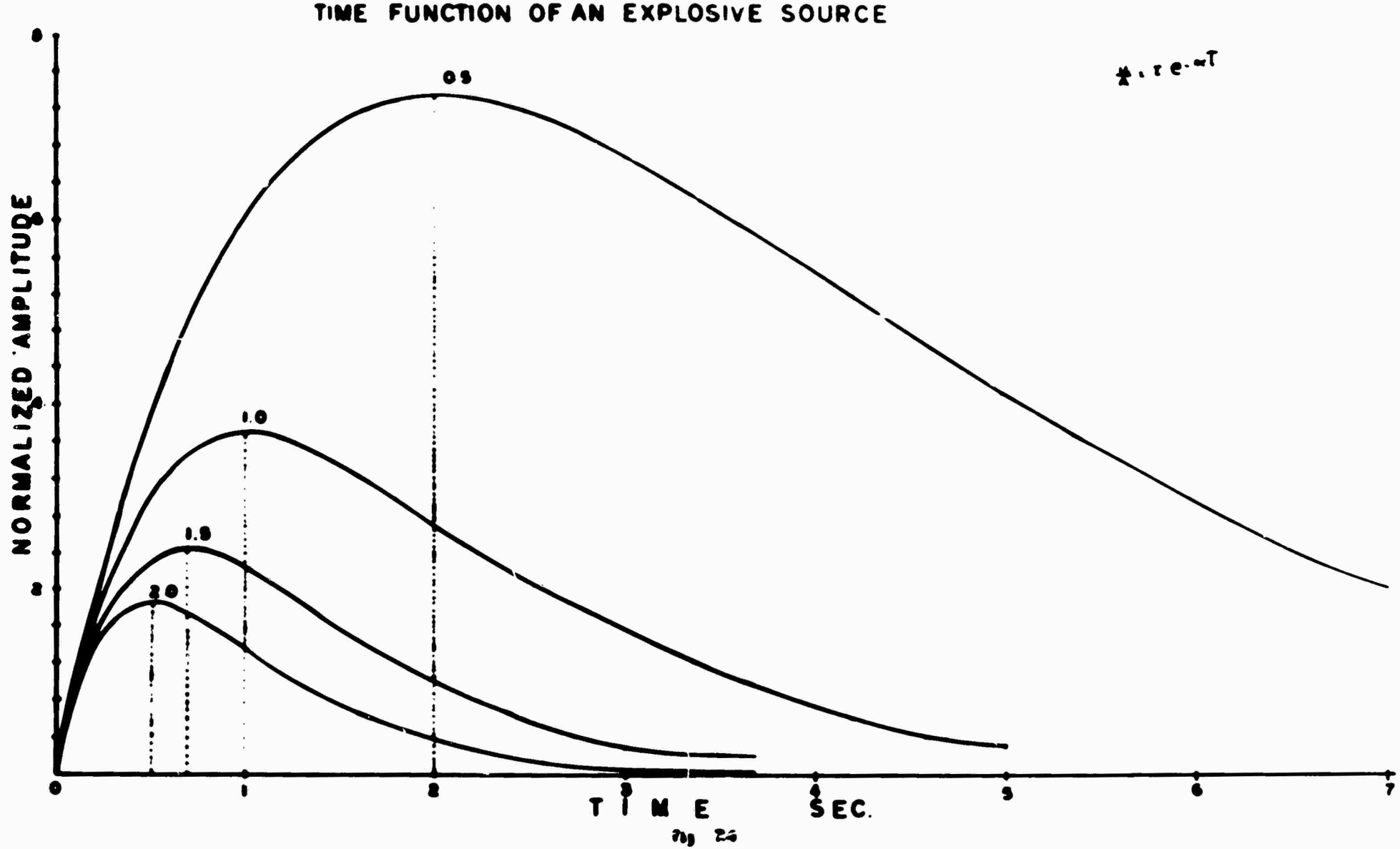
TIME FUNCTION OF AN EXPLOSIVE SOURCE
$A \cdot \tau e^{-\alpha T}$
0.5
1.0
1.5
2.0
NORMALIZED AMPLITUDE
0
1
2
3
4
5
6
7
TIME SEC.

Fig 24

TIME FUNCTION FOR A FAULT

$\frac{1}{A} \cdot e^{-\alpha t} \sin \omega t$

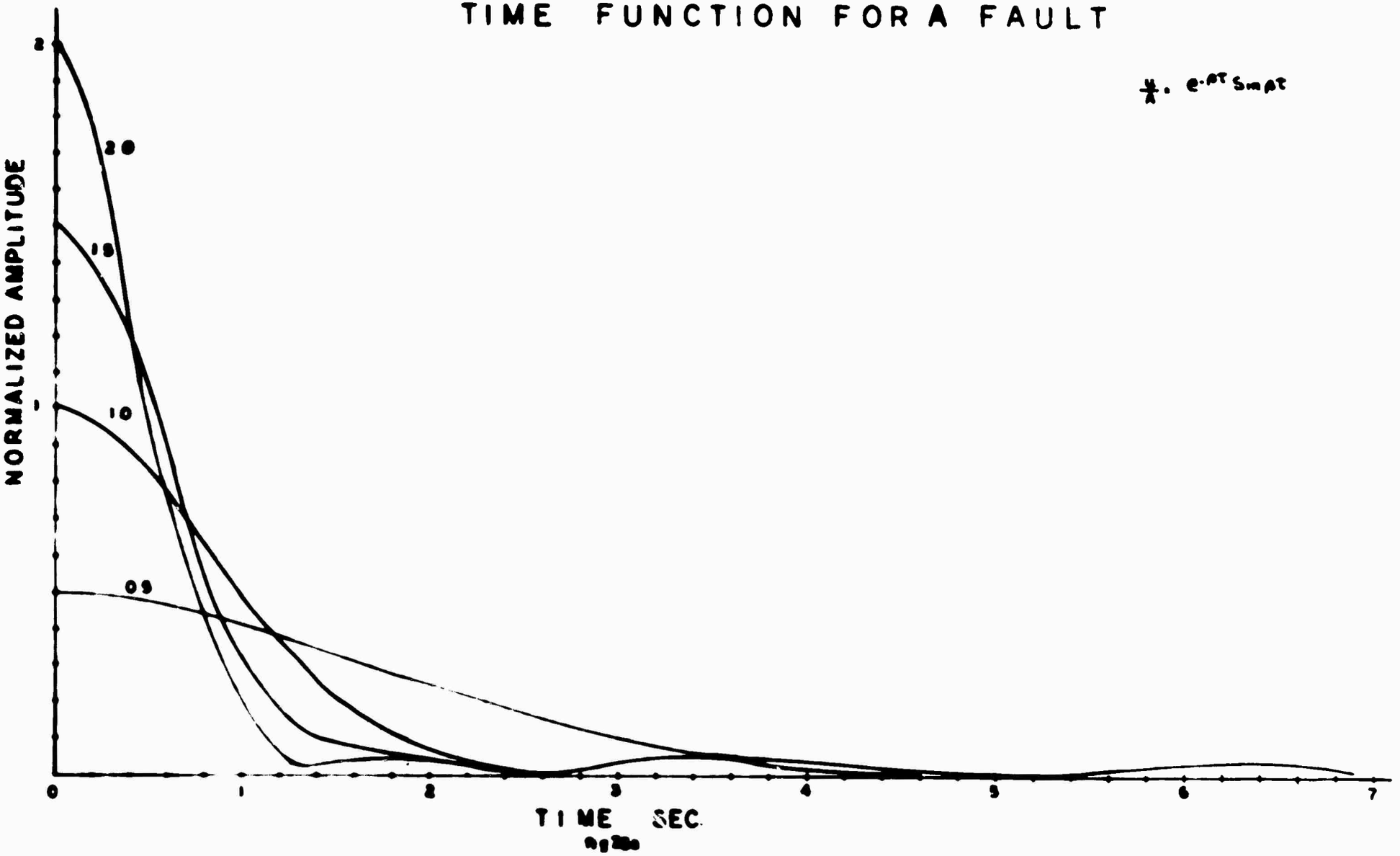

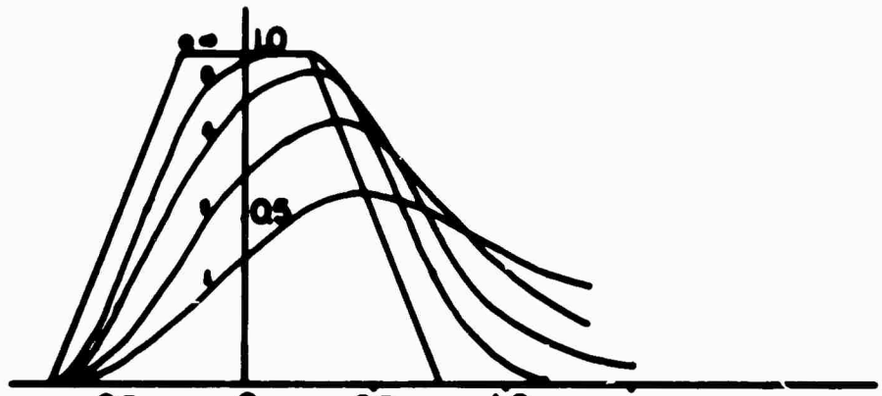

Fig 25

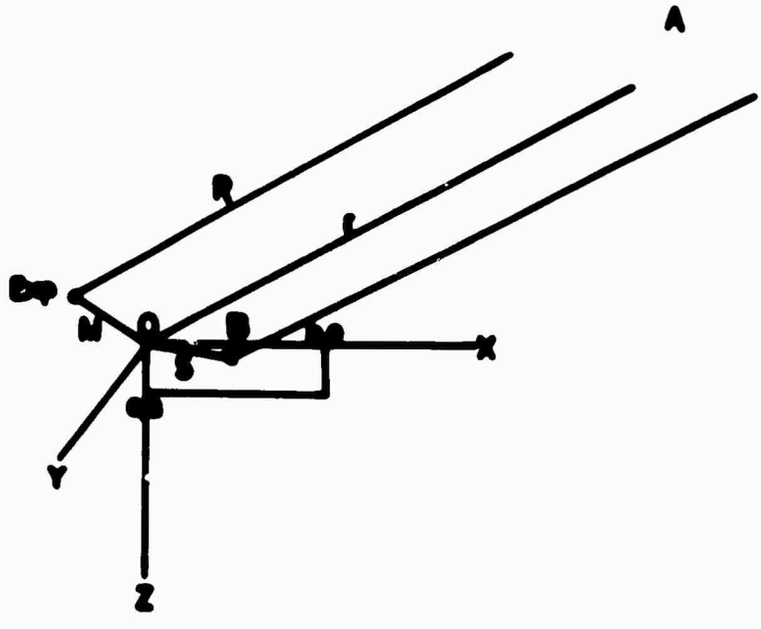

Fig 26

P PULSES FROM EARTHQ TRIGGERED BY EXPLOSIONS

R=DISTANCE FROM FAULT TO STATION

:OC.

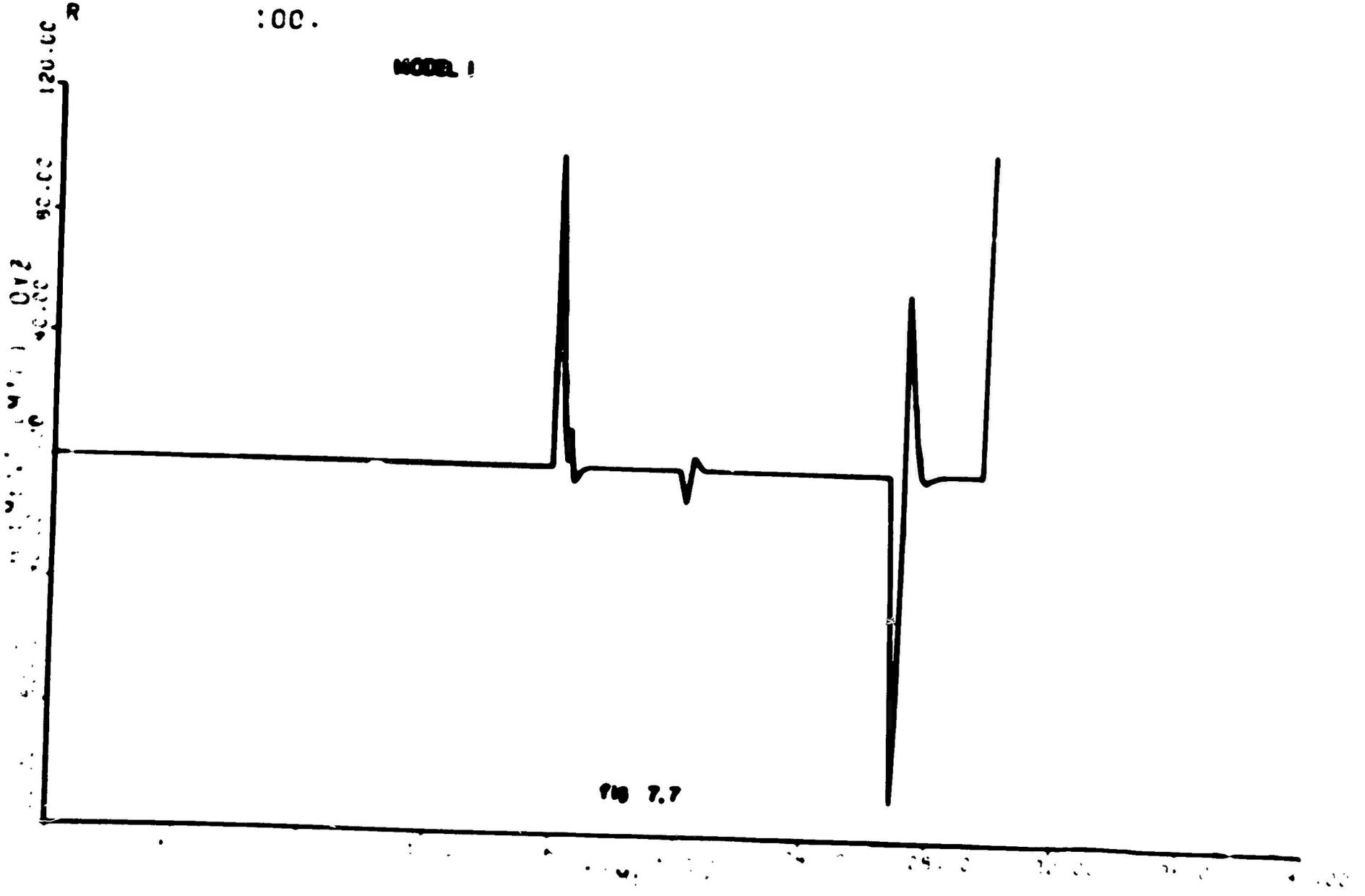

FIG 7.7

MODEL I

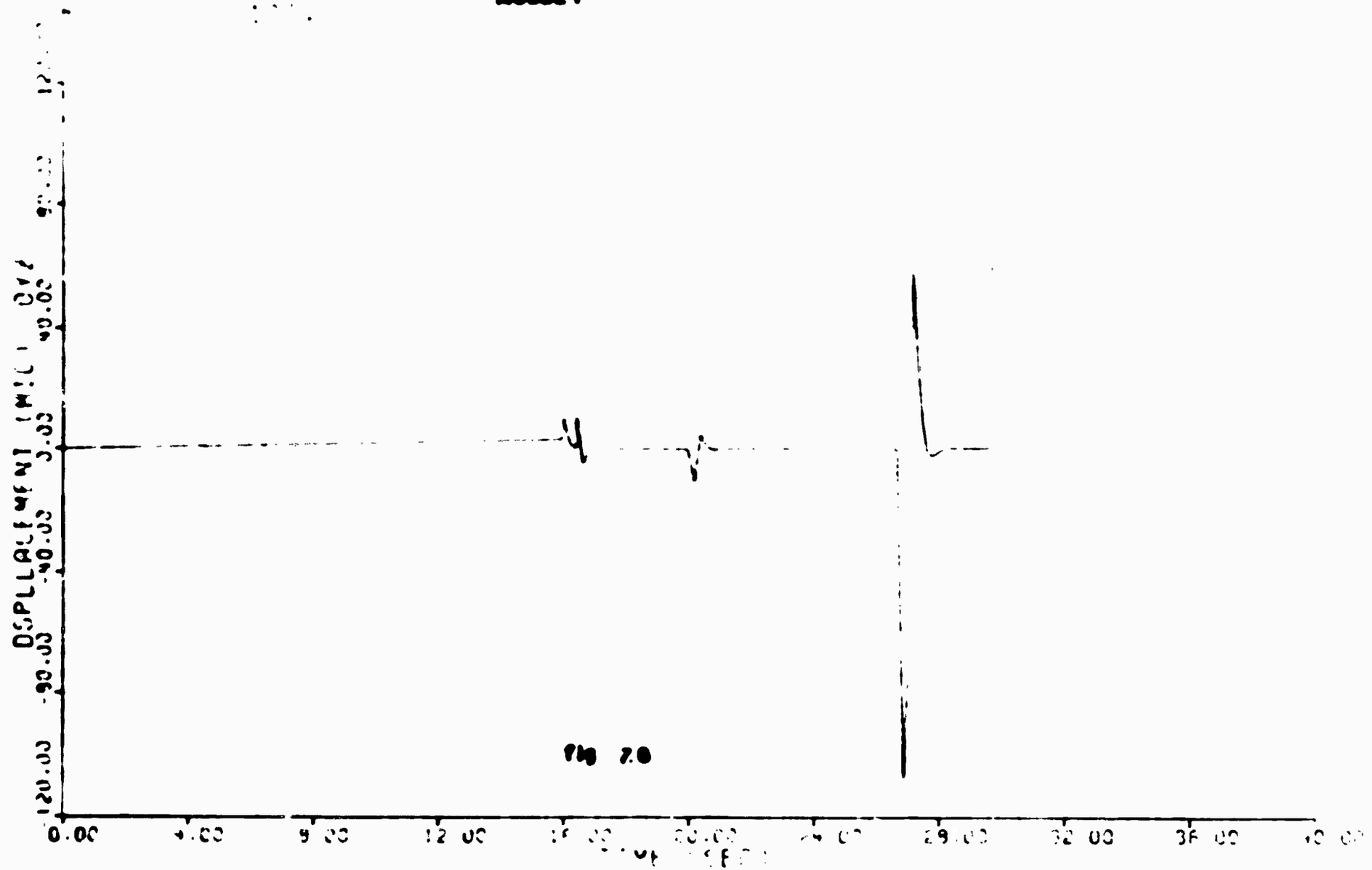

Fig 2.8

P PULSES FROM EARTHQ TRIGGERED BY EXPLOSIONS

R=DISTANCE FROM FAULT TO STATION

100.

fig 7.9

P PULSES FROM EARTHQ TRIGGERED BY EXPLOSIONS

MODEL 3

R 100. 0.

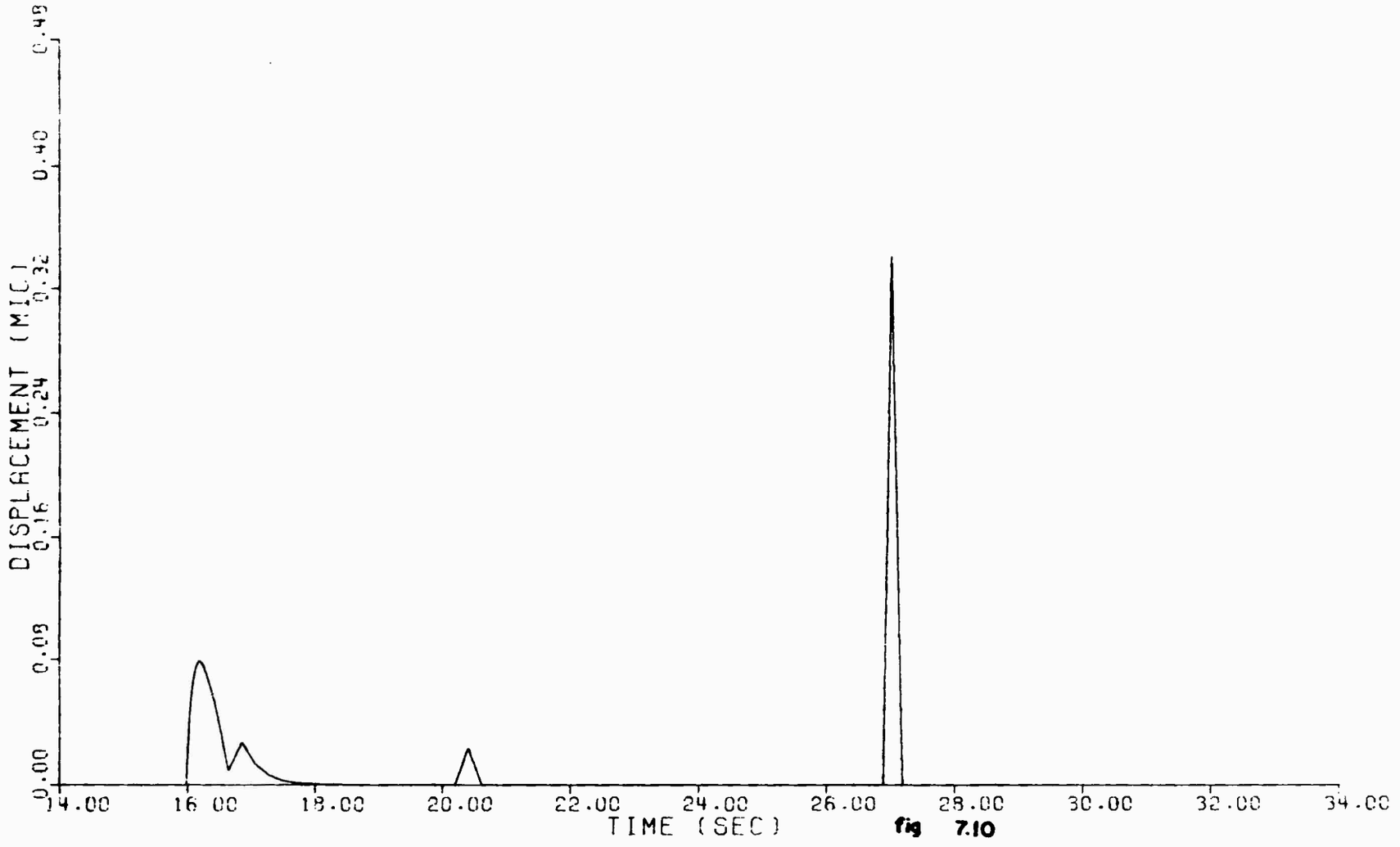

fig 7.10

8.

A study of smaller BENHAM aftershocks, begun on a project with the U.S. Geological Survey during the summer of 1969, was completed under the Contract during this report period, and a paper prepared for publication. The title of the paper is "Smaller Aftershocks of the BENHAM Nuclear Explosion," by William Stauder. The Abstract follows:

The examination of the BENHAM aftershocks is extended to 162 earthquakes approximately an order of magnitude smaller than those previously studied. The spatial distribution of these smaller events is similar to that found for larger events examined by Hamilton and Healy. Focal mechanisms are also similar to those of the larger aftershocks: dip-slip along northeasterly trending zones, generally strike-slip along a north-south trending zone west of the shot-point. About one-third of the mechanism solutions are ambiguous, capable of either interpretation. Amplitude data are successfully used to resolve the ambiguity in about half these cases by selecting the solution which gives a notably lesser value of the variance, $\sum (A_{i\ obs} - kA_{i\ calc})^2/N$ of the amplitude residuals. The value of $\underline{k}$ is related to the magnitude of the shocks. A $\underline{b}$ value of 1.09 indicates that aftershocks of the explosion follow a recurrence rate normal for regional earthquakes or aftershock sequences.

Focal Mechanisms

9. An Application of P Wave Stationary Phase Approximation in Determining Source Parameters by Equalization Procedures.

W. Stauder and M. Lalliana

A stimulus for the use of P wave amplitude data in determining source parameters arises from the personal observation of similarity of wave-form of the P wave from station to station for a given earthquake and of the diminishing of amplitude of the initial P wave at stations which after analysis and comparison of all the data are shown to be near nodal lines. This personal experience was made more objective in a study by Nuttli (Nuttli and Gudaitis, 1966).

Nuttli measured the amplitude of the first half-cycle of the P wave at numerous stations for the Kodiak Island earthquake of February 6, 1964. These amplitude data, corrected only for instrumental response, are shown in Figure 9.1. The scatter in the data is considerable.

The fault plane solution of this particular earthquake is known (Stauder and Bollinger, 1966). The theoretical P wave amplitude radiated by a double couple point source in a homogeneous medium is given by the relation

$$u_p = \frac{1}{4\pi\rho} \frac{xy}{\alpha^3 R^3} K'\left(t - \frac{R}{\alpha}\right) \qquad (1)$$

where ρ is the density, α the P wave velocity, R distance along the ray, $K(t)$ the source time function, and x and y the space coordinates of an observing point with respect to the mechanism axes. Nuttli corrected the observed amplitudes by dividing by the factor xy appropriate to each station.

The results are shown in Figure 9.2. The character of the symbols in the figure is related to the distance of a point from a nodal line, or, equivalently, to the magnitude of the factor xy. It is noted that the scatter is considerably reduced, with the exception of a few points for which values of xy are less than 0.1, i.e., points near nodal lines. By perturbing the mechanism solution by only a few degrees in the dip and dip directions of the nodal planes, a solution was obtained for which even these exceptions disappeared and for which the residuals in observed versus calculated amplitudes were a minimum.

The final solution obtained in this way is shown in Figure 9.3. The line drawn on the figure is the amplitude variation expected from geometric spreading only, based on the Jeffrey-Bullen P wave travel time curve for 0.00H. The correspondence between the observed amplitudes corrected for focal mechanism and the theoretical amplitudes is good. One may conclude that the chief factor in the scatter of P wave amplitude data is the effect of the radiation pattern at the source.

These observations suggest the possibility of seeking a focal mechanism solution for which some quantity, say the variance, S, of the observed versus computed amplitudes is a minimum, where

$$S = \frac{\sum_{i=1}^{N} (A_{i\,obs} - A_{i\,calc})^2}{N} \qquad (2)$$

In principle this is, of course, a well established technique, that of the body-wave equalization procedure which was proposed by Ben-Menahem et al. (1965) and has been applied to a number of earthquakes (Teng and Ben-Menahem, 1965; Ben-Menahem et al., 1968; Khattri, 1969). In a recent paper Chandra (1970) has further applied the method of equalization of P wave spectral amplitudes to determine the focal mechanism of five earthquakes, and has compared the results with solutions from the first motion of P and from the polarization of the S wave. He found close agreement in the solutions determined independently by the three procedures.

In the application here proposed, however, there is question not so much of the spectral amplitudes of P equalized to the source as of the amplitude of the first half-cycle of the P wave observed in the time domain. That is, the amplitude of the first half-cycle of the P wave is considered to represent the spectrum of the wave at the predominant period of the P wave. This is a stationary phase approximation. Teng and Ben-Menahem first used the term in this connection and applied the stationary phase approximation technique to the SH waves of the Banda Sea earthquake (Teng and Ben-Menahem, 1965). Chandra (1970b) has applied the same technique systematically to the P waves for a group of eight earthquakes. He found that the stationary phase solutions agreed with solutions previously determined by equalization of the P wave spectra.

A stationary phase approximation, since it utilizes only the first half-cycle, or even the first quarter cycle (P wave onset to first peak or trough) may be considered to sample the direct P arrival, uncontaminated by converted waves in the crust beneath the stations or in the neighborhood of the source. It is potentially applicable, therefore, to shallow focus earthquakes as well as to the isolated signals of P waves from deep focus shocks.

Even after equalization to the source, P wave amplitudes will vary in absolute value depending upon the magnitude of the earthquake. In order to compare equalized amplitudes to calculated amplitudes a normalizing factor must be introduced. For this, following Jarosch (1968), we let

$$A_{i\,obs} = k\,A_{i\,calc} + e_i \qquad (3)$$

where $A_{i\,obs}$ is the observed amplitude at the ith station

$A_{i\,calc}$ is the calculated amplitude as given by eq.(1)

k is a constant to be determined

e_i is the error in the ith observation.

In order to minimize the sum of the squares of the errors, e_i, we choose k so that

$$k = \frac{\sum A_{i\,obs}\,A_{i\,calc}}{\sum A_{i\,calc}\,A_{i\,calc}} \qquad (4)$$

A value of k may be so obtained for any orientation of the source axes. But a search program is introduced in order

to seek that orientation of the source axes for which

$$\frac{\Sigma (\pm A_{i,obs} - A_{i,calc})^2}{N} \qquad (5)$$

is a minimum. A best fitting solution is thus obtained in a manner quite analogous to the procedure proposed by Ben-Menahem et al. (1965) in the equalization and comparison of spectral amplitudes.

An illustrative example, and a presentation of the results in a plane other than the geographic plane, may help to summarize both the method and a limitation common to all equalization techniques. Figure 4 presents the conventional P wave first motion and S wave polarization mechanism solutions for a Hokkaido earthquake of October 23, 1965. It is noted that the azimuthal coverage of stations about the epicenter is rather good, and that one nodal plane is well determined by the P wave first motion. The positions of both nodal planes may be fixed by a best fit to the S wave polarization data.

In order to apply the equalization of the amplitudes to the focal sphere by the stationary phase approximation, the amplitudes and periods of the first half-cycle of the P wave were determined at 25 stations. These observations were then equalized to the source by taking into account the effect of the instrument and of the crust, and by compensating for geometric spreading and absorption in the mantle. The results of the search program are displayed in Figure 9.5.

The observed equalized amplitudes are presented on the left, the calculated amplitudes for the best fitting orientation of the focal axes on the right.

As has been pointed out by users of this technique, the graphs of Figure 4) are a two dimensional presentation of what in reality is a three dimensional figure; the irregularities of the amplitude diagrams are a function not of azimuthal dependence but of difference in the take-off angle at the source. For example, Figure 9b shows the variation in amplitude as a function of azimuth corresponding to the greatest and to the least take-off angle for the particular observations used in the examination of this earthquake. While either curve is smooth, it is readily seen that if rays corresponding to different take-off angles are plotted on a polar graph a quite irregular figure can result. Hence the star-like shape of the observed and calculated amplitude plots.

While for surface waves it is necessary to present a radiation pattern in a geographic plane, this does not seem to be necessary, or even of particular advantage, for the reduction and presentation of body wave amplitude data. A presentation in terms of the focal axes may be more instructive.

In terms of spherical coordinates referred to the source axes, the amplitude of the P wave on the surface of a sphere of radius R (see eq. (1)) is given by

$$u_p = \frac{\sin^2\theta \sin 2\varphi}{4\pi\rho v^3 R} K'\left(t - \frac{\rho}{v}\right) \qquad (6)$$

where φ is measured in the xy plane, or in the plane of the forces, and θ is measured from the A or B (null) axis. The variation with φ is the familiar four-lobed P wave radiation pattern. Both φ and θ are readily related to the azimuth and take-off angles of a given ray through the direction cosines of the mechanism axes relative to the geographic axes. The amplitude along a ray making an angle θ may in turn be reduced to the amplitude of a ray leaving a source of the same strength at an angle $\theta = \pi/2$ by dividing the observed amplitude by $\sin^2\theta$. In this way the radiation pattern is reduced to the xy plane or plane of the forces. Or, equivalently, one views the radiation pattern from the B axis, looking toward the xy plane.

Figure 4.7 presents the amplitude data of the Hokkaido earthquake in this fashion. One sees immediately the effect of the nodal line and the degree of closeness of fit of the observed P wave amplitudes with the calculated amplitudes for the orientation of the focus selected. One sees as well, and more graphically than in other presentations, the limitation in the distribution of data over the focal sphere. Even with good geographic distribution of observations, the data points are spread over barely a quarter of the xy plane.

In cases however, where the distribution in the xy plane covers several quadrants (strike slip faulting in a vertical plane) a presentation as in Figure may serve to identify the plane of faulting and the direction rupture propagation; the lobes will be asymmetric, enlarged in the direction of the rupture.

A final reference to the quantity k determined above (eq. (4)). If we let $\bar{A}$ be an average value of the amplitude on the focal sphere, then

$$\bar{A}_{obs} = k \bar{A}_{calc}$$

and since

$$M \propto \log \bar{A}_{obs}$$

we have $M \propto \log (k\bar{A}_{calc})$

or $M \propto \log k + \log \bar{A}_{calc}$.

The value of $\bar{A}_{calc}$ is obtained by the relation

$$\bar{A}_{calc} = \frac{\int 2\pi g \, dS}{\int dS} = .424$$

Thus the value of k may be used to determine a magnitude derived simultaneously from many observations of the P wave amplitude and corrected for the effect of the radiation pattern of the source.

The above techniques are being applied systematically to the study of earthquakes in the Kurile Islands and in Peru-Ecuador. The results will be helpful both in support of focal mechanism studies and in the determination of dominant mechanisms of a region, necessary for establishing regional mechanism corrections.

References

Ben-Menahem, A., S. W. Smith, and T. L. Teng (1965). A procedure for source studies from spectrums of long-period seismic body waves, BSSA, 55, 203-235.

Ben-Menahem, A., H. Jarosch, and M. Rosenman (1968). Large scale processing of seismic data in search of regional and global stress patterns, BSSA, 58, 1899-1932.

Chandra, U. (1970a). Comparison of focal mechanism solutions obtained from P and S wave data, JGR, 75, 3411-3420.

Chandra, U. (1970b). Stationary phase approximation in focal mechanism determination, BSSA, 60, (in press.)

Jarosch, H. S. (1968). Body wave magnitude and source mechanism, Seismic Data Lab. Report 225, Teledyne, Inc.

Khattri, K. N. (1969). Focal mechanism of the Brazil deep-focus earthquake of November 3, 1965, from the amplitude spectra of isolated P waves, BSSA, 59, 691-704.

Muttli, O. W., and V. V. Gudaitis (1966). On the amplitude of long period P waves (Abstract), Earthquake Notes, 37, p. 24.

Stauder, W., and G. A. Bollinger, (1966). The focal mechanism of the Alaska earthquake of March 28, 1964, and of its aftershock sequence, JGR, 71, 5283-5296.

Titles to Figures

Figure 1. Amplitudes of first half-cycle of the P wave, corrected only for instrumental response, Kodiak Island earthquake of February 6, 1964.

Figure 2. Amplitudes of first half-cycle of the P wave corrected for focal mechanism as determined by Stauder (1966).

Figure 3. Amplitude of first half-cycle of the P wave corrected for adjusted focal mechanism. Solid line is the amplitude expected on the basis of the Jeffreys-Bullen travel time tables.

Figure 4. Conventional first motion of P and polarization of S mechanism solution for the Hokkaido earthquake of October 25, 1965.

Figure 5. Observed amplitudes (left figure) equalized to the source, and the calculated P amplitudes (right figure) for best fitting double couple source, earthquake of October 25, 1965.

Figure 6. Variation in calculated P wave amplitude for take-off angles corresponding to the [illegible] and least value of L_n for stations represented in Figure 5.

Figure 7. Amplitude data for the Hokkaido earthquake reduced to the xy plane.

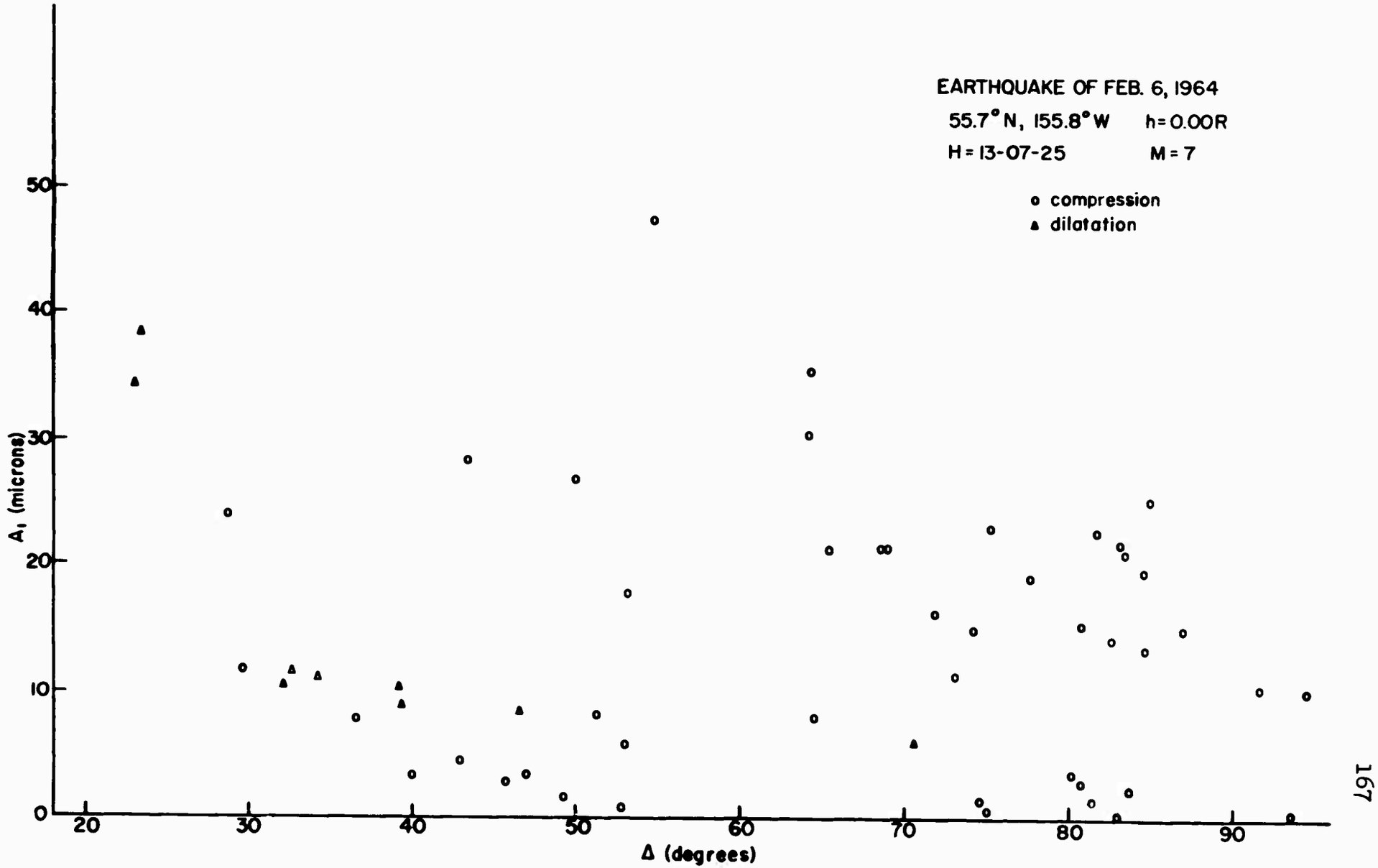
EARTHQUAKE OF FEB. 6, 1964
55.7° N, 155.8° W h=0.00R
H = 13-07-25 M = 7
o compression
▲ dilatation
A, (microns)
Δ (degrees)
0
10
20
30
40
50
20
30
40
50
60
70
80
90

Fig. 9.1

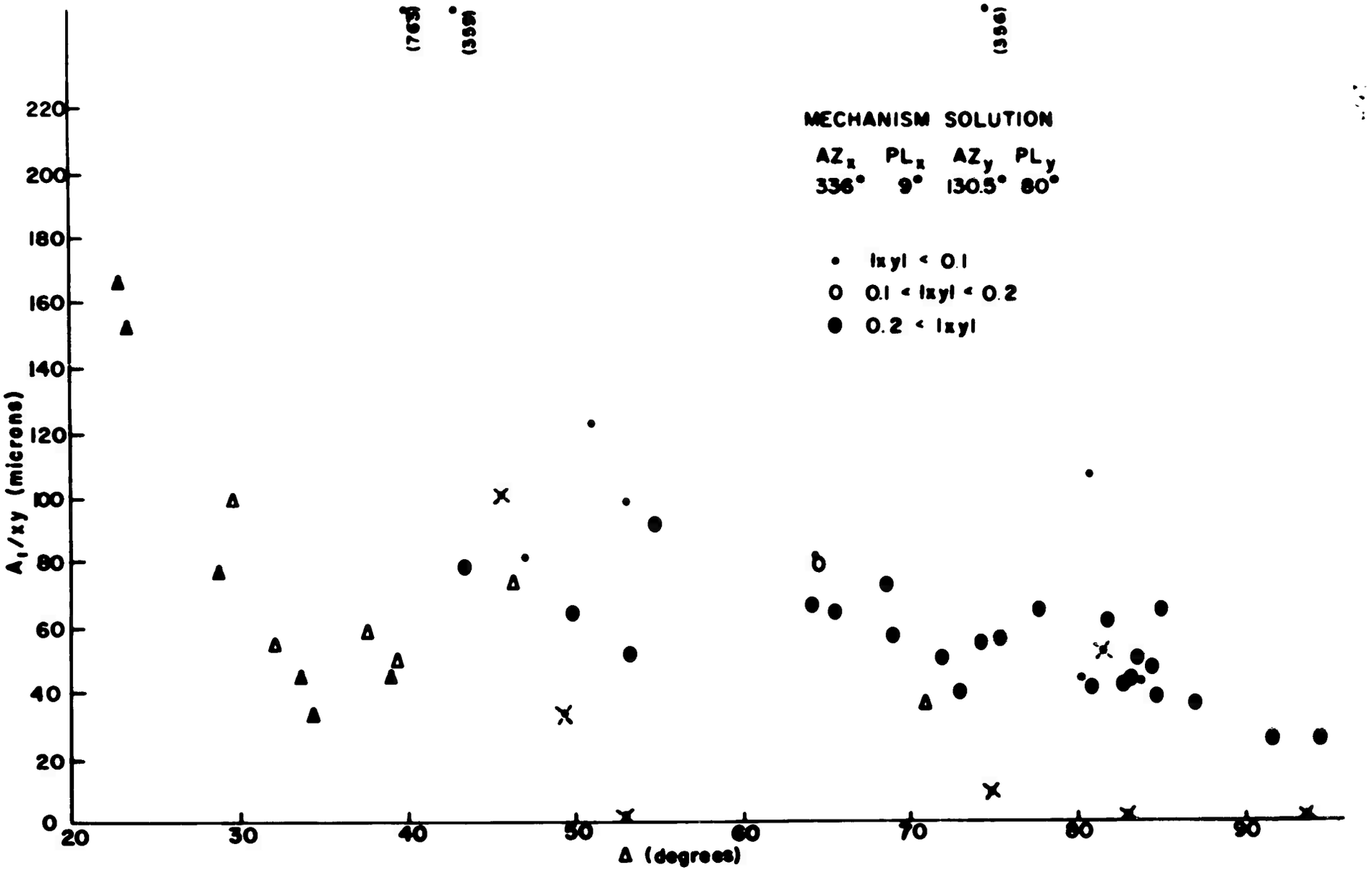
MECHANISM SOLUTION
AZx PLx AZy PLy
336° 9° 130.5° 80°
• |xyl < 0.1
○ 0.1 < |xyl < 0.2
● 0.2 < |xyl
A1/xy (microns)
Δ (degrees)
0
20
40
60
80
100
120
140
160
180
200
220
20
30
40
50
60
70
80
90

Fig. 9.2

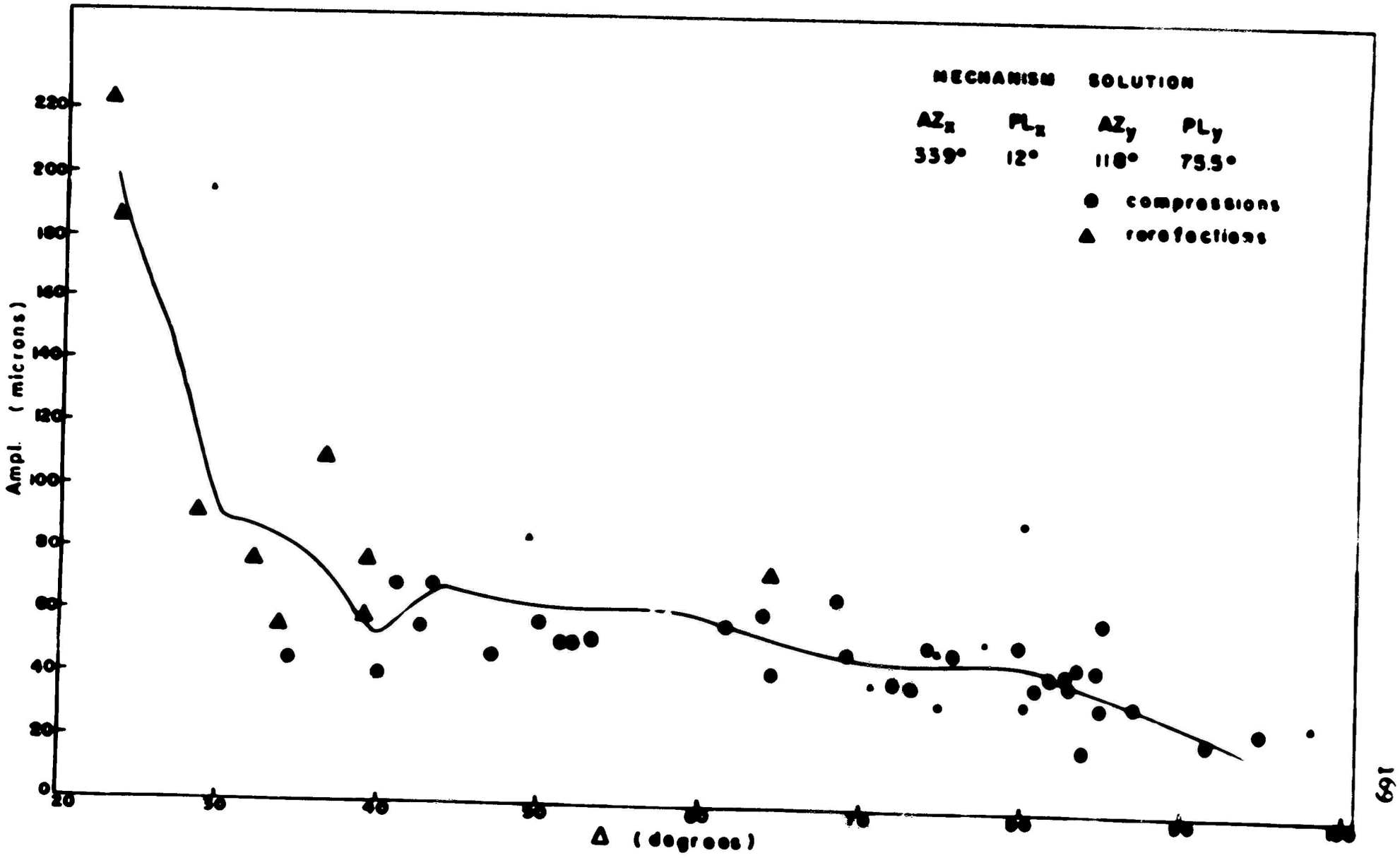
MECHANISM SOLUTION
AZ_x PL_x AZ_y PL_y
339° 12° 118° 75.5°
compressions
rarefactions
Ampl. (microns)
0
20
40
60
80
100
120
140
160
180
200
220
20
30
40
50
60
70
80
90
100
Δ (degrees)

Fig. 9.3

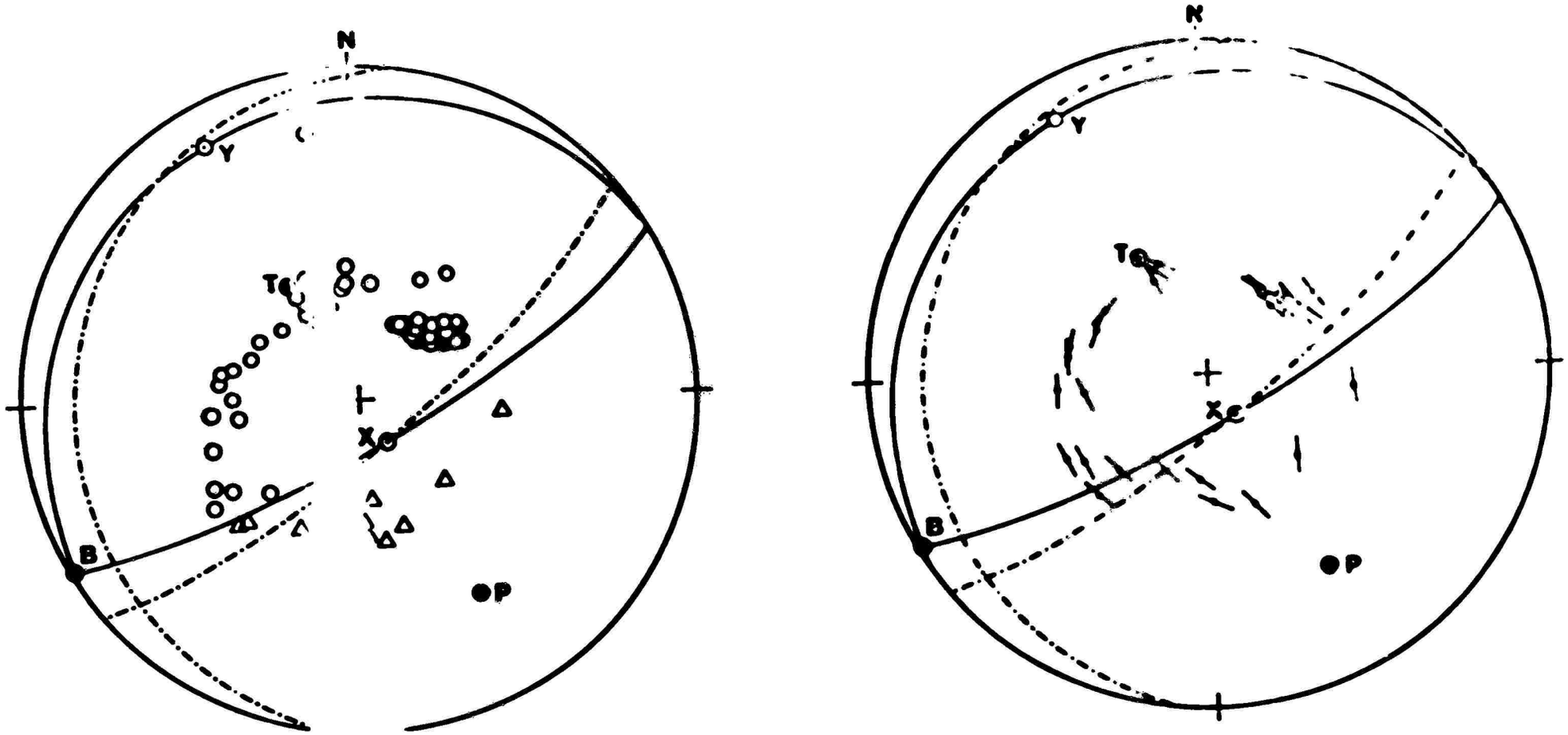

FIG 9.4

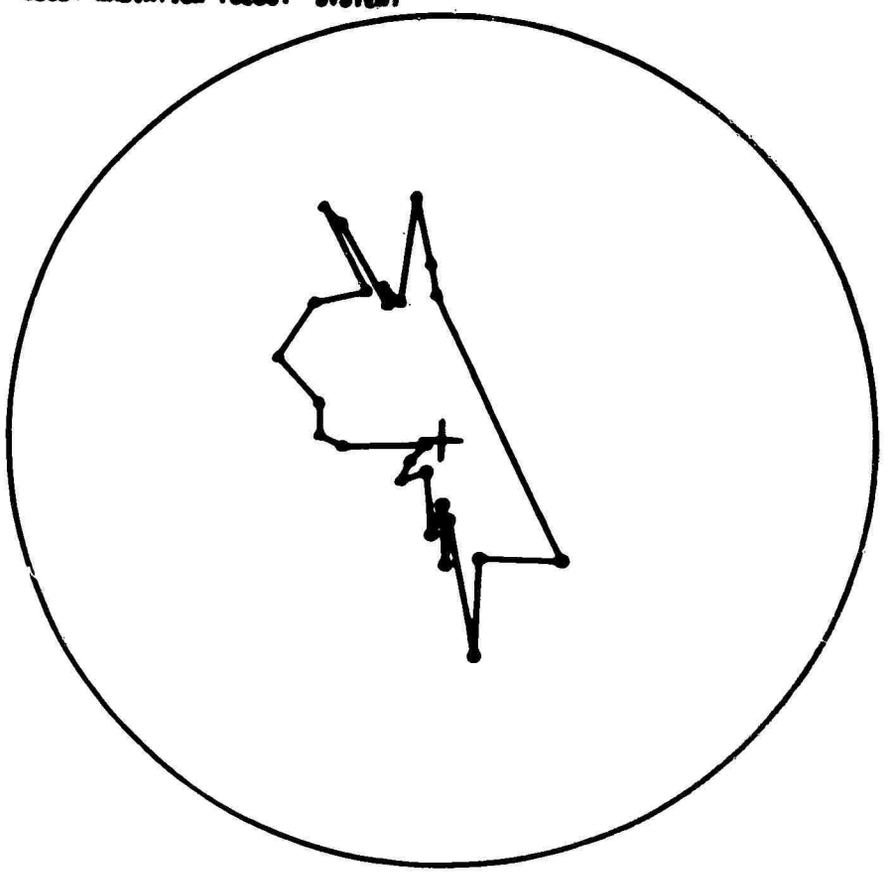

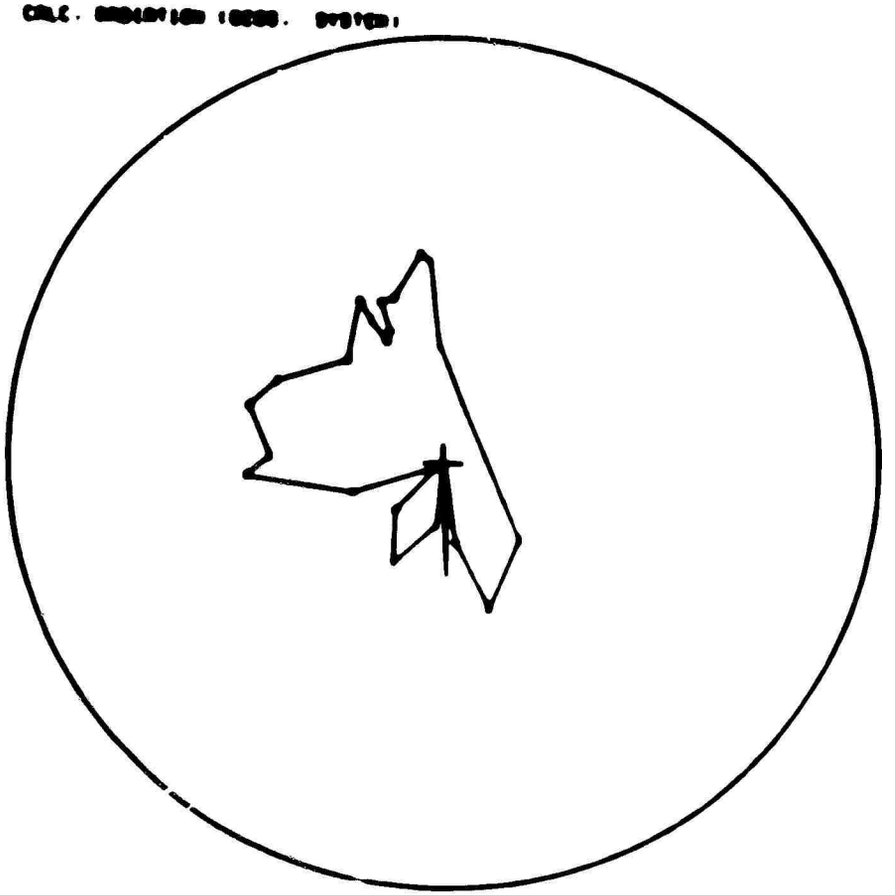

Fig. 9.

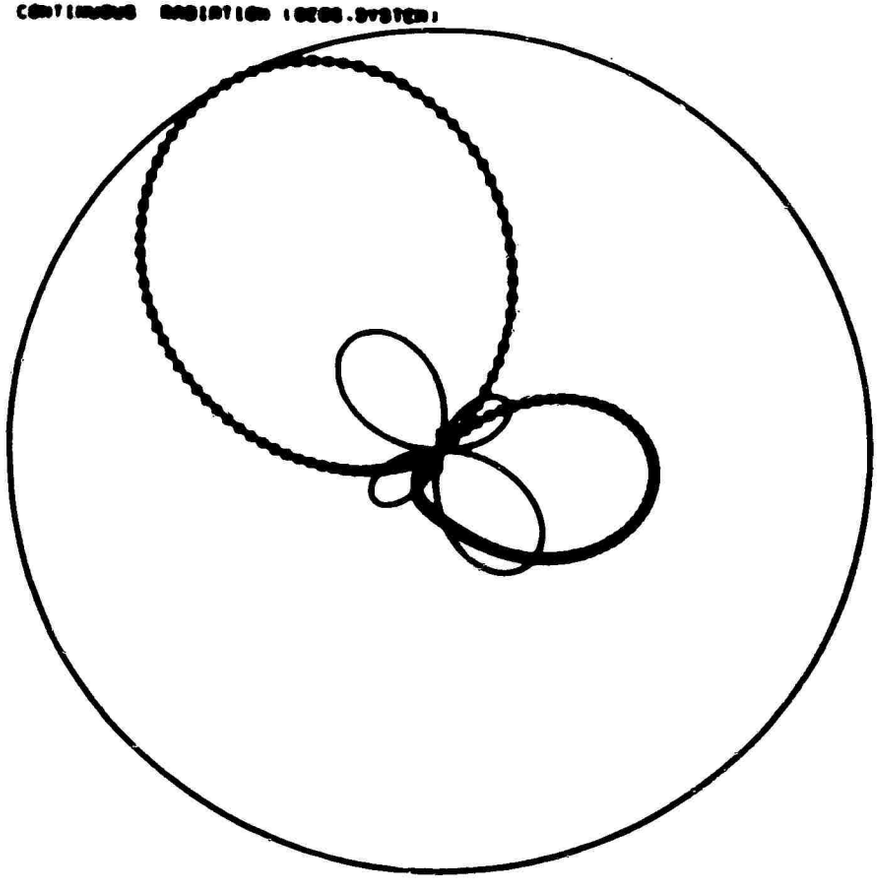

Fig. 9.6

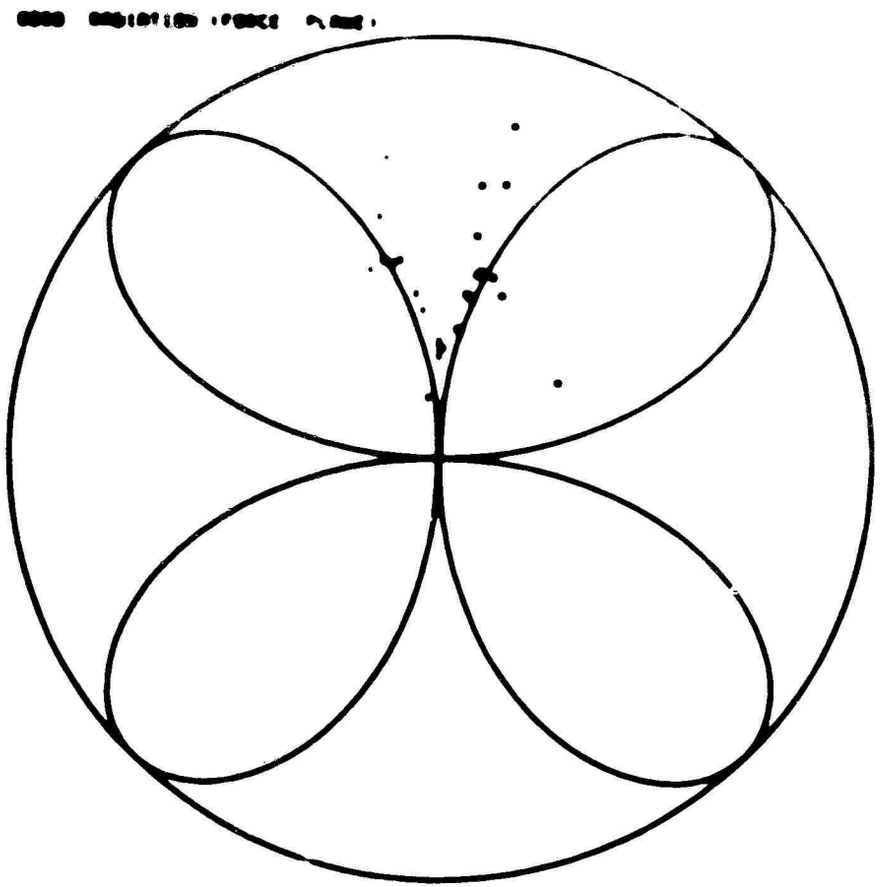

Fig. 9.7

10. Source Parameters of Earthquakes from Spectra of Rayleigh Waves

A. Udias

A. Length of Fault and Velocity of Rupture.

Ben-Menahem (1961) has developed the expressions for the far field displacements of Rayleigh waves radiating from a propagating fault of finite dimensions. The model of the fault is a surface of length b and width d. The propagating fracture is represented by a point source propagating along the b dimension with a velocity v and radiating energy as it propagates. For a vertical strike-slip fault and a propagating double couple the displacement of the vertical component of the Rayleigh wave is given by

$$U_z^R(\omega) = \frac{\sin 2\theta}{\sqrt{r}} g_R(\omega) \sqrt{k_R} \left| \frac{\sin X_R}{X_R} \right| e^{i\left(\varphi_R + \frac{3\pi}{4}\right)} \qquad (1)$$

where

$$X_R = \frac{\pi b f}{c_R}\left(\frac{c_R}{v} - \cos\theta\right) \qquad (2)$$

The effect of the finite dimensions is included in the factor $\chi_R(\omega, \theta)$. To isolate this factor Ben-Menahem defined the directivity function, D, as the ratio of the spectral amplitudes of the surface waves corresponding to waves leaving the source in opposite directions.

$$D = \frac{U_\beta^2(\theta)}{U_\beta^2(\theta+\alpha)} = \frac{\sin X_\alpha(\theta)\; X_\beta(\theta+\alpha)}{\sin X_\beta(\theta+\alpha)\; X_\alpha(\theta)} \qquad (3)$$

Since the only factors which depend on θ in eq. (1) are $\sin X_\beta/X_\beta$ and $\sin\theta$, we can generalize the expression for the directivity to be the ratio of the spectral amplitudes at two stations corresponding to rays leaving the source with an arbitrary angle, α, between them. Thus

$$D_\alpha = \frac{U_\beta^2(\theta)}{U_\beta^2(\theta+\alpha)} = \frac{\sin\left[\frac{\pi b f}{c_\beta}\left(\frac{c_\beta}{v} - \cos\theta\right)\right]^2 \left(\frac{c_\beta}{v} - \cos(\theta+\alpha)\right) \sin 2\theta}{\sin\left[\frac{\pi b f}{c_\beta}\left(\frac{c_\beta}{v} - \cos(\theta+\alpha)\right)\right]^2 \left(\frac{c_\beta}{v} - \cos\theta\right) \sin 2(\theta+\alpha)} \qquad (4)$$

Minima in this function occur at zeros of the numerator, that is, at values of the argument of the sine function

$$\frac{\pi b f}{c_\beta}\left(\frac{c_\beta}{v} - \cos\theta\right) = n\pi \;, \quad n = 0, 1, 2, \ldots.$$

Maxima occu at zeros of the denominator, or for

$$\frac{\pi b f}{c_\beta}\left[\frac{c_\beta}{v} - \cos(\theta+\alpha)\right] = n\pi \;, \quad n = 0, 1, 2, \ldots.$$

The values of the frequency at which either maxima or minima occur can be used to determine the fault length b. For example, for the first order extrema

$$b = \frac{c_\beta}{f_{max}\left[\frac{c_\beta}{v} - \cos(\theta+\alpha)\right]} = \frac{c_\beta}{f_{min}\left(\frac{c_\beta}{v} - \cos\theta\right)} \qquad (5)$$

The directivity function, D, as defined originally (eq. (1)) was used with R or G waves of consecutive order recorded at the same station. This procedure minimizes the sources of error, but reduces the use of the method to earthquakes sufficiently large to generate return surface waves or waves which circle the earth more than once. In theory nothing prevents using direct Rayleigh or Love waves recorded at different stations distributed at arbitrary but differing azimuths about the epicenter. In this event the more general directivity function, D_{α}, (eq. (4)) applies. Allowance must be made, of course, for differences in epicentral distance, path of propagation, etc. This procedure makes it possible to apply the method to earthquakes smaller than M = 7.

The advantage of applying the more generalized expression for the directivity is that stations can be selected at which the Rayleigh waves are well recorded without the constraint of being 180° apart in azimuth. Since the directivity function is normalized, the amplitudes in the spectral ratios must be reduced to a common distance. This is done through the equation

$$\bar{A}_2 = A_2\left(\frac{\sin\Delta_1}{\sin\Delta_2}\right)^{1/2} e^{-(\Delta_1-\Delta_2)\gamma} \qquad (6)$$

As an example, the method here proposed is applied to the Aleutian Island earthquake of July 4, 1966. The two nodal planes of P are assumed to be known, and are taken

from Stauder (1962). Fig. 4(a).1 shows the orientations, AA' and BB', of these planes and also indicates the stations and their distribution about the source at which the direct Rayleigh waves were used in the analysis. The Rayleigh waves at these stations were digitized and a Fourier analysis made of the digitized data. In this process care must be taken to select a suitable time window, for it is important to exclude from the analysis any interference from later arrivals, lateral refractions, etc.

Given the spectra, as many combinations as possible of spectral ratios are formed. By application of equation (5), repeated from above

$$b = \frac{c_a}{f_{max}\left[\frac{c_a}{v} - \cos(\theta - \alpha)\right]} - \frac{c_a}{f_{min}\left(\frac{c_a}{v} - \cos\theta\right)} \qquad (5)$$

a value of b can be obtained from the first maximum or first minimum of any one of these spectral ratios. In so doing it is necessary to assume a value of v, the velocity of rupture. In fact, when using only the amplitude portion of the spectra there is no independent way of determining the fracture velocity, v. However, if many ratios are used for the calculation of b, we may assume different values of v and from these select that v which gives the least standard error for the mean value of b. In this manner we obtain a simultaneous estimate of both b and v.

A by-product of the method when a sufficient number of stations around the epicenter are used is the determination, through the proper choice of θ of the plane of faulting from the two nodal planes and the direction of fracture.

Figs.10.2 & 10.3 show two examples of the spectral ratios for the earthquake of July 4, 1966. The points in the figures are obaervational values of the spectral ratio for the pairs of stations indicated. The solid lines are the computed directivity function for the fault length, fracture velocity, and direction of fracture assumed for the best fit to the data. While there is some variation in the observed from the computed spectral ratio, the minima and maxima are well defined. For this Aleutian Island earthquake the NS striking plane is selected as the plane of faulting, with the fracture propagating southward. This is in keeping with the interpretation of this earthquake as an arc-arc transform fault.

Fig.10.4 shows a similar application to an earthquake in the Azores. The focal mechanism was determined by Sykes (1967). The earthquake is strike-slip, with epicenter on a fracture zone.

B. Seismic Moment.

The seismic moment is calculated following the work of Aki (1966) and the theoretical results of Ben-Menahem and Harkrider (1964) from the spectral amplitudes of the vertical component of the Rayleigh waves at periods sufficiently large that the point source approximation of the source is valid.

Assuming a step function for the source time function the value of the moment is given by

$$M_o = \frac{|U(\omega)|(2\pi r)^{1/2} C_R e^{\gamma r}}{N_{rz}|\chi(\theta)|} \qquad (7)$$

$U(\omega)$ is the spectral amplitude, r the distance, γ the attenuation coefficient, C_R the phase velocity, N_{rz} the Rayleigh wave singlet transfer function and $\chi(\theta)$ the radiation pattern function as defined by Ben-Menahem and Harkrider.

For the earthquakes studied here we calculated the moment at two values of the period, 100 and 50 seconds. For these periods the uncertainties in the assumed phase velocity and attenuation coefficient are small. The results are given in Table 1.

C. Stress Drop, Seismic Energy, and Average Dislocation.

Values for the stress drop, σ, and average dislocation, $\bar{w}$, have been found from the above determined values of the moment and fault length using the relations

$$\bar{w} = \frac{M_o}{\mu A} = \frac{M_o}{\mu b d} \qquad (8)$$

$$\sigma = \frac{1}{2} \frac{w_m \mu}{d} \qquad (9)$$

where

$$w_m = \frac{4}{\pi} \bar{w} \qquad (10)$$

The value of μ was taken as 3.3×10^{11} and the fault width equal to 10 km for the Aleutian earthquake and 5 km for that in the Azores. The results, again, are given in Table 1.

References

Aki, K. (1966). Generation and propagation of G waves from the Hiigata earthquake of June 16, 1964, 2. Estimation of earthquake moment, released energy, and stress-strain drop from the G wave spectrum, Bull. Earthquake Res. Inst., Tokyo Univ., 44, 73-88.

Ben-Menahem, A. (1961). Radiation of seismic surface-waves from finite moving sources, BSSA, 51, 401-435.

Ben-Menahem, A., and D. G. Harkrider (1964). Radiation patterns of seismic surface waves from buried dipolar point sources in a flat stratified earth, JGR, 69, 2605-2620.

Stauder, W. (1968). Mechanism of the Rat Island earthquake sequence of 4 February 1965 with relation to island arcs and sea-floor spreading, JGR, 73, 3847-3858.

Sykes, L. R. (1967). Mechanism of earthquakes and nature of faulting on the mid-oceanic ridges, JGR, 72, 2131-2153.

TABLE 1		JULY 4, 1966 18^h ALEUT	JULY 4, 1966 12^h AZORES
m_b		6.5 ± 0.4	5.7 ± 0.3
M_o 10^{25}	dyne cm	14 ± 3.7	0.24 ± 0.09
b	km.	35 ± 0.4	18 ± 1.8
d	km	10	5
v	km/sec	1.5	1.5
$\bar{w}$	cm	120	6.6
σ	bars	43	2.8

Titles to Figures

Figure 1. Orientation of nodal planes, AA', BB', and azimuthal relation of stations selected for surface wave analysis, Aleutian Island earthquake of July 4, 1966.

Figure 2. Spectral ratio for station pair ATU/AFI. Plotted points correspond to observational value: solid line to the theoretical spectral ratio for the values of b and v indicated, Aleutian Island earthquake of July 4, 1966.

Figure 3. Spectral ration for station pair ANP/BHP, Aleutian Island earthquake of July 4, 1966.

Figure 4. Spectral ratio for station pair TRI/IST, Azores earthquake of July 4, 1966.

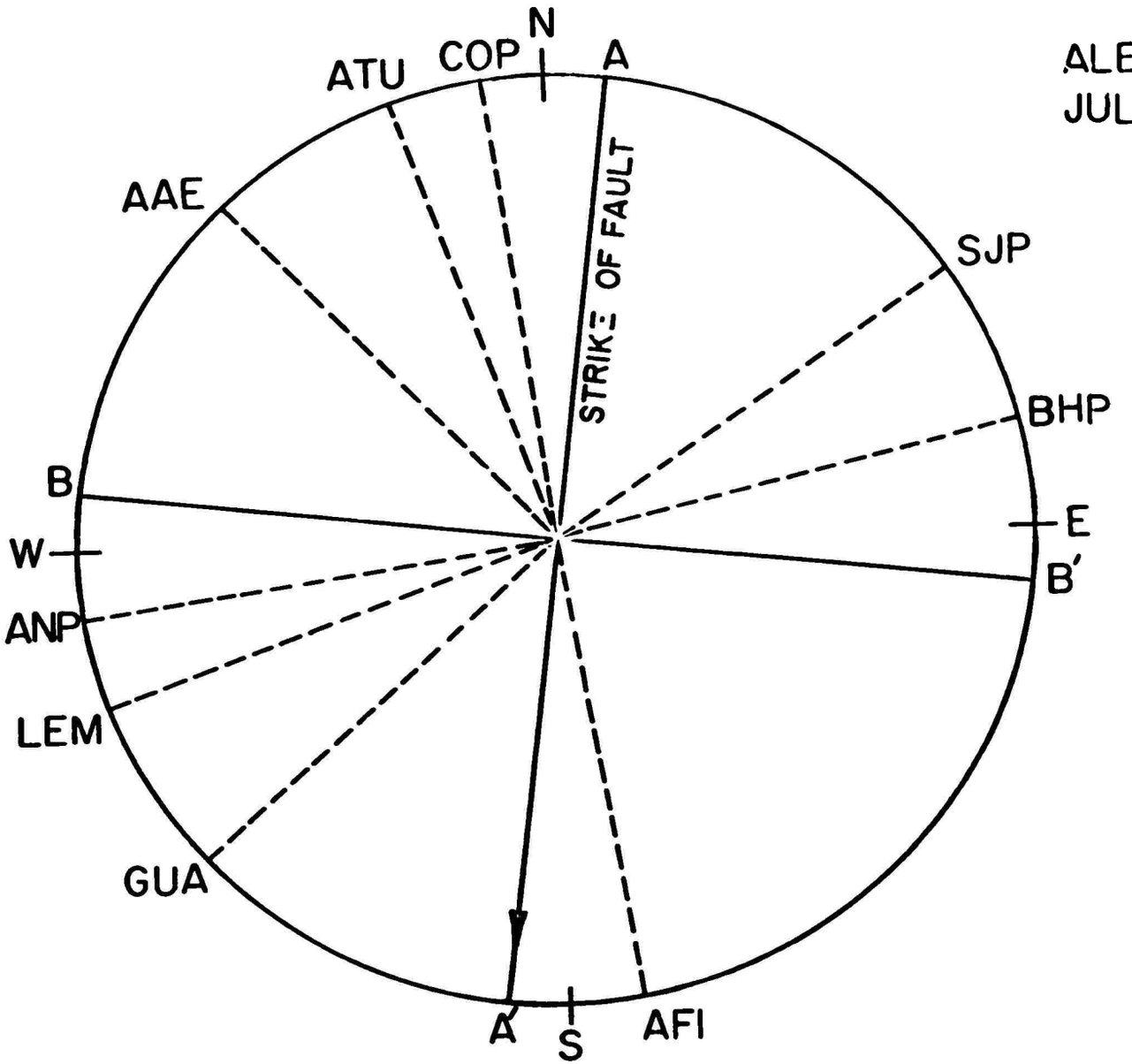

ALEUT
JULY 4, 1966

Fig. 10.1

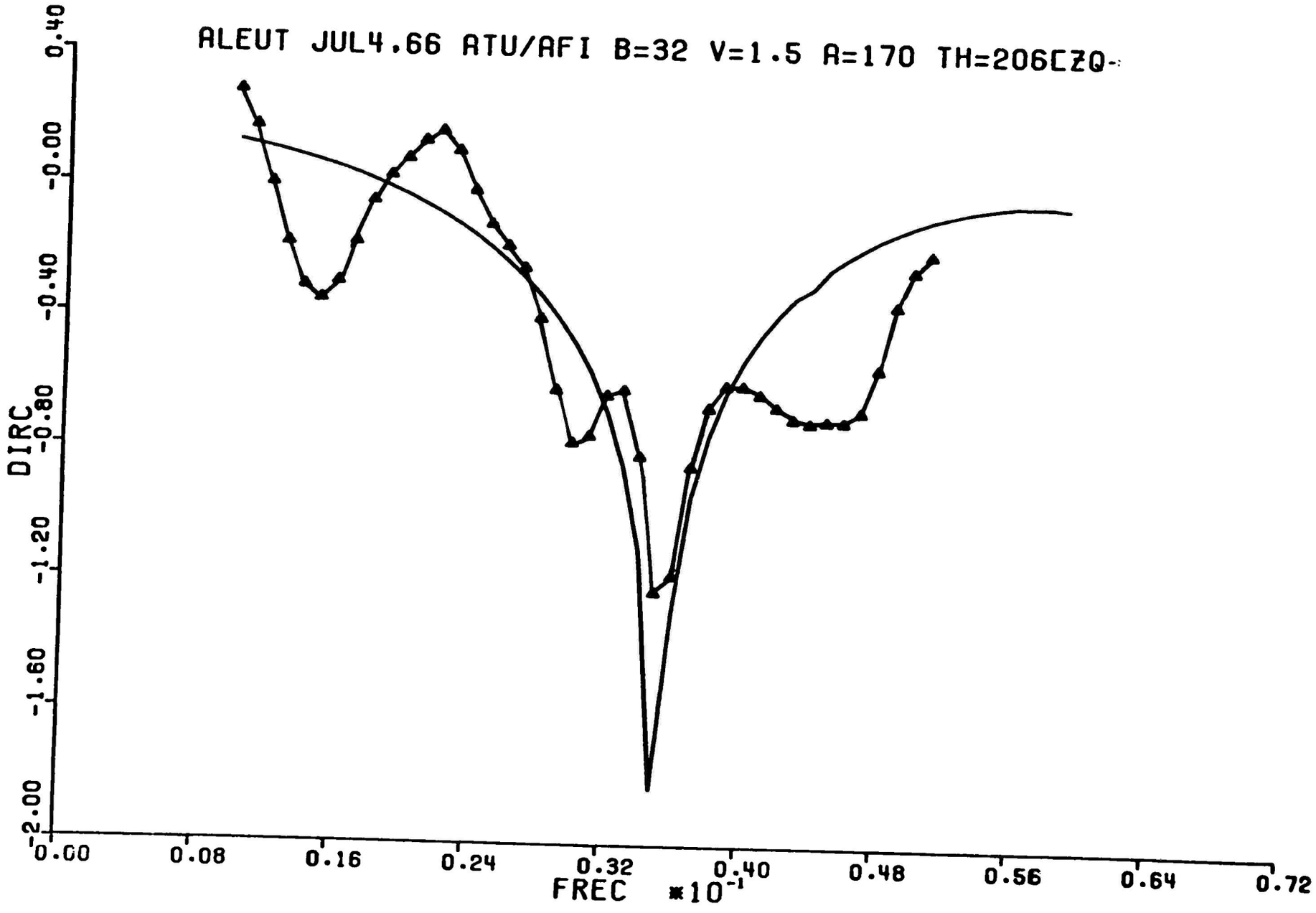
ALEUT JUL4.66 ATU/AFI B=32 V=1.5 A=170 TH=206CZQ-
DIRC
0.40
-0.00
-0.40
-0.80
-1.20
-1.60
-2.00
0.00
0.08
0.16
0.24
0.32
0.40
0.48
0.56
0.64
0.72
FREC *10-1

Fig. 10.2

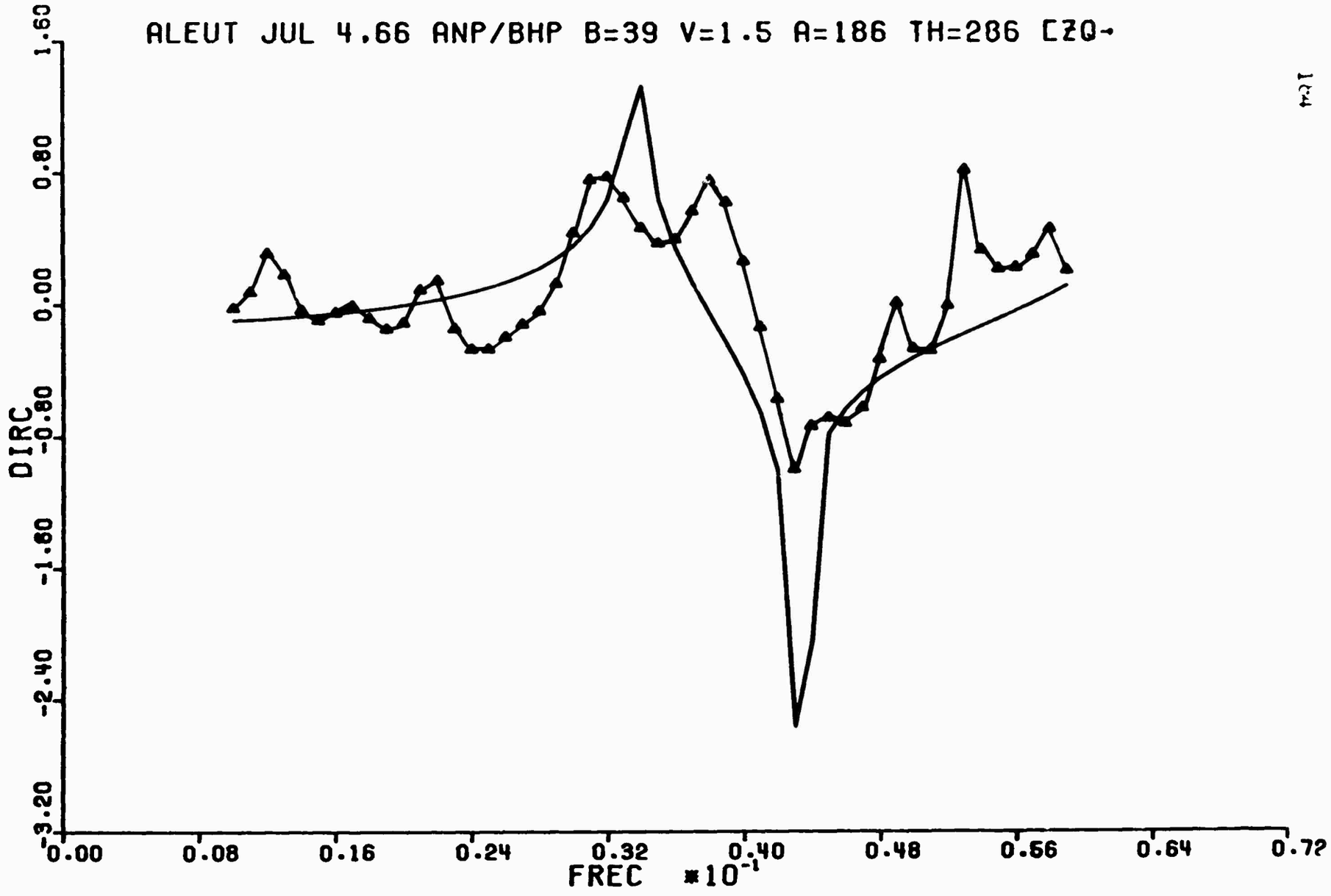
ALEUT JUL 4.66 ANP/BHP B=39 V=1.5 A=186 TH=286 CZQ-
DIRC
1.60
0.80
0.00
-0.80
-1.60
-2.40
-3.20
0.00
0.08
0.16
0.24
0.32
0.40
0.48
0.56
0.64
0.72
FREC *10⁻¹

Fig. 10.3

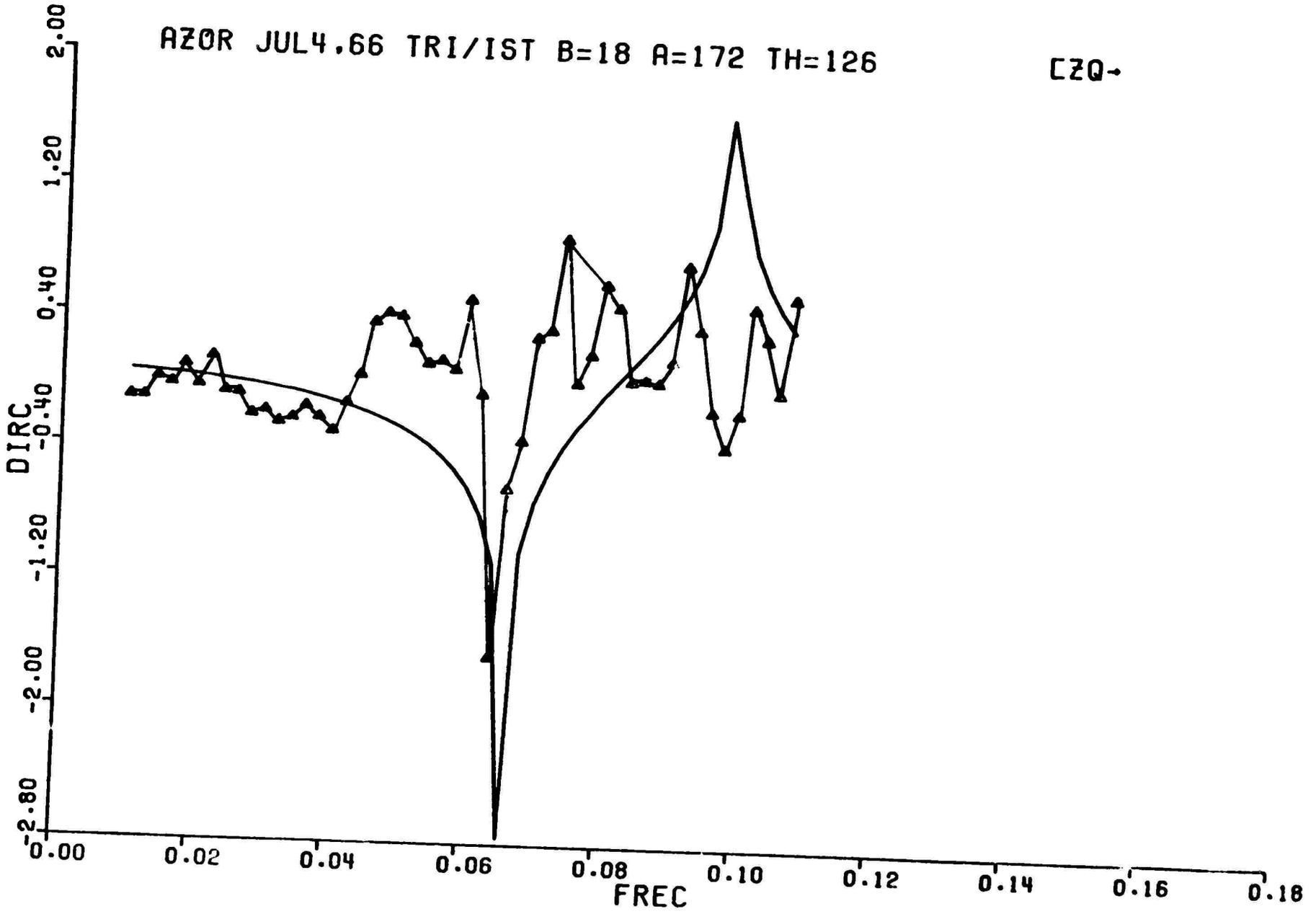
AZOR JUL4.66 TRI/IST B=18 A=172 TH=126
CZQ-
DIRC
2.00
1.20
0.40
-0.40
-1.20
-2.00
-2.80
0.00
0.02
0.04
0.06
0.08
0.10
0.12
0.14
0.16
0.18
FREC

Fig. 10.4

Regional Seismicity

11. Southeast Missouri Seismic Network

Ram Agrawal

The immediate objective of this research has been to study the seismicity of the New Madrid zone on the basis of small earthquakes ($2.4 < m_b < 3.5$) recorded by portable short-period sensitive seismographs. The long-range goal is to determine the relationship of the spectral properties of the seismic waves to the earthquake parameters, especially focal depth and magnitude.

Geology of the New Madrid Area.

The area, geologically, is essentially confined within the borders of the northern part of the Mississippi embayment. This embayment is a broad northward extension of the Gulf Coastal plain. This area is bounded on the west and north by the Ozark Uplift, and on the east by the Illinois Basin. Both of these major features are made up of sedimentary rocks of Paleozoic age. Structurally, the embayment is a large downwarped region of Paleozoic rocks opening to the Gulf of Mexico, filled to the level of present surface with deposits, mostly unconsolidated, ranging in age from Cretaceous to recent. A schematic geological cross-section W-E at latitude 36°N is shown here.

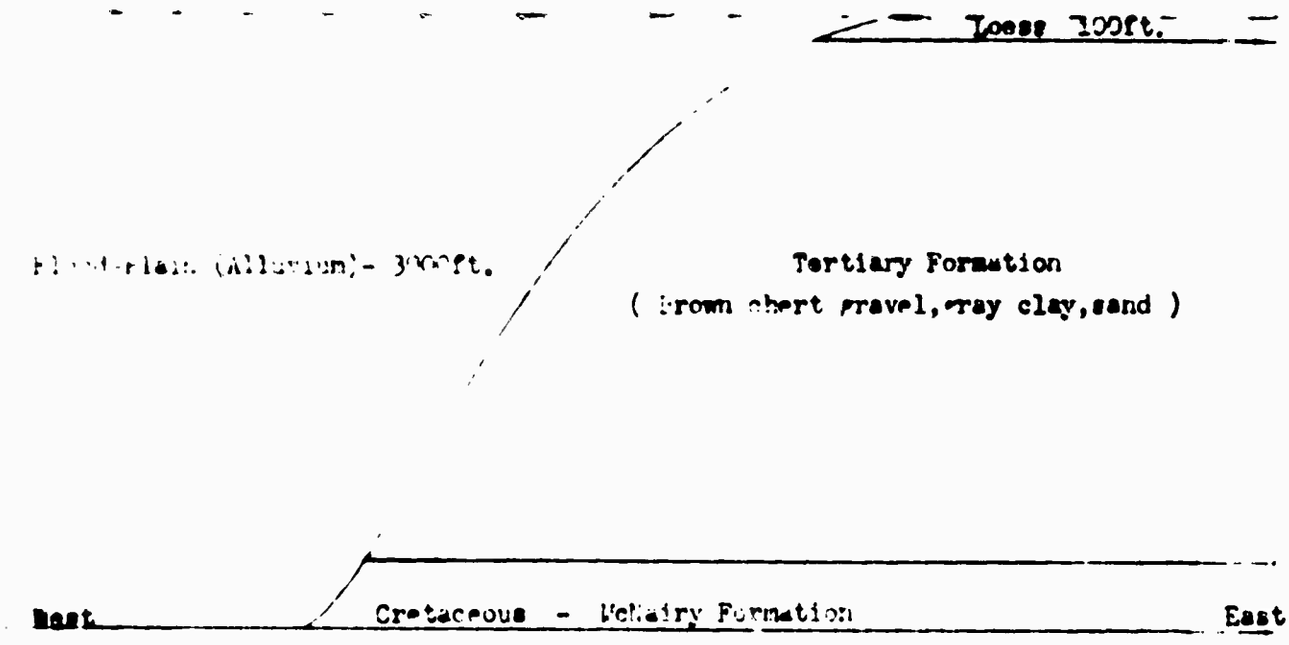

Location of Stations

A three-station seismic network has been operating in western Tennessee since October 1969, with the following specifications:

Samburg(S)

Long.: 89.303°W

Lat.: 36.416°N

Elevation: 138 meters.

The station is on Tertiary rock. Recording is on magnetic tape, played back in the laboratory on a Brush oscillograph. Three instruments; one vertical component, one horizontal N-S and another horizontal E-W, are operating. The natural period, and peak magnification of the instruments are as follows:

Instrument	Natural Period	Amplifier-Gain	Peak Magnification	Frequency at in cps
Vertical	1 sec	150	33K	13.5
		500	106K	13.5
Horizontal (N-S)	1 sec.	150	63K	11.0
		500	208K	11.0
Horizontal (E-W)	1 sec	150	47K	12.0
		500	146K	12.0

The noise level at Samburg has been found to be 5 millimicron peak to peak at 11.0 cps.

Lassiter (L)

Long.: 89.352°W

Lat.: 36.330°N

Elevation: 108 meters.

This station, about 11 km distant from Samburg on Tertiary rock, consists of one vertical component seismograph with natural period 0.4 sec and peak magnification is 110K at 2.5 cps. Recording is on an Autocorder.

Tiptonville (T)

Long.: 89.507°W

Lat.: 36.443°N

Elevation: 85 meters.

A vertical component seismometer with natural period 1 sec is located on alluvium at a distance of 18 km from Samburg. Recording is on magnetic tape.

In addition, another station is operated in Missouri about 80 km from the three in Tennessee:

Greenville (G)

Long.: 90.395°W

Lat.: 37.053°N

Elevation: 168 meter

A vertical component seismometer with period 1 sec and peak magnification 10^5 at 2.5 cps recorded on an Autocorder is operated there.

Epicenter Location Technique

From a model in which all stations are assumed to lie on a horizontal plane and all crustal layers, of constant velocity, are assumed to be bounded by horizontal planes, two computer programs have been developed for determining hypocenters:

(1) Using Pg-arrival times - t_1, t_2, t_3, t_4 at the four stations (Westphal & Lange 1967). Where t_1 - time of arrival of Pg at the nearest station.

(2) Using Pg-arrival times at three stations and (Sg-Pg) interval at the nearest station.

Both programs compute focal depth, but only in a few cases were meaningful depths obtained. Seismic events recorded from March to May 1970 have been studied.

In Table 1-A and B epicentral coordinates, origin time and focal depths are given.

The following velocity structure (McEvilly, 1964) was used to locate the epicenters:

V_P	V_S	Density	Thickness
6.1 km/sec	3.5 km/sec	2.7 gm/cc	11 km
6.4 km/sec	3.68 km/sec	2.9 gm/cc	9 km
6.7 km/sec	3.94 km/sec	2.9 gm/cc	18 km
8.15 km/sec	4.75 km/sec	3.3 gm/cc	

The epicenters were located on the basis of one of the following alternate assumptions:

1. depth less than 11 km
2. depth between 11 km and 20 km.

The results from the first assumption are given in Table 1A and those from the second in Table 1B.

Interpretation of the Epicenter Plot.

Epicenters thus obtained were plotted. Most of the epicenters lie from 35° to 37°N and from 89° to 90°W. There are two clusters of epicenters; one near the New Madrid bend of the Mississippi River and another at the border of Missouri and Arkansas. However, both clusters of epicenters lie along a line running from S 35°W to N35°E, which is more or less parallel to the course of the Mississippi River as shown in Fig. 11.1. The epicenters in Fig. 11.1 are under assumption 1. above. This line of epicenters is in good agreement with the line of epicenters based on historical data for 1811-1964 (Heinrich, 1941, Stauder, 1965, McGinnis, 1963).

The above line of epicenters is also in good agreement with the direction of faults located by Mateker (1968) using

gravity and well-log data. The events do not fall on any of Mateker's faults, but in between the two that bound the upper end of the embayment.

Depth of Focus

For two events, depth of the source has been found to be around 12 km and that for one event 17 km. These are expected values in this region. In three cases tentative values of focal depth of 100-200 km were found. This is an unexpected result and must be verified by further analysis. The tentative spatial distribution of these six events along the line of epicenters ($S35^{o}W$ to $N35^{o}E$) is shown in Fig. 11.2.

Any definite relationship between the shallow and deep focus events cannot be given because of the limited data. For most of the events, computed depth of the focus has been found to be imaginary. Thus, effort is still going on to develop a method to compute the focal depth of such events. It has been judged that only if the epicenter is within the network and also very close to one of the stations, the focal depth computed is reliable.

Time Residual in Pg-Arrival.

Residual in Pg-arrival times using three-station technique of epicenter location has been found to be about $\pm$ 0.3 sec. But in four-station technique it is about $\pm$ 2.0 secs, because of the limited control at Greenville station, which is about 80 km from the tripartite network.

Magnitude Determination.

There was no calibration function available to calculate the magnitude of local earthquakes in the New Madrid area. A relation for the calculation of magnitude has been developed using Pg.

Development of the Magnitude Calibration Function.

Let us assume the magnitude relationship as follows:

$$m_b = a + \log \frac{A}{T} \left(\frac{\text{micron}}{\text{sec}}\right) + b \log D \text{ (km)} \qquad (1)$$

where

A - ground motion in microns

T - period of Pg

D - hypocentral distance in km

$$D^2 = h^2 + \Delta^2$$

h - focal depth

Δ - epicentral distance in km.

a and b are constants

a - varies from event to event

b - depends upon the local geological conditions.

Thus, for about sixteen earthquakes $\log \frac{A}{T}$ and log D are calculated at Samburg and Greenville, assuming focal depth to be 12 km, and are shown in Table II.

Then $\log \frac{A}{T}$ vs log D curve has been plotted. The shapes of the straight lines thus drawn for each event are measured as shown in Table II. The average slope turned out to be tan 65°; i.e. b = tan 65° = 2.15.

The magnitude of the event of March 27, 1970, $03^h\ 44^m$, was calculated to be 3.5 by Dr. O. Nuttli using Pn. Taking this earthquake as a standard one, a line of slope of 2.15

was drawn passing through the point ($\log \frac{A}{T}$, log D) for Samburg as shown in Fig. 11.3. This line cuts $\log \frac{A}{T}$ axis at 1.63 where log D = 1.0. Thus on substitution the values of m_b, $\log \frac{A}{T}$ and log D in equation (1),

$$3.5 = a + 1.63 + 2.15 \times 1.0$$

$$a = -3.78 + 3.50 = -0.28.$$

Therefore, magnitude relationship on the basis of 16 earthquakes using Pg becomes

$$m_b = -0.28 + \log \frac{A}{T} \left(\frac{\text{micron}}{\text{sec}}\right) + 2.15 \log D \quad .$$

Magnitude of all the events were calculated using this relationship and are shown in Table II. The magnitude varies from 2.4 to 3.5.

Justification of the Magnitude Formula.

The magnitude of the event March 27, 1970, $02^h\ 21^m$, was calculated to be 2.5 by Dr. O. Nuttli, and by this relationship also it has been found to be 2.5. Hence the above magnitude relationship seems to be reasonable; however, for better magnitude relationship more data are needed.

Discrimination of Earthquake and Blast.

At about 100 km from the tripartite network there are mining districts where frequent blasting is done. Thus the discrimination of local earthquake and blast in the New Madrid area is very difficult. However, the following criteria have been used for discrimination:

1. <u>On the basis of epicenter location</u>. Epicenters of some of the events have been found to be in the known mining districts; for example, the events of Apr. 19,

1970, $10^h\ 11^m$, and Mar. 28, 1970, $07^h\ 38^m$.

2. On the basis of appearance of seismograms. The seismograms of strip mine explosions and local earthquakes have been shown in Fig. 11.4. As a general rule, records from industrial explosions in the Illinois-Missouri area feature a well developed, short-period surface wave-train, such as that seen in Fig. 11.4 b, which may easily be recorded to distances of 200 km and greater. The records from small earthquakes, on the other hand, are notably lacking in the surface wave trains.
3. On the basis of ratio of Pg to Sg. Ratios of Pg to Sg have been calculated for all the events and are shown in Table II. It has been found that a) $Pg/Sg \leq 1$ for earthquake, b) $Pg/Sg > 1$ for blast. For example, $Pg/Sg = 1.71$ for the event of Mar. 28, 1970, $07^h\ 38^m$.

Seismicity of New Madrid Zone.

From the recording of Mar.-May, 1970, it has been found that in a month six events occurred. In the following table the number of events of a particular magnitude are shown:

No. of events in three mo.	m_b
2	2.4
3	2.5
3	2.8
1	3.0
1	3.2
2	3.5

The range of magnitudes in the present data set is too small to permit the determination of a meaningful slope for the log N vs m_b curve.

Conclusion.

On the basis of the earthquakes occurring from 1962-69 as reported by USCGS, it has been concluded that there are only five events per year in the Southeast Missouri area. However, this network recorded about six events per month during March-May, 1970.

In view of this fact, though at present the results are not complete, it is anticipated that continued recording will result in a more accurate picture of seismicity.

References

Asada, T. (1957). "Observations of nearby micro-earthquakes with ultra sensitive seismometers," J. Phys. Earth, 5, 83-113.

Evernden, J. F. (1967). "Magnitude determination in U.S.," Bull. Seism. Soc. Am., 57, No. 4, 627.

Heinrich, Ross R. (1941). "A contribution to the seismic history of Mo.," Bull. Seism. Soc. Am., 31, No. 3, 187-224.

Malone, Stephen D. (1969). "Focal determination of micro-earthquakes using a tri-partite seismic array," Earthquake Notes, vol. XL, No. 3, 31-40.

Mateker, E. J. (1968). "Earthquakes in Missouri," Bull. of Washington University, 46-51.

McEvilly, T. V. (1964). "Central U.S. crust-upper mantle structure from Love and Rayleigh wave phase velocity inversion," Bull. Seism. Soc. Am., vol. 54, 1997-2015.

McGinnis, Lyle D. (1963). "Earthquakes and crustal movement as related to water load in the Mississippi Valley region," Ill. State Geol. Survey, Urbana, Circular 344, 1-20.

Kisslinger, C. (1965). Excerpt from a report on the seismicity of the St. Louis area.

Nuttli, Otto W., William Stauder and Carl Kisslinger (1969). "Travel-time tables for earthquakes in the central United States," Earthquake Notes, 40, 19-28.

Oliver, J., A. Ryall, J. N. Brune and D. B. Slemmons (1966). "Micro-earthquake activity recorded by portable seismographs of high sensitivity," Bull. Seism. Soc. Am., 56, 899-924.

Sanford, A. R. and C. R. Holmes (1962). Micro-earthquakes near Socorro, New Mexico," J. Geophys. Res., 67, 4449-4459.

Stauder, William, S.J., J. Dowling and W. H. Jackson (1964). "The Billiken calibration shot in southeast Missouri," Scientific Report 4, Contract AF 19(604-7399), Saint Louis University. 26 pp.

Stauder, William, S.J. (1965). A report on the seismic activity of southeast Missouri," Special Report, Dept. of Geophysics and Geophysical Engineering, Saint Louis University, 14 pp.

Stauder, William, S.J., and Allan Ryall (1967). "Spatial distribution and source mechanism of micro-earthquakes in Central Nevada," Bull. Seism. Soc. Am., 57, 1317-1345.

Stewart, S. W. (1968) "Crustal structure in Missouri by seismic refraction methods," Bull. Seism. Soc. Am., 58, 291-323.

Westphal, W. H. and A. L. Lange (1967). "Local seismic monitoring - Fairview Peak Area, Nevada," Bull. Seism. Soc. Am., 57, 1279-1298.

Table 1-A

Date 1970	Origin Time H M S	Epicentral Coordinates Long. in Deg. W	Lat. in Deg. N	Focal Depth in Km	Remark
March 18	22 42 31.39	90.13	35.93	X	*
27	03 44 29.08	89.48	36.55	11.88	*
28	07 38 30.31	98.32	28.46	X	*
April 08	06 03 50.26	89.53	36.53	X	*
May 08	03 41 44.54	90.01	35.67	81.47	*
	08 59 46.94	89.89	35.98	X	*
	10 29 48.63	88.43	35.92	X	*
22	03 52 33.79	90.02	36.06	X	*
	23 50 37.69	89.63	36.16	11.22	*
23	08 04 16.29	90.06	35.48	X	*
	11 24 03.97	89.82	36.63	X	*
28	23 39 10.83	89.55	36.43	5.22	*
30	05 02 58.75	89.05	37.04	150.86	*
March 27	02 21 34.51	89.59	36.58	X	#
	03 44 27.79	89.51	36.60	18.10	#
28	07 38 29.47	95.82	30.77	X	#
April 11	00 59 55.62	89.61	36.26	X	#
14	04 39 10.76	89.44	36.33	11.83	#
19	10 11 23.37	86.77	40.11	X	#

V_P = 6.1 km/sec

V_S = 3.5 km/sec

X - Depth Imaginary

* - Three Station Data Technique

- Four Station Data Technique

Table 1B

Date 1970	Origin Time H M S	Epicentral Coordinates Long. in Deg. W	Lat. in Deg. N	Focal Depth in km	Remark
March 18	22 42 31.38	90.21	35.93	X	*
28	02 21 34.91	89.58	36.58	X	*
	03 44 29.07	89.49	36.57	11.44	*
28	07 38 30.29	96.67	29.98	X	*
April 08	06 03 58.99	89.64	36.35	184.35	*
11	00 59 55.54	89.40	36.65	X	*
14	04 39 13.44	89.41	36.42	X	*
May 08	03 41 58.44	90.02	35.57	81.08	*
	08 58 46.89	89.89	35.92	X	*
	10 29 48.62	88.28	35.85	X	*
22	03 52 33.76	89.16	35.67	X	*
	23 50 37.65	89.60	36.11	13.03	*
23	08 04 16.28	90.08	35.35	X	*
	11 23 58.84	90.39	35.84	X	*
28	23 39 10.71	89.51	36.41	17.12	*
30	05 02 58.61	89.95	37.09	157.18	*
March 27	02 21 35.05	89.58	36.57	X	#
	03 44 28.48	89.50	36.59	14.34	#
28	07 38 30.13	96.10	30.49	X	#
April 11	00 59 56.47	89.59	36.28	X	#
14	04 39 12.01	89.43	36.36	X	#
19	10 11 23.29	86.50	40.40	X	#

Table II

S.N.	Date 1970	Origin Time[1] H M S	S-P	Pg/Sg	Frequency in cps	Samburg log A/T	Samburg log D	Greenville Log A/T	Greenville log D	b = tanθ θ in deg.	m_b
1	March 18	22 42 31.39	0.98 (T)	0.41	9.5	-0.25	1.97	-	2.11	-	3.7 ?
2	27	02 21 34.51	1.56 (T)	0.50	9.5	-0.44	1.53	-1.49	1.95	66	2.5
3		03 44 27.79	2.11 (T)	0.92	7.8	+0.56	1.49	-1.73*	2.36*	68.5	3.5
4	28	07 38 29.47	1.57 (T)	1.71	9.5	-	-	-	-	-	-
5	April 08	06 03 50.26	21.50 (L)	0.11	3.3	-1.85	1.41	-1.33	1.99	-	2.7
6	11	00 59 55.62	2.20 (T)	0.11	7.7	-0.65	1.54	-1.70	2.06	62.5	2.4
7	14	04 39 10.76	0.45 (T)	0.48	9.8	-0.65	1.31	-0.95	2.07	28	2.5
8	19	10 11 23.37	5.50 (L)	-	-	-	-	-	-	-	-
9	May 08	03 41 44.54	15.20 (L)	0.22	3.3	-0.78	2.02	-1.30	2.20	70	3.2
10		08 59 46.94	7.40 (L)	0.30	3.3	-0.73	1.85	-	2.11	-	3.0
11		10 29 48.63	2.50 (L)	0.27	7.5 (S)	-0.55	2.00	-1.30	2.34	65	3.5
12	May 22	03 52 33.79	3.50 (L)	0.82	3.3	-0.64	1.89	-1.77	2.07	80	2.8
13		23 50 37.69	5.21 (S)	0.72	7.8	-0.66	1.62	-1.17	2.09	42	2.8
14	May 23	08 04 16.29	2.90 (L)	0.38	2.5	-0.85	2.10	-	2.25	-	3.4
15		11 24 03.97	1.60 (L)	1.00	10.0	-0.78	1.72	-1.47	1.85	78.5	2.5
16	May 28	23 39 10.83	2.80 (L)	0.87	9.8 (S)	-0.36	1.41	-1.62	2.01	64	2.4
17	30	05 02 58.75	20.40 (S)	0.48	7.8	-0.48	1.87	-1.77	2.07	82	2.8
										Av.θ = 65°	
										b = 2.15	

* Oxford Data

1 Table I-A

SEISMICITY - SE MISSOURI

1911-1964

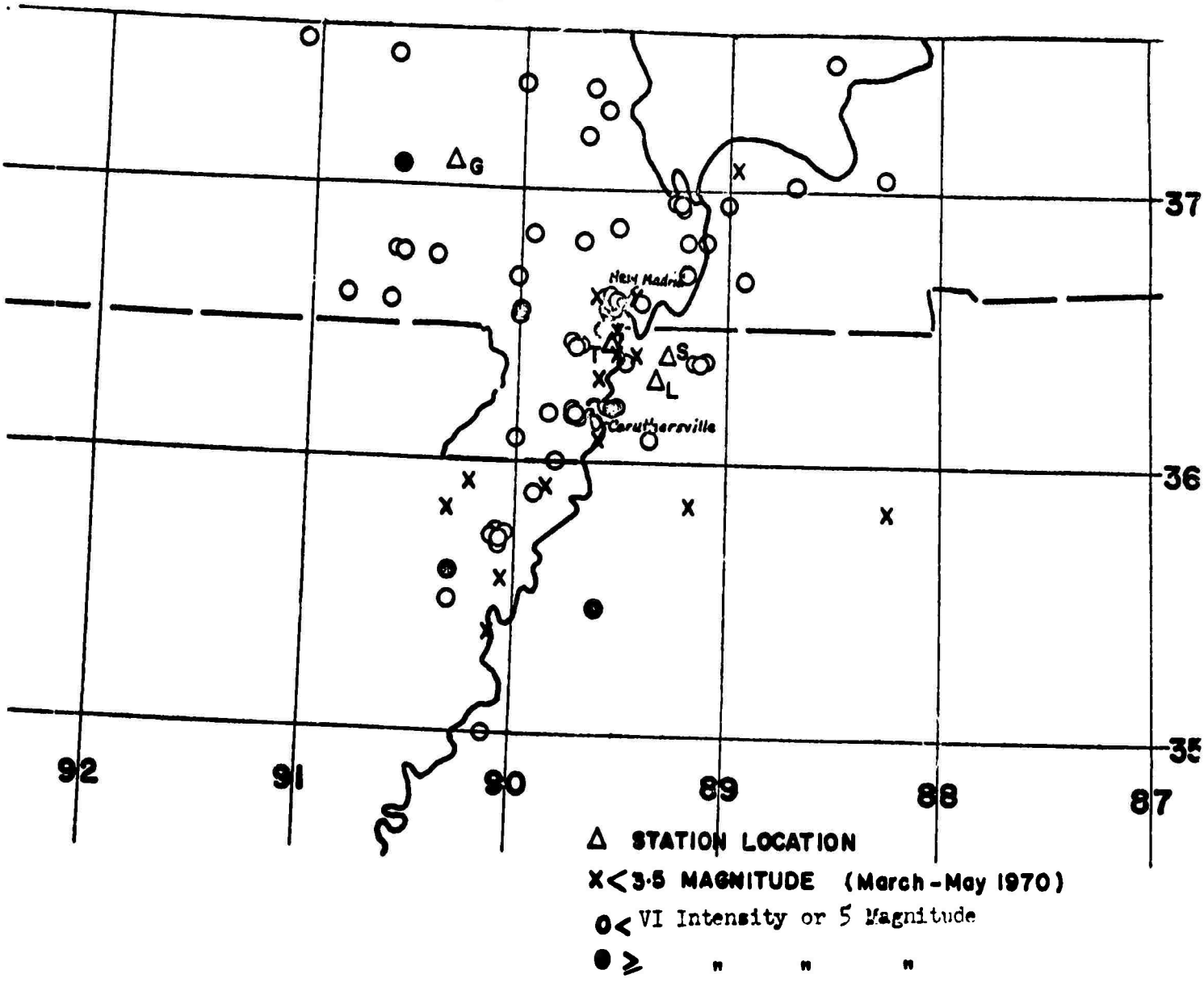

(After Stauder W, 1965)

Fig.11.1

Spatial Distribution of Foci.

S.N.	Date 1970	Origin Time[1] H M S	Focal Depth in km	m_b
S_1	May 22	23 50 37.65	13.03	2.8
S_2	May 28	23 39 10.71	17.12	2.4
S_3	March 27	03 44 29.07	11.44	3.5
D_1	May 08	03 41 58.44	81.08	3.2
D_2	April 08	06 03 58.99	184.35	2.7
D_3	May 30	05 02 58.61	157.18	2.8

1 - Table I-B

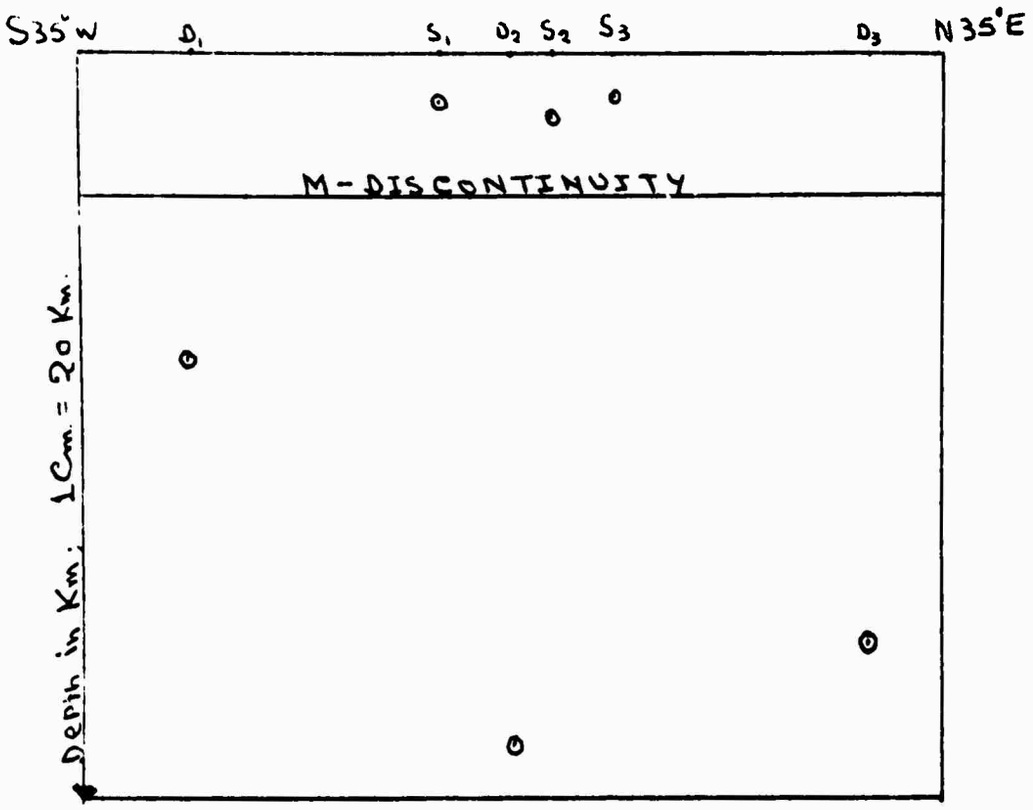

Fig.11.2

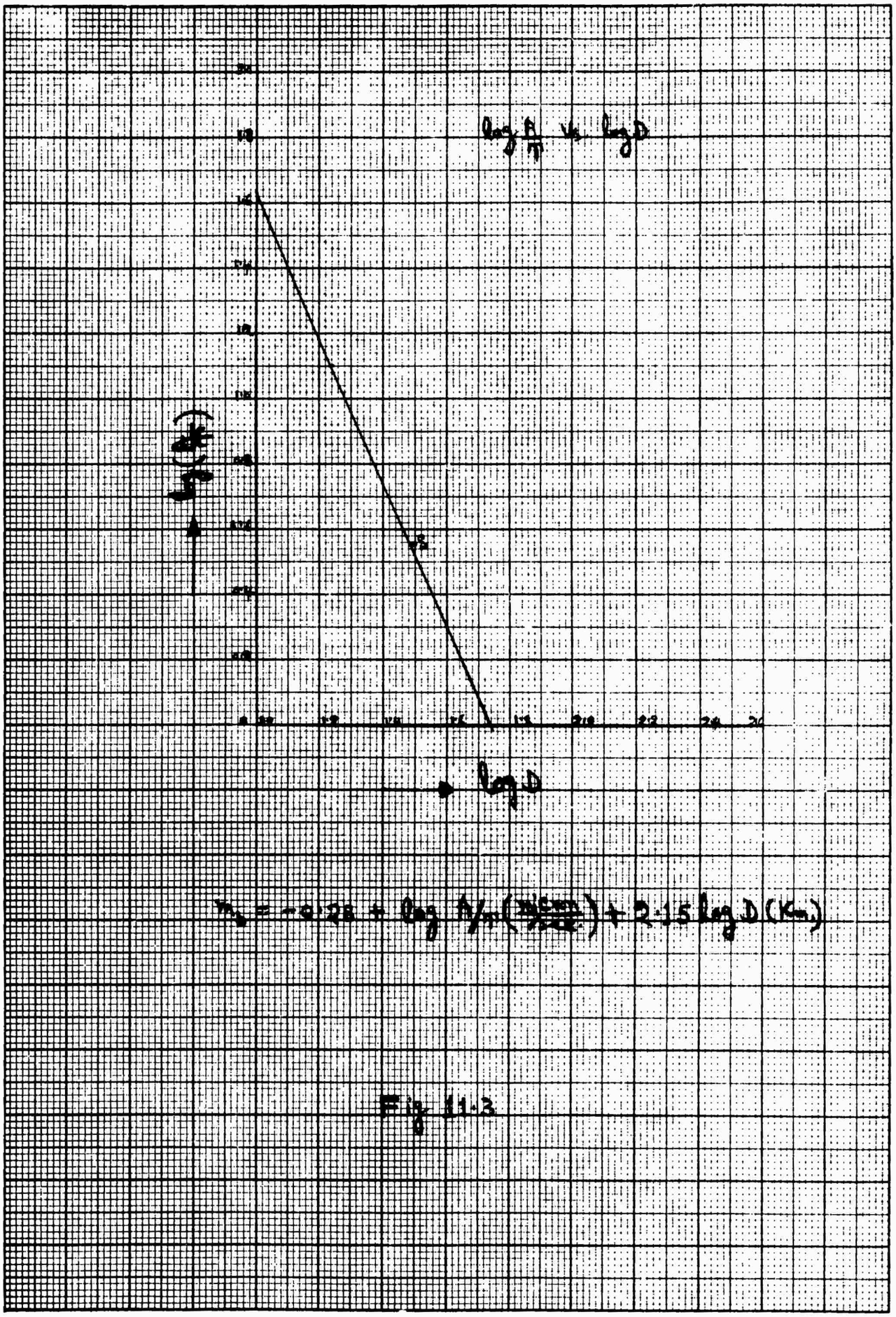

Fig 11.3

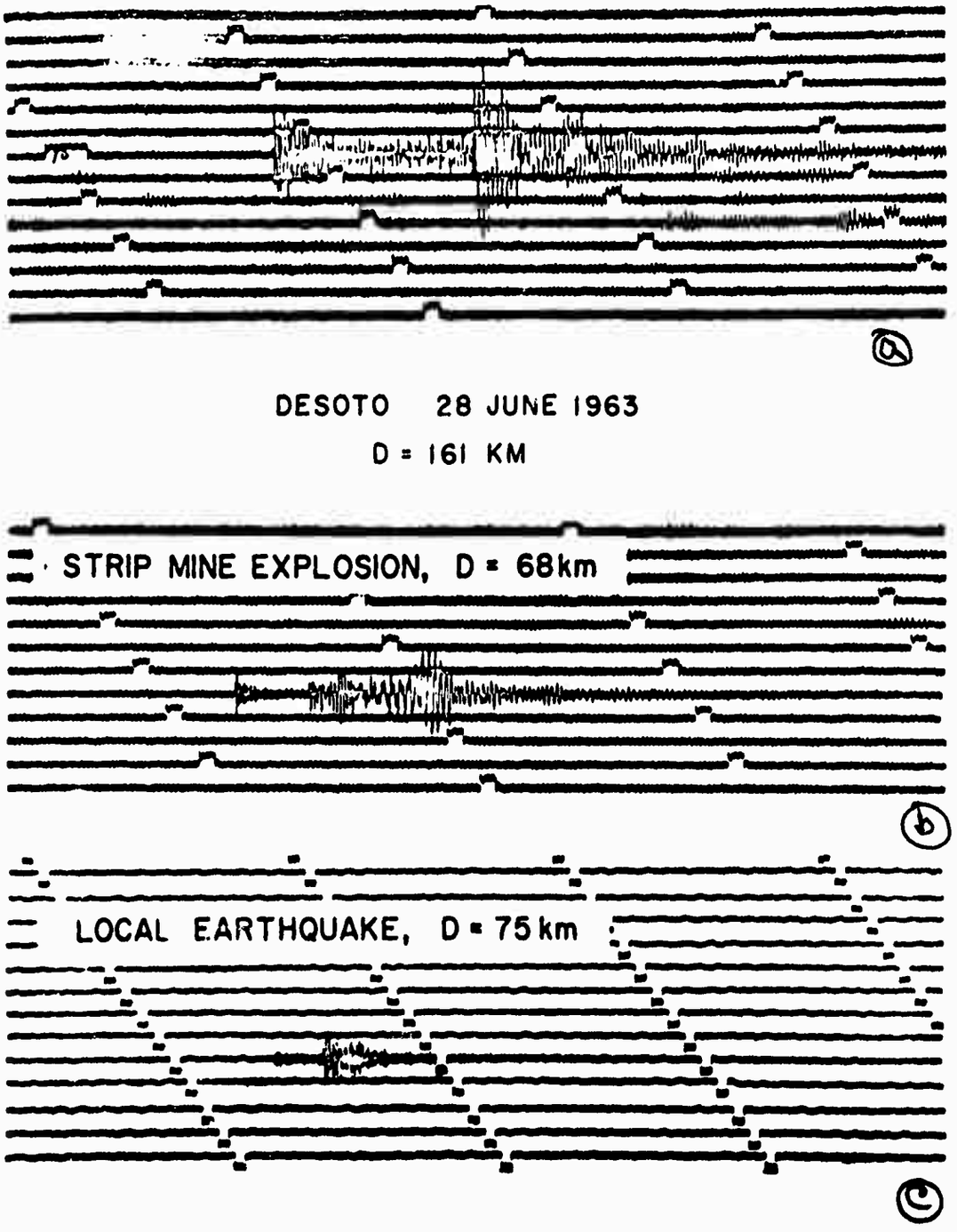

Figure 11.4. Comparison of records from BILLIKEN and other small seismic sources of the Missouri area.
a) (top) BILLIKEN record at DeSoto, Missouri,
b) (middle) strip mine explosion, also recorded at DeSoto.
c) (bottom) small local earthquake recorded near Poplar Bluff.

(After Stauder,W.et.al.1964)

Unclassified

Security Classification

DOCUMENT CONTROL DATA · R & D

(Security classification of title, body of abstract and indexing annotation must be entered when the overall report is classified)

1. ORIGINATING ACTIVITY (Corporate author)
Saint Louis University
School of Engineering and Earth Science
St. Louis, Missouri 63103

2a. REPORT SECURITY CLASSIFICATION
Unclassified

2b GROUP

3. REPORT TITLE

RESEARCH IN SEISMOLOGY

4. DESCRIPTIVE NOTES (Type of report and inclusive dates)
Scientific. Interim. - 1 September 1969 - 31 August 1970

5. AUTHOR(S) (First name, middle initial, last name)

Carl Kisslinger

6. REPORT DATE
1 September 1970

7a. TOTAL NO. OF PAGES
204

7b. NO. OF REFS
99

8a. CONTRACT OR GRANT NO.
F 19628-70-C-0036
ARPA Order No. 0292

b. PROJECT NO.
8652

c. DoD Element 62701D

d. Dod Subelement n/a

9a. ORIGINATOR'S REPORT NUMBER(S)
Annual Technical Report No. 1

9b. OTHER REPORT NO(S) (Any other numbers that may be assigned this report)
AFCRL-70-0582

10. DISTRIBUTION STATEMENT
1 - This document has been approved for public release and sale; its distribution is unlimited.

11. SUPPLEMENTARY NOTES
This research was supported by Advanced Research Projects Agency

12. SPONSORING MILITARY ACTIVITY
Air Force Cambridge Research Laboratories (LWW)
L. G. Hanscom Field
Bedford, Massachusetts 01730

13. ABSTRACT

Research related to the detection, location, and identification of underground nuclear explosion devoted to several major problem areas has been completed. Effects of earth structure and focal mechanism on body-wave magnitude determinations have been investigated, and empirical relations between nuclear yield and Rayleigh wave magnitudes established for selected seismograph stations. Calculations of crustal transmission coefficients for P-waves have been extended to take into account dip and the results applied to observations of laboratory explosion and deep earthquakes. A model for the triggering of earthquakes by explosions based on finite-strain theory has been suggested, the superposition of the explosion-generated and triggered-earthquake-generated P-wave computed for single models, and aftershocks of the Benham event analyzed. Methods of using P-wave and Rayleigh wave spectra for determining earthquake mechanisms have been developed and applied. A small local network for detecting and locating low magnitude earthquakes in southeast Missouri has yielded good data on current local seismicity.

DD FORM 1 NOV 1473

Unclassified

Security Classification

14 KEY WORDS	LINK A		LINK B		LINK C	
	ROLE	WT	ROLE	WT	ROLE	WT
Seismology						
Nuclear explosions						
Earthquake magnitude						
Earthquake energy						
Earthquake triggering						
Transmission coefficients						
Dipping layers						
Earthquake mechanisms						
P-waves						
Rayleigh waves						
Explosion aftershocks						
Nuclear yield						